University of New Mexico
UNM Digital Repository

8-31-2011

Two pulse per cavity lasers and their applications

Andreas Schmitt-Sody

Follow this and additional works at: https://digitalrepository.unm.edu/phyc_etds
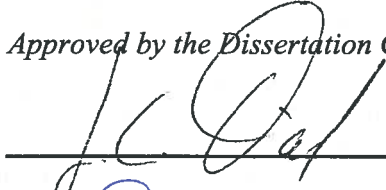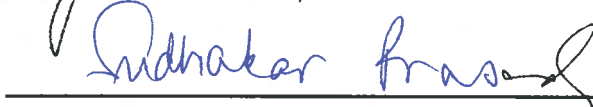
Andreas Schmitt-Sody
Candidate

Physics and Astronomy
Department
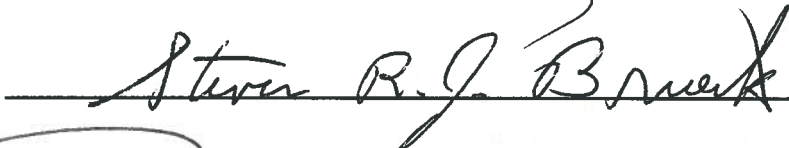
This dissertation is approved, and it is acceptable in quality
and form for publication:

Approved by the Dissertation Committee:

_____, Chairperson

Sudhakar Prasad

Steven R. J. Brueck

Two pulse per cavity lasers and their applications

by

Andreas Schmitt-Sody

MS, University Of New Mexico, 2007

DISSERTATION

Submitted in Partial Fulfillment of the
Requirements for the Degree of

Doctor of Philosophy
Physics

The University of New Mexico

Albuquerque, New Mexico

July, 2011

Dedication

To Hansi

Acknowledgments

I owe thanks and appreciation to many people for helping and guiding my research efforts. I apologize to anyone I may have omitted.

First, I would like to thank Dr. Jean-Claude Diels for his patience, support, and advice over the last six years. Also, I need to thank my committee members for taking the time to read this manuscript: Dr. Prasad, Dr. Sheik-Bahae, and Dr. Brueck. A big thank you goes to all my current and former student group members and I thank them for their advice and helping hand during the experiments. I especially want to mention Dr. Andreas Velten, with whom I worked on the OPO experiment, Dr. Oliver Chalus for his patience in mentoring me during the first few years, and Dr. Ladan Arissian for her contribution to this project. Other group members who have helped me in my research are Dr. Alex Braga, Shermineh Rostami, Xuan Luo, Xiaozhen Xu, Koji Masuda, Chengyong Feng, Jeremy Yeak, Mikael Hosatte, Daniel Mirrel, and Martha Navarro. Finally, Dr. David D. Smith was a very helpful collaborator and gave valuable input to publications and experiment.

Lastly, I have to thank my wife Ugne for her support, encouragment helping me through the tough motivational times and trying to make my English better.

Two pulse per cavity lasers and their applications

by

Andreas Schmitt-Sody

ABSTRACT OF DISSERTATION

Submitted in Partial Fulfillment of the
Requirements for the Degree of

Doctor of Philosophy
Physics

The University of New Mexico

Albuquerque, New Mexico

July, 2011

Two pulse per cavity lasers and their applications

by

Andreas Schmitt-Sody

MS, University Of New Mexico, 2007

PhD. Physics, University of New Mexico, 2011

Abstract

Lasers have been around now for over 50 years. Initially it was said that it is an invention without an application. Since then it turned out that lasers are valuable tools for applications like mapping atomic transitions or interferometric measurements. The research presented here will show one type of lasers, a two-pulse-per cavity mode-locked laser, its applications and analyze its practical and theoretical limits.

An analysis of a two pulse per cavity mode-locked laser is presented as analogy to a quantum mechanical two level system. It can be shown that our lasers with two independent pulses propagating inside the cavity can be coupled via a scattering medium and will behave exactly the same way as a two level atom driven by a step function electric field. This analogy is providing a new insight into the dynamics of two-pulse coupling in mode-locked ring lasers.

The most important application of a mode-locked laser with two intracavity pulses is Intra-cavity phase interferometry (IPI). The unique feature of mode-locked lasers,

where a pulse to pulse phase shift is converted into a frequency, can be used for very sensitive phase measurements that outperform standard interferometers. Two pulse trains with the same repetition rate from the same cavity and a different phase shift will show a beatnote signal directly proportional to this phase shift when interfered on a detector. It leads to an good signal strength since all modes of the frequency comb contribute to the signal. In this dissertation, I will describe the advancement of IPI with our standard Ti:Sapphire cavities to the measurement of magnetic fields. Also another cavity, Optical Parametric oscillators (OPO) can be used for IPI. I will be showing two different implementations, intra-cavity pumped and extra-cavity pumped and their usefulness to phase interferometry by presenting a new method to measure the non-linear index of a material. In the end, a discussion about the theoretical limit of the sensitivity and resolution is provided for both, the Ti:Sapphire and OPO system.

Contents

Contents

Contents

Contents

Contents

List of Figures

List of Figures

List of Figures

List of Tables

Glossary

Δ x   displacement

$\Delta\varphi$ differential phase shift

k   wave vector

I   Intensity

$\tilde{\mathcal{E}}(t)$ comeplex electric field envelope

$\mathcal{E}(t)$ real electric field envelope

τ_p pulse width

ω_0 angular center frequency of pulse

φ phase

Ω angular frequency variable in the Fourier domain

τ_{RT} cavity roundtrip time

ν optical frequency

f$_{CEO}$ carrier to envelope offset frequency

T   integration time, coherence time

Glossary

L	cavity length
n_2	non-linear refractive index
λ	wavelength
n	ordinary refractive index
B	magnetic flux
V	Verdet constant
W	Energy
T_{OC}	output coupler transmission
l_{tot}	total cavity losses
P	power
θ	spontaneous emission factor
$\tilde{r}$	scattering coefficient
Ψ	wave function
α_1, α_2	gain factors
g	mutual gain coefficent (includes mutual saturation terms)
ρ_{ij}	density matrix elements
κ E	Rabi frequency

Chapter 1

Introduction

Lasers have been in existence for over 50 years. The first laser was built by Maiman in 1960 and used a ruby crystal for the gain material [2]. Initially it was said that lasers were considered an invention without an application. However, since the 1950s, lasers have become invaluable tools. Applications range from mapping out atomic transitions through narrow linewidth continuous wave (CW) lasers to cutting materials. During CW laser development, pulsed lasers also generated growing interest. The pulsed lasers' broad spectrum and high peak intensities and peak power were used for most nonlinear optical experiments. The first pulsed laser, a ruby Q-switched laser, was reported shortly after the initial invention of the laser by McClung and Hellwarth [3], reaching megawatt (MW) peak powers. Two years later, the first report of active mode-locking was published [4]. Within a few decades, most broadband laser types were able to be mode-locked, starting with dye lasers in the 1970s to Ti:Sapphire lasers toward the end 1980s to semiconductor lasers. Ti:Sapphire lasers are presently the most frequently used laser for mode-locking, to create short pulses, because their broad gain bandwidth of more then 300nm [5] allows for pulse widths as short as 5fs and average output powers of up to 1W out of the oscillator, a far leap from the 1950s era lasers.

The dissertation is describing two applications of a mode-locked laser with two pulse per cavity. One of the application, called two level analogy, of these two-pulse-per-cavity lasers will be described in the dissertation in Chapters 2 and 3. Classical analogies of quantum mechanical systems aid visualization and better understanding of quantum mechanical systems only. From previous research, a simple electrical circuit showed an elegant analogy of the interaction of an electric field with a three level quantum mechanical system [6]. The two-level analogy discussed in Chapter 3, provides new insight to the two-pulse coupling in mode-locked ring laser dynamics instead of the frequently researched quantum mechanical systems. The two-level analogy uses two independent pulses propagating inside the cavity and couples the pulses via a scattering medium. The research shows the system will behave the same as a two level atom driven by a step function electric field, but provides insight into mode-locked ring laser dynamics. The analogy's practical application is a sensor for scattering measurements.

Other applications of mode-locked laser vary from pump probe experiments to frequency combs. One important application with frequency combs is the optical frequency standard for precise clocks, developed from the laser pulse trains' inherent characteristics of equally spaced delta-functions in the frequency domain and the wide spectrum of fs pulses. Since the comb spacing is in the radio frequency (RF) band, the RF signal from the laser can be locked to a standard RF signal given by microwave oscillators. The RF signal locking provides an accurate time standard. Due to the low noise and high stability of the mode-locked Ti:Sappphire laser, it can provide an accurate frequency standard when locked to atomic transitions and the the laser cavity is stabilized with cumbersome systems. This accurate frequency standard can be used for testing basic physics principles, or used for precise pin-pointing in global positioning systems (GPS).

Nevertheless, precision measurements are still possible even with unstabilized mode-locked lasers as the research presented here will show. Unstabilized mode locked lasers use the phaseshift of the carrier wave underneath the pulse envelope to convert the phaseshift into a frequency, called intracavity phase interferometry (IPI), the second application of a two-pulse per cavity laser descussed in the dissertation. The resulting frequency induces a frequency shift of the entire comb. The frequency shift is measured by normal heterodyne beating using a reference pulse train with the same repetition rate. The sequential phaseshift from pulse to pulse in the pulse train can occur inside of the laser cavity or outside with a Doppler shift. Inside a mode-locked cavity, circulating pulses can acquire a phaseshift at each rountrip due to the difference in group and phase velocity. Using two pulses, one signal and one reference to acquire the opposite phaseshift with respect to each other, provides, at the output of the laser, two pulse trains of equal repetition rate as needed for heterodyne detection. Since the pulses share the same cavity, fluctuations, in principle, affect both pulses the same way. If no phase noise is introduced by the measurement, the laser does not need any special stabilization setup. IPI theory is discussed in detail in Chapter 4.

Only a few laser systems can be used for IPI. The first IPI experiment used a dye laser system. mode-locked with a saturable absorber dye jet [7]. Five years later, Ti:Sapphire lasers that were mode-locked with a saturable absorber dye jet improved the overall stability of the beatnote signal from a bandwidth of 100Hz to 1Hz. Due to the disadvantages of the dye jet, synchronously pumped optical parametric oscillators (OPO) were investigated [8]. This dissertation discusses experiments to improve the OPO cavity for IPI as well as different applications, like optical magnetometry. The OPO experiments and applications are discussed in Chapters 5 and 6, respectively. Limitations to beatnote bandwidth are discussed in Chapter 5.

One disadvantage of using OPOs is the need for high power mode-locked pump sources. Ti:Sapphire lasers have the power and pulse duration needed to pump OPOs but, in addition to high costs, a problematic Q-switching is present. A cascade of four lasers are needed during the OPO lasing process, which is inefficient. The four laser setup includes the diode laser pumping the Nd:vanadate laser and doubling the frequency to 532nm to pump the Ti:Sapphire. The cumbersome setup is a driver for developing a high-power, mode-locked semiconductor laser. Relatively high output power was achieved with fairly narrow pulse widths of 500fs. Since the output power was not sufficient for pumping an OPO, the research shifted to a different semi-conductor laser: optically pumped, vertical emitting, external cavity semiconductor laser (optically pumped VECSEL). VECSEL experiments and results are discussed in Chapter 5.

Chapter 2

Theory of the Two level System Analogy

2.1 Introduction

A second experiment conducted with two-pulse-per-cavity lasers is the two-level system analogy briefly introduced in Chapter 1. The two-level system analogy experiment will be described in the next two chapters. The analogy provides new insight to the two-pulse coupling occurring in mode-locked ring lasers. The experiment couples two independent pulses propagating inside the same cavity via a scattering medium and will behave exactly the same way as a two level atom driven by a step function electric field.

Various analogies exist for quantum mechanical systems using classical examples. For instance, the quantum mechanical interaction of a field with a three level system had a simple electrical circuit analogy [6]. However, most available analogies are related to a three level system. This experiment investigates the analogy between

5

a two-level system and a mode-locked laser with two circulating intracavity pulses. The large variety of pulsed interrogation techniques of two level systems [9], first discovered in nuclear magnetic resonance [10], and later applied to optical transitions, may innovate new detection methods in ring and linear lasers.

A general description of the analogy between a two level system and a bidirectional ring laser is presented in Section 2.2. Because the laser is mode-locked, with two pulses circulating in the cavity, this characteristic provides flexibility to impose various types of coupling between the two pulses, as discussed in Section 2.3. The standard two-level system has a well defined ground-state, an initial condition for most interactions. Section 2.4 shows the density matrix equations of a two-level system applied to the ring laser, as well as the Bloch vector diagram of Hellwarth-Vernon-Feynman [11].

2.2   Ring laser and the Two-Level System

The atomic or molecular system considered in this analogy has two quantum states with opposite parity and can be coupled by a dipole transition. The two levels are distinguished by their energy. In the ring laser under consideration, the states $|1\rangle$ and $|2\rangle$ are two rotation senses of a ring laser. The probability of each direction (clockwise and counterclockwise) is monitored through the pulse energy in the corresponding direction. The two levels of the quantum-mechanical system are coupled by an electromagnetic wave of frequency ω nearly equal to the transition frequency ω_0. Either situation uses the slowly varying approximation. For the quantum-mechanical two-level system, the transition rates and detuning $\Delta\omega = \omega_0 - \omega$ are negligible compared to ω and ω_0. Similarly in the ring laser example, the transition rate between $|1\rangle$ and $|2\rangle$, as well as the difference in cavity resonances for the two rotation senses,

6

Chapter 2. Theory of the Two level System Analogy

are negligible compared to the carrier frequencies.

A sketch of a laser with two pulses circulating in the cavity is presented in Fig. 2.1 (a), and its two-level analogue in Fig. 2.1 (b). A ring laser is taken as an example, but the analogy also applies to a linear cavity cavity with two circulating pulses. In the Schrödinger description of a dipole transition $|1\rangle \rightarrow |2\rangle$ interacting near resonance with an electric field $E = \frac{1}{2}(\tilde{\mathcal{E}}\exp(i\omega t) + c.c.)$, the wave function ψ is written as a linear combination of the basis: $\psi(t) = a_1(t)|1\rangle + a_2(t)|2\rangle$. Slowly varying coefficients c_i, defined by $a_i = c_i \exp(\pm i\omega_0 t)$ are substituted to the a_i in the Schrödinger equation, resulting in the set of differential equations (see, for instance, Ref [12]),

$$\frac{d}{dt}\begin{pmatrix} c_1 \\ c_2 \end{pmatrix} = \begin{pmatrix} i\frac{\Delta\omega}{2} & i\frac{1}{2}\kappa\tilde{\mathcal{E}} \\ -i\frac{1}{2}\kappa\tilde{\mathcal{E}}^* & -i\frac{\Delta\omega}{2} \end{pmatrix}\begin{pmatrix} c_1 \\ c_2 \end{pmatrix},$$ (2.1)

where $\kappa|\tilde{\mathcal{E}}| = p|\tilde{\mathcal{E}}|/\hbar$ (p being the dipole moment of the transition) is the Rabi frequency. In the ring laser analogy, the coefficients $c_i(t)$ correspond to the complex field amplitudes $\tilde{\mathcal{E}}_i$ (the tilde indicating a complex quantity) of each pulse circulating in the ring cavity (round-trip time τ_{RT}), as sketched in Fig. 2.1. The state of the system is also defined by $\psi(t) = \tilde{\mathcal{E}}_i(t)|1\rangle + \tilde{\mathcal{E}}_2|2\rangle$. The evolution equation of these fields is

$$\frac{d}{dt}\begin{pmatrix} \tilde{\mathcal{E}}_1 \\ \tilde{\mathcal{E}}_2 \end{pmatrix} = \frac{1}{\tau_{RT}}\begin{pmatrix} \tilde{r}_{11} & \tilde{r}_{12} \\ \tilde{r}_{21} & \tilde{r}_{22} \end{pmatrix}\begin{pmatrix} \tilde{\mathcal{E}}_1 \\ \tilde{\mathcal{E}}_2 \end{pmatrix} = \frac{1}{\tau_{RT}}||R|| \cdot ||E||.$$ (2.2)

In order to have an equivalence between Eqs. (2.1) and (2.2), the matrix $||R||$ should be *Anti-Hermitian*, which imposes that $\tilde{r}_{21} = -\tilde{r}_{12}^* = -\tilde{r}^*$ and that $\tilde{r}_{ii}$ be purely imaginary. It can also easily be verified that this is the only form of interaction

7

matrix for which energy is conserved $d/dt[|\tilde{\mathcal{E}}_1|^2 + |\tilde{\mathcal{E}}_2|^2] = 0$. The general case where $||R||$ is neither Hermitian nor Anti-Hermitian is discussed in Section 2.3.

The real parts of the diagonal elements of the matrix $||R||$ represent gain and loss in the cavity. In steady state, the gain and loss are in equilibrium, and the real parts of $\tilde{r}_{kk}$ are zero. A gain (or absorber) with a recovery (relaxation) time longer than $\tau_{RT}/2$ will cause transients in population. In the cavity sketched in Fig. 2.1 (a), an electro-optic phase modulator imposed an opposite phase shift ($\Delta\phi/\tau_{RT}$ and $-\Delta\phi/\tau_{RT}$) in either direction, thereby modifying the resonance of the cavity for the pulse $\tilde{\mathcal{E}}_1$ by $\Delta\omega/2 = \Delta\phi/(2\tau_{RT})$, and for pulse $\tilde{\mathcal{E}}_2$ by $-\Delta\omega/2 = -\Delta\phi/(2\tau_{RT})$. These detuning terms contribute to the diagonal terms of the matrix $||R||$: $\tilde{r}_{11} = -\tilde{r}_{22} = i\Delta\phi/2$

2.3 Conservative Versus Dissipative Coupling

2.3.1 The Symmetric Coupling Case

The mutual coupling terms $\tilde{r}_{ij}$ have taken numerous forms in the ring laser literature [13, 14], which mainly addresses CW lasers. While Symmetric Coupling is considered, it is not conservative and does not lead to an equivalence with the two-level equations. The traditional approach has been to represent the scattering coupling distributed in the whole cavity by an equivalent complex "scattering coefficient" $\tilde{r}_{12} = \tilde{r}_{21} = \tilde{\xi} = \xi \exp(i\theta)$. This coefficient couples symmetrically, at each round-trip, a fraction ξ of one beam into the other, with an average phase factor θ [15, 16, 13]. Writing for the fields $\tilde{\mathcal{E}}_1 = \mathcal{E} \exp(i\varphi_1)$ and $\tilde{\mathcal{E}}_1 = \mathcal{E} \exp(i\varphi_1)$; substituting in Eqs. 2.2 and separating the real and imaginary parts leads to the standard equations for the laser gyro. In particular, the real part leads to an expression for the total intensity change, which
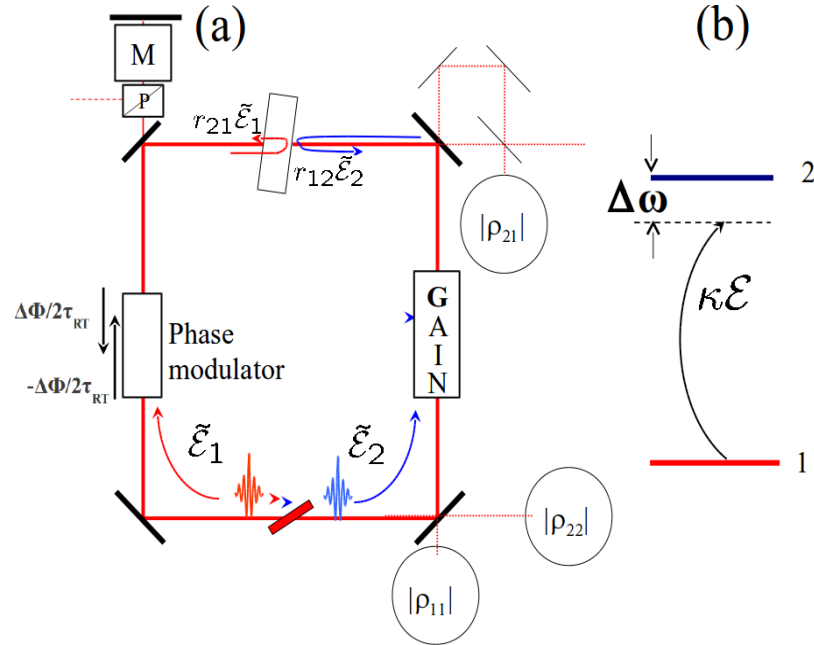
Figure 2.1: Sketch of the analogy between a ring laser and a two level system. (a) The bidirectional mode-locked ring laser, where two circulating pulses meet in a saturable absorber jet. An interface, positioned at or near the opposite crossing point of the two pulses, controls the amplitude of the coupling parameter $\tilde{r}_{ij}$. The laser with two pulses circulating in its cavity is the analogue of the two-level system; the circulating intensities in the laser, measured for each direction by quadratic detectors, are the diagonal elements (populations) of the density matrix of the equivalent two-level system. The absence of the phase modulation corresponds to the two levels being on resonance, driven at the Rabi frequency $\kappa\mathcal{E}$ by a resonant field (the Rabi frequency $\kappa\mathcal{E}$ correspond to the frequency r_{12}/τ_{RT} in the ring analogy). The backscattering at the interface thus provides a coherent coupling (Rabi cycling) between the two states, while other non coherent decays tend to equalize the population in the two directions, and washed out the phase information. The detuning $\Delta\omega$ in (b) corresponds to the phase difference per round-trip $\Delta\phi/\tau_{RT}$ in (a), imposed by an electro-optic phase modulator driven exactly at the cavity round trip time. A beat note detector measuring the interference between the two fields, records the off-diagonal matrix element. A combination of a Pockel's cell M and polarizer P controls a feedback of the clockwise pulse into the counterclockwise one.

is proportional to:

$$\frac{1}{2}\frac{d}{dt}(\tilde{\mathcal{E}}_1\tilde{\mathcal{E}}_1^* + \tilde{\mathcal{E}}_2\tilde{\mathcal{E}}_2^*) = \frac{1}{2}(\tilde{\mathcal{E}}_1\frac{d\tilde{\mathcal{E}}_1^*}{dt} + \tilde{\mathcal{E}}_2\frac{d\tilde{\mathcal{E}}_2^*}{dt} + c.c.) =$$
$$\frac{2\xi\cos\theta}{\tau_{RT}}Re(\tilde{d})Re(\tilde{\mathcal{E}}_1\tilde{\mathcal{E}}_2^*). \tag{2.3}$$

The derivative of the phase difference $\psi = \varphi_2 - \varphi_1$ is calculated by extracting the imaginary part of the expression for the derivative of the electric fields,

$$\frac{\partial\psi}{\partial t/\tau_{RT}} = \Delta\omega - \left\{\xi\left[\frac{\mathcal{E}_1}{\mathcal{E}_2}\sin(\psi-\theta) + \frac{\mathcal{E}_2}{\mathcal{E}_1}\sin(\psi+\theta)\right]\right\}. \tag{2.4}$$

It is only for $\theta = \pi/2$ that this coupling is conservative, per the equation for conservation of energy (2.3). This particular condition, combined with $\tilde{\mathcal{E}}_1\tilde{\mathcal{E}}_2$, is the one for which the coupling $\xi\exp(i\theta)$ does not introduce any dead band [17], as seen in the expression (2.4) for the derivative of the differential phase [18].

Unlike CW laser, the amplitude and phase coupling coefficients $\tilde{r}_{12}$ and $\tilde{r}_{21}$ can be easily controlled in the case of bidirectional mode-locked ring laser. The coupling, with $\tilde{\xi}$ purely imaginary, can be created by a thin dielectric layer normal to the beam, in the limit of vanishing thickness. Such a layer can be described by a polarization $\tilde{P} = N\alpha_p\delta(z)\tilde{E}$, where α_p is the polarizability of the layer of dipoles of density N. Inserting this polarization into Maxwell's wave equation, and integrating across the dielectric layer while taking into account the continuity of the tangential field, leads to the following expressions for the complex reflection coefficient $\tilde{r}_d$ and transmission coefficient $\tilde{t}_d$.

$$\tilde{r}_d = \frac{-i\beta}{1+i\beta}, \tag{2.5}$$

$$\tilde{t}_d = \frac{1}{1+i\beta}, \tag{2.6}$$

where $\beta = (2\pi)^2 N\alpha_p/\lambda$, λ being the wavelength of the light. It can be easily verified that the coupling of the two fields $\tilde{\mathcal{E}}_1$ and $\tilde{\mathcal{E}}_2$ by such layer conserves the total energy $|\tilde{\mathcal{E}}_1|^2 + |\tilde{\mathcal{E}}_2|^2$, consistent with $|r_d|^2 + |t_d|^2 = 1$ and $\tilde{r}_d\tilde{t}_d^* + \tilde{r}_d^*\tilde{t}_d = 0$, as long as β is real.

2.3.2 The Nonsymetric Coupling Case

Mode-locked lasers are particularly interesting, because the localized radiation in the cavity enables a selection of a truly conservative coupling. Instead of a small coupling structure compared to the wavelength as considered above, this section will discuss an interface (that could include a coating) between two media.

The coupling, localized at the crossing point of the two circulating pulses, can be produced by the reflection at a dielectric interface between two media 1 and 2, for which $\tilde{r}_{12} = \tilde{r}$ and $\tilde{r}_{21} = -\tilde{r}^*$, which unsurprisingly corresponds to an Anti-Hermitian matrix. The total intensity change introduced by this coupling is zero, as expected for a conservative coupling. Further, the phase relation between the two reflections at either sides of the interface is a consequence of energy conservation.

Following the approach of Spreeuw *et al* [19], the matrix $||R||$ can be written in Eq. (2.2) as a sum of a conservative (here, Anti-Hermitian) matrix $||A||$ and a dissipative matrix $||H||$:

$$||R|| = ||A|| + ||H|| =$$

$$\begin{pmatrix} i\frac{\Delta\phi}{2} & \tilde{r}_{12} \\ -\tilde{r}_{12}^* & -i\frac{\Delta\phi}{2} \end{pmatrix} + \begin{pmatrix} \alpha_1 & -\tilde{g} \\ -\tilde{g}^* & \alpha_2 \end{pmatrix} \tag{2.7}$$

In Fig. 2.1 (a), the phase shift $\pm\Delta\phi/2$ imposed on either pulse 1 and 2 by the electro-optic phase modulator, divided by the round-trip time τ_{RT}. corresponds to the detuning of the analogue two-level system. The differential frequency $\Delta\omega$ can

also be caused by rotation, Fresnel drag, Faraday effect *etc...* In the "dissipative matrix" $||H||$, α_1 and α_2 are the net gain (loss) coefficients for the two beams. The mutual saturation term of the gain contributes also to the real part of $\tilde{g}$.

2.4   Density matrix equations

Eq. 2.2 can be r-ewritten in terms of the intensities in either rotation sense $\rho_{22} = \tilde{\mathcal{E}}_2 \tilde{\mathcal{E}}_2^*$ and $\rho_{11} = \tilde{\mathcal{E}}_1 \tilde{\mathcal{E}}_1^*$, and the quantities $\rho_{12} = \tilde{\mathcal{E}}_1 \tilde{\mathcal{E}}_2^*$ and $\rho_{21} = \tilde{\mathcal{E}}_2 \tilde{\mathcal{E}}_1^*$:

$$\frac{d(\rho_{22} - \rho_{11})}{dt/\tau_{RT}} = -4\mathrm{Re}(\tilde{r}_{12}\rho_{21}) \qquad (2.8)$$
$$+2\alpha_2\rho_{22} - 2\alpha_1\rho_{11}$$

$$\frac{d\rho_{21}}{dt/\tau_{RT}} = -i\Delta\omega\tau_{RT}\rho_{21} + \tilde{r}_{12}^* (\rho_{22} - \rho_{11})$$
$$+(\alpha_1 + \alpha_2)\rho_{21} - \tilde{g}^*(\rho_{22} + \rho_{11}) \qquad (2.9)$$

$$\frac{d(\rho_{22} + \rho_{11})}{dt/\tau_{RT}} = 2\alpha_2\rho_{22} + 2\alpha_1\rho_{11} - 4\mathrm{Re}(\tilde{g}\rho_{21}). \qquad (2.10)$$

For the pure conservative case, $||H|| = 0$, this system of equations reduces to Eqs. (2.8,2.9) [with $d/dt(\rho_{11} + \rho_{22}) = 0$], in which one recognizes Bloch's equation for a two level system driven off-resonance by a step function Rabi frequency of amplitude $\tilde{r}/\tau_{RT}$ [11]. The difference in intensities $(\rho_{22} - \rho_{11})$ is the direct analogue of the population difference between the two levels. The off-diagonal matrix element ρ_{21} is the interference signal obtained by beating the two outputs of the laser on a detector. As in the case of the two-level system, the phenomenological relaxation rates γ can be introduced for the energy relaxation (diagonal matrix element) and γ_t for the coherence relaxation (off-diagonal matrix elements). The physical meaning of the transverse relaxation time $1/\gamma_t$ is the mutual coherence time of the two pulse trains. For a constant "detuning" $\Delta\omega$, γ_t is related to the beat note bandwidth. Combination of the non conservative coupling g and the loss α results in energy

and coherent relaxation rates γ and γ_t. A general conservative case may involve the dissipative matrix, with the condition that $\rho_{22} + \rho_{11}$ is a constant.

The detuning term in Eq 2.9 may include a contribution from the Kerr effect $\Delta\omega_{Kerr}$ = $\Delta\omega_{SPM}+\Delta\omega_{XPM}$. The Kerr-induced self-phase modulation $\Delta\omega_{SPM}$ takes place in all components where the pulses do not cross such as the gain medium, and the phase modulator in Fig. 2.1,

$$\Delta\omega_{SPM} = \frac{1}{\tau_{RT}}(\frac{2\pi n_{2s}l_s}{\lambda})(\rho_{22} - \rho_{11}), \tag{2.11}$$

where n_{2s} and l_s are the nonlinear index and length of the nonlinear medium involved in self-phase modulation. The Kerr-induced cross-phase modulation ω_{XPM} takes place in all components where the pulses do cross, such as the saturable absorber in the example of Fig 2.1.

$$\Delta\omega_{XPM} = \frac{1}{\tau_{RT}}(\frac{4\pi n_{2x}l_x}{\lambda})\sqrt{\rho_{11}\rho_{22}}, \tag{2.12}$$

where n_{2x} and l_x are the nonlinear index and length of the nonlinear medium involved in cross-phase modulation. The Kerr effect thus introduces two nonlinear terms of the form $C_s(\rho_{22} - \rho_{11})$ and $C_x\sqrt{\rho_{11}\rho_{22}}$ in Equ. 2.10. In the experimental setup presented here, these terms are smaller by a factor of 10^5 than other contribution and will be neglected. However, situations exist when these terms are important and can lead to a determination of Kerr coefficients [20].

The mirror vibrations contribute to the beatnote bandwidth (i.e. each pulse sees random differences in the cavity length of the order of the mirror motion over a time of $\tau_{RT}/2$). This broadening mechanism is equivalent to inhomogeneous broadening. The gain (loss) terms α_i can be seen as contributions to the population from other levels. In an inversion driven laser, $\alpha_1 \approx \alpha_2 = \alpha$ is an intensity dependent relaxation that exists only in transients, since $\alpha = 0$ (gain = loss) when the laser is at equilibrium. This situation occurs also in a two-level system when both levels (1) and (2) are strongly coupled to a third level (laser medium pumped to zero inversion).

2.5 Summary

The theoretical framework for the two-level analogy was described in this chapter. The intensity dynamics equation of two pulses in a cavity, coupled through a scattering medium can be rewritten in a density matrix form. The equations are exactly the same as the Bloch equation of a two-level system coupled with a step-function electric field. Experimentally, the model validity can be tested by monitoring the intensity evolution of the two pulses in a millisecond time scale. The off-diagonal elements also can be monitored since the term $\rho_{12} = \tilde{\mathcal{E}}_1 \tilde{\mathcal{E}}_2^*$ is the same as the interference of the two pulses and the term determining the beatnote for the IPI experiments.

Chapter 3

Experimental Implementation of the Two-Level Analogy

3.1 Introduction

Several lasers can be used to test the theory presented in Chapter 2. The laser systems differ by the gain and loss media parameters and can display different transient dynamics. A mode-locked ring Ti:Sapphire was used to demonstrate the experiments. The electronics were one of the primary challenges to establish the initial condition. For a two-level system, the initial condition has the following set-up: the lower level is fully populated and the upper level empty. The laser's energy travels in one direction and the laser is operating uni-directional. Ways to establish a preferential rotation state in the ring laser are proposed in Section 3.2. The electronics used to establish the initial condition are described in 3.3. Finally, the experimental demonstration of the two-level analogy is presented.

3.2 Initial Condition

In order to observe Rabi cycling, the system should be initially in a "ground state," where the intensity of one of the pulses dominate. Several methods are possible to achieve this goal:

1. Inserting a non-directional coupling in the cavity

2. Using a directional gain that can be controlled externally

3. Coupling from one direction to the other outside of the cavity; by feeding the pulse back into the one direction, in time and space, the other direction is extinguished

3.2.1 Non Directional Coupling

Non-directional coupling was not used for the experiment, but is included to discuss all the possible set-ups for the initial condition. Non-directional coupling can be achieved with a combination of thin (compared to the wavelength) dielectric or gain (absorbing) layers [21]. Equation 2.5 gives an expression for the reflection coefficient of a dielectric thin layer. In the case of a gain layer, as in an optically pumped quantum well, $\beta - ib$, where b is a real number, and the expressing for the complex reflection coefficient of the gain layer is

$$\tilde{\xi}_g = \frac{b}{1 - b} \tag{3.1}$$

A combination of a gain (L) and dielectric layer (R), an eighth of wavelength apart (total propagation $\exp(-ikz) = \exp(-i\pi/2) = -i$), will have a different reflection

coefficient when irradiated from the left ($\tilde{R}_L$) or from the right ($\tilde{R}_R$:

$$\tilde{R}_L \approx i(\frac{r_d}{i} - \xi_g) \approx 0$$
$$\tilde{R}_R \approx \xi_g + \frac{r_d}{i}. \tag{3.2}$$

Since the gain layer is providing energy to the light field, the coupling is not conservative. This type of non-reciprocal coupling provides the ideal initial condition, if the coupling can be applied as a step function. A structure with a single gain layer cannot have sufficient gain for laser operation. Instead a MQW structure with 19 gain layers and 4 dielectric layers was designed and tested in ring lasers [22, 21]. Both unidirectional and quasi-unidirectional (depending on the pump power) operations were demonstrated. Because of the large number of layers, this structure has a too narrow bandwidth (1 nm) to be used with ultrashort pulses

3.2.2 Directional Gain and Faraday Rotation

In a synchronously pumped OPO, the gain travels with the pump pulse. By inserting the ring laser's OPO crystal in a linear pump cavity, two counter-circulating pulses are created (one at each passage of the pump) [23]. The relative intensity of the pump pulse determines the relative intensity of the circulating signal pulses. The OPO is an interesting system in relation to this analogy, because there is no coupling between the circulating pulses introduced by the gain. The linear cavity presented in Chapter 5 can also be used for such an experiment.

Another approach to unidirectionality is directional losses such as can be introduced by a Faraday rotator. The Faraday rotation can be seen as the analogue of fluorescence decay, which transfers energy from the upper level to the lower level while conserving the total population. In the laser, the saturation properties of the gain

medium cause an approximate conservation of the population.

3.2.3   External Feedback

External feedback is the approach used in this experiment. In order to define the initial condition, the output pulse from one direction is extracted, and feedback (<1%) with a mirror, after appropriate optical delay, is reflected into the opposite direction. By using a fast switch (turn-off time of less than the cavity round-trip time of 10 ns) at the Pockels cell, the coupling is turned off to let the fields in the cavity evolve.

3.3   Electronics

3.3.1   Avalanche Transistor Circuit

One of the experiment's challenges was to apply the quarter wave voltage on the Pockels cell in less than a round trip. For Q-Switching or amplifiers, a transistor bank is standardly used to achieve the fast switching time required. The avalanche break down mechanism is used to get fall or rise times less then 10 ns. The avalanche breakdown is achieved by carefully choosing the amount of transistors in a series. The total voltage applied, divided by the amount of transistors is just above the break down voltage of each transistor individually. Then, a switching signal is applied to one of the transistors. The voltage on each transistor exceeds the break down voltage and the avalanche effect occurs. Typical voltages needed for a quarter wave voltage are between 1.5 and 3 kV depending on the material and size of the crystal. In figure 3.1 the circuit schematic is shown.
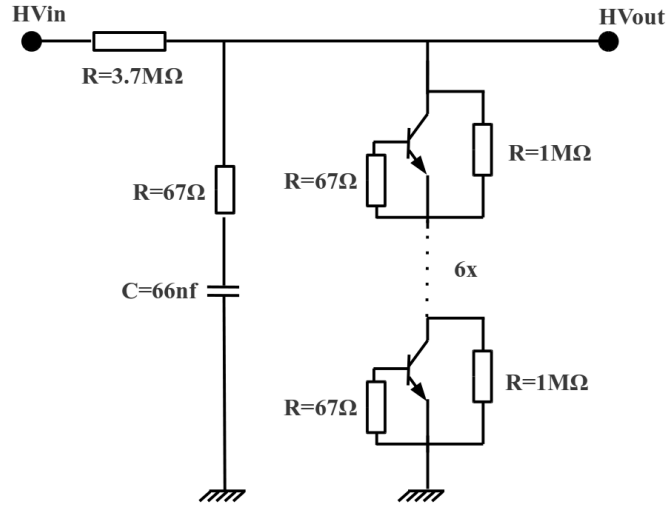
Figure 3.1: The schematic of the avalanche transistor circuit

A typical switching signal is displayed in Figure 3.2 and 3.2. However, the problem begins from the very slow rise time after the switching occurred. The capacitors slowly recharge and the desired voltage level (in this case 0V) is only achieved for a short amount of time (less then a few microseconds). Experimenting with several different capacitor values did not extend the recharging time significantly to the needed time constant (several milliseconds). Since the intensity oscillation was expected to be in milliseconds, another approach needed to be pursued.

3.3.2   Mercury switch

Another suitable switch for the experiment is a mercury switch. The basic principle is applying a small switching voltage and moving a mercury bubble to connect two wires. Mercury is an almost perfect conductor with negligible resistance. The mercury switch's advantage, compared to the avalanche transistor circuit, is the switch can be on or off for as long as the switching voltage is applied or turned off. However,
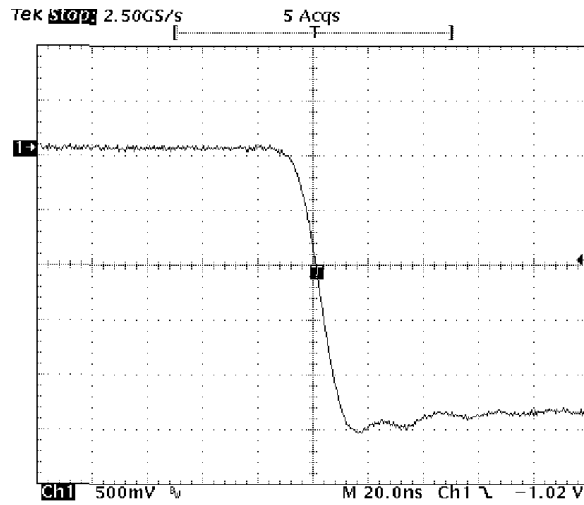
Figure 3.2: The fall time (switching time) is less then 10ns
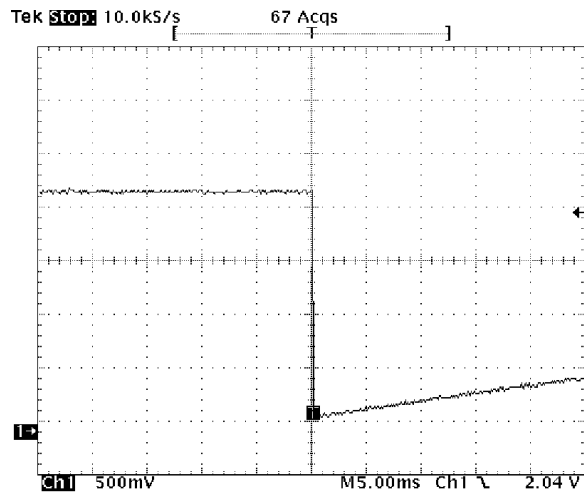
Figure 3.3: The rise time could not be hold constant for more then about 5ms.

the fast, commercial available mercury switches can only be used for a voltage level of several hundred of volts. Hence, a low voltage modulator was purchased to accommodate the voltage level where the quarter wave voltage is approximately 300V.

In figure 3.4 the layout of the circuit board and in 3.5 a typical switching behavior is shown.
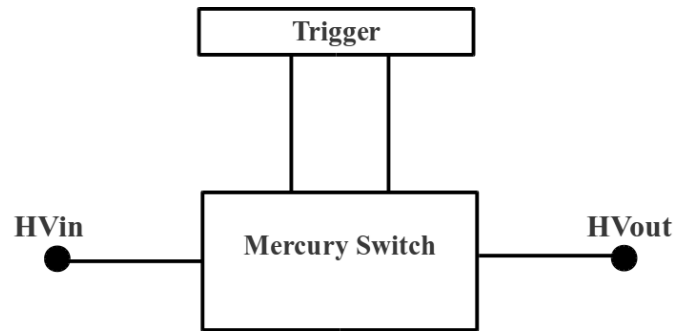
Figure 3.4: A simple schematic of the mercury switch is shown.
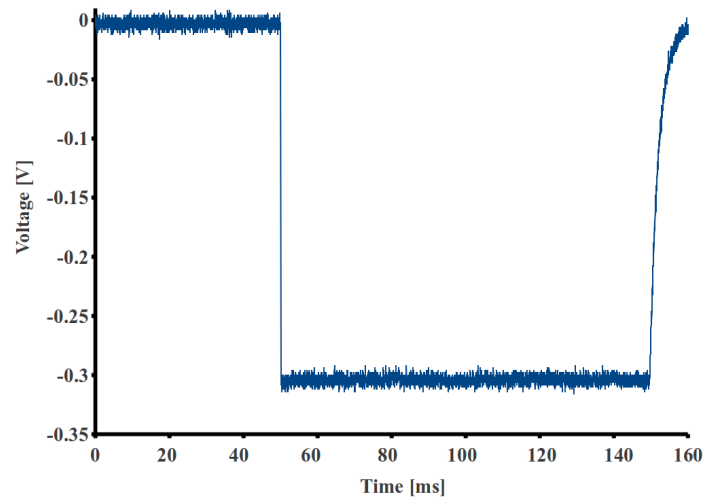
Figure 3.5: Switching behavior of the mercury switch for approximately 300V. A square pulse was applied to the switch.

A square pulse, provided by a Berkeley nucleonics corporation function generator with an amplitude of 12V, is applied with a pulse width of several milliseconds. The fall time is in the desired region of less than 10ns as shown in figure 3.6. The desired voltage level can be achieved for as long as the switch pulse is applied as needed
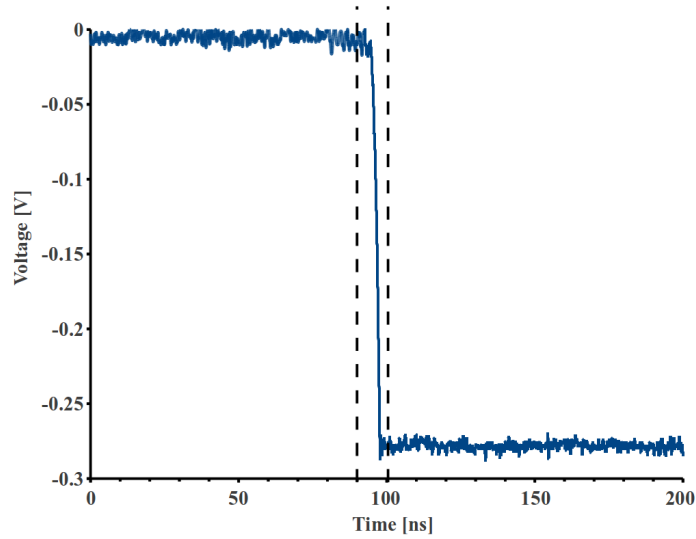
Figure 3.6: Switching behavior of the mercury switch for approximately 300V. The fall time is indicated to be less then 10ns.

for the experiment. The rise time is much longer in the order of a few milliseconds (Figure 3.6) but has no effect on the experiment since the desired voltage level of zero Volts can be maintained for a lengthy period.

3.4 Experimental Demonstration of the Two-Level Analogy

3.4.1 The Laser

The analogy can be tested with a variety of laser systems, which will differ by the gain and loss media parameters. In the synchronously pumped OPO, the gain is a few percent and the mutual saturation parameter is zero. In the ring Ti:sapphire laser chosen for this demonstration, the gain balances the losses for a coefficient α of

approximately 0.08.

The experimental system is a ring Ti:sapphire-laser (Pump power= 5W, 8% loss per round-trip in a 3.1 m cavity with four prisms [24]) mode-locked with a dye jet as a saturable absorber, resulting in 30 ps pulses at 800 nm. The following analogies can be tested:

1. Rabi cycling of the population difference

2. For the resonant case ($\Delta\omega = 0$), the Rabi frequency is proportional to the "driving force" that is the backscattering coefficient $|\tilde{r}|$,

3. The Rabi cycling for the population difference $(\rho_{22} - \rho_{11})$ and the off diagonal element ρ_{21} are 90° out of phase

4. Existence of a longitudinal and transverse relaxation time

5. For the off resonant case, the Rabi cycling is at the following frequency $\sqrt{\Delta\omega^2 + (|\tilde{r}|/\tau_{RT})^2}$.

3.4.2   Rabi Cycling on Resonance

In the measurements that follow, the system is "at resonance"; i.e. $\Delta\omega = 0$). An example of "Rabi cycling" is shown in Fig. 3.7. The counterclockwise intensity (ρ_{22}) is plotted as a function of time [Fig. 3.7]. The clockwise intensity ρ_{11} (not shown) is complementary. The system is prepared so that the ρ_{11} is initially populated (ρ_{11} = 0.8, ρ_{22} = 0.2). As the feedback that creates the initial state is switched off at $t = 1$ ms, there is a fast (approximately 10 μs) transient. This rise time reflects combined dynamics of the gain and cavity, as the laser adapts to the different (now symmetrical) cavity losses. This rise time corresponds roughly to the fluorescence lifetime of the upper state of Ti:sapphire. The "Rabi cycling of the "population difference" $\rho_{22} - \rho_{11}$ is plotted in Fig. 3.8.
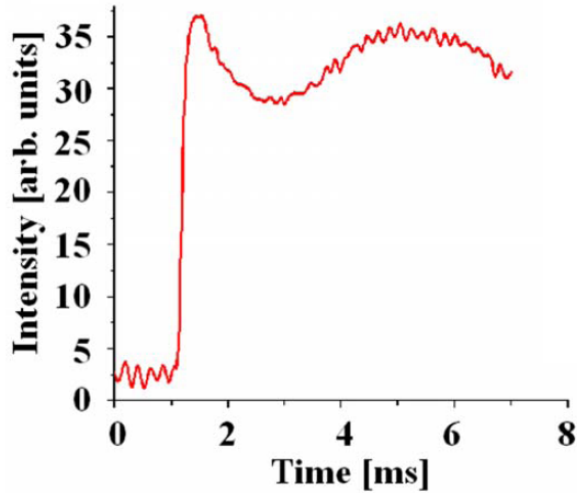
Figure 3.7: The evolution of the intensity in the counterclockwise direction is shown after switching the Pockels' cell. The intensity at clockwise direction is 180° out of phase with this graph, with population dropping from the maximum initial value. The fast initial transient reflects the gain and cavity dynamics associated with the sudden change in cavity loss at the switching time. Thereafter, a slow oscillation due to population transfer or Rabi oscillation between two directions is observed.

The beanote frequency can also be recorded (off-diagonal element $|\rho_{12}|$) as sketched in Fig. 2.1(a). From the Bloch vector model of Feynman, Hellwarth and Vernon [11], the oscillation of the diagonal elements and the off-diagonal element are 90° out of phase. This property can be seen in Fig. 3.9.

The Rabi frequency $|\tilde{r}|/\tau_{RT}$ can be varied by changing the position of the scattering surface, as shown in Fig. 3.10. The maximum value measured [24] for this interface corresponds to a backscattering coefficient of $|\tilde{r}| \approx 1 \cdot 10^{-6}$. Note that the Rabi frequency provides a direct measurement of very minute backscattering coefficients, without the need to trace a complete gyroscopic response as in Refs. [24, 25].

In the case of a two-level system, the phenomenological "longitudinal" and "transverse" relaxation times have been identified as energy relaxation time (fluorescence
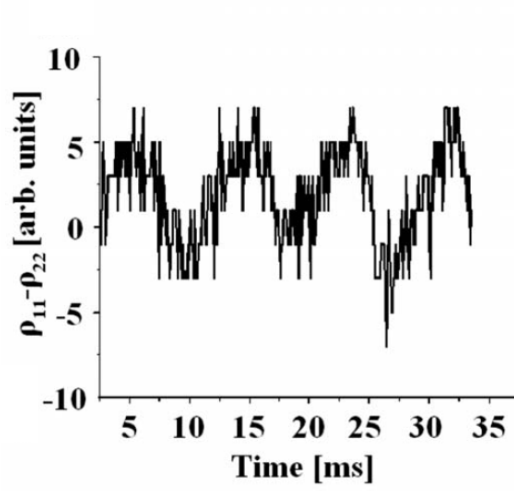
Figure 3.8: Population difference showing the Rabi cycling.
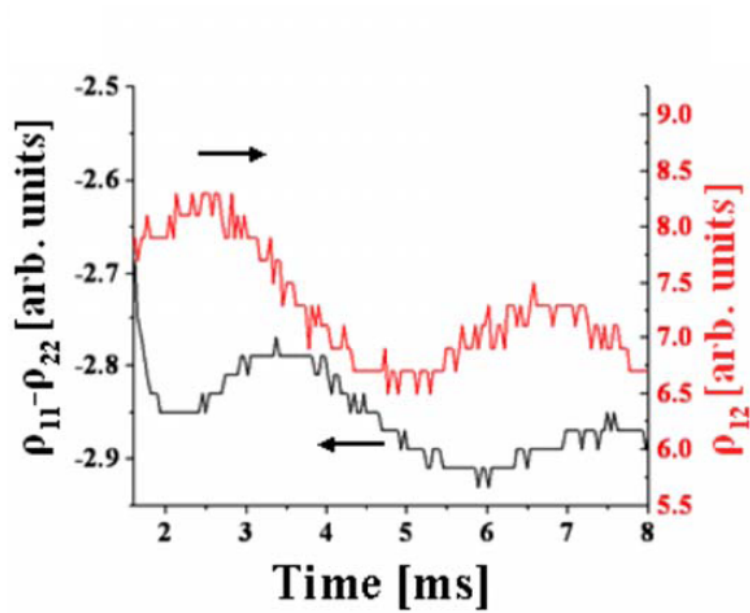
Figure 3.9: Comparison of the oscillation of the population difference $\rho_{22} - \rho_{11}$ and the off-diagonal element (beat note) ρ_{12}.
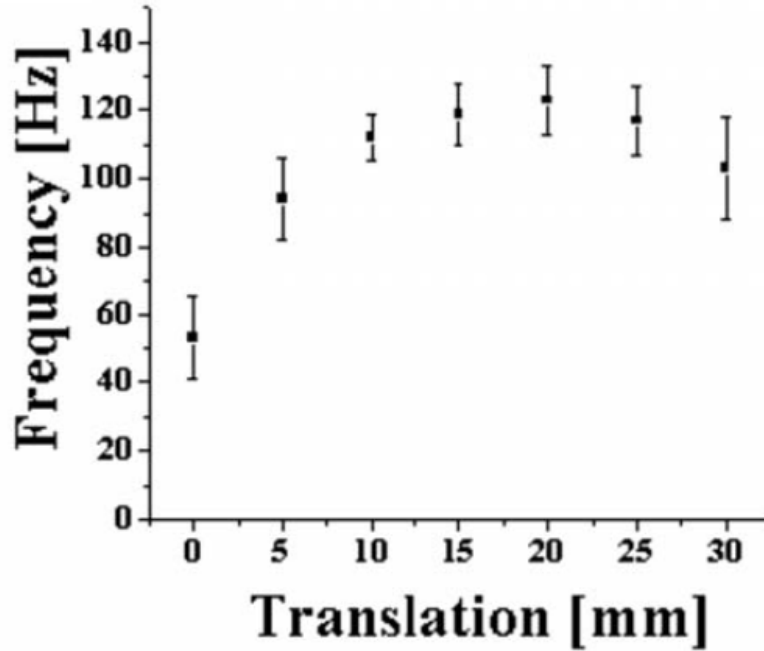
Figure 3.10: Rabi frequency as a function of position of the glass at the meeting point of the two directions. Translation of the glass-air interface along the beam result in different values of coupling $\tilde{r}$.

decay) and phase relaxation time (due for instance to atomic collisions). Figure 3.11 shows a measurement of the decay of the Rabi oscillation for the diagonal and off-diagonal elements. The decay is measured by fitting the Fourier transform of the measurement to a Lorentzian, and measuring its FWHM. The values are 27 and 30 Hz shown in Fig. 3.12. As noted previously, there are at least two origins to the off diagonal element decay: mirror vibration and coupling through absorption (gain). The latter affects equally the diagonal and off-diagonal elements. The former can be seen as a type of "inhomogeneous broadening", since the origin is in random cavity length fluctuation, expressed as randomness in the value of $\Delta\omega$. The approximately 30 Hz bandwidth of both decays is consistent with 0.3 μm amplitude
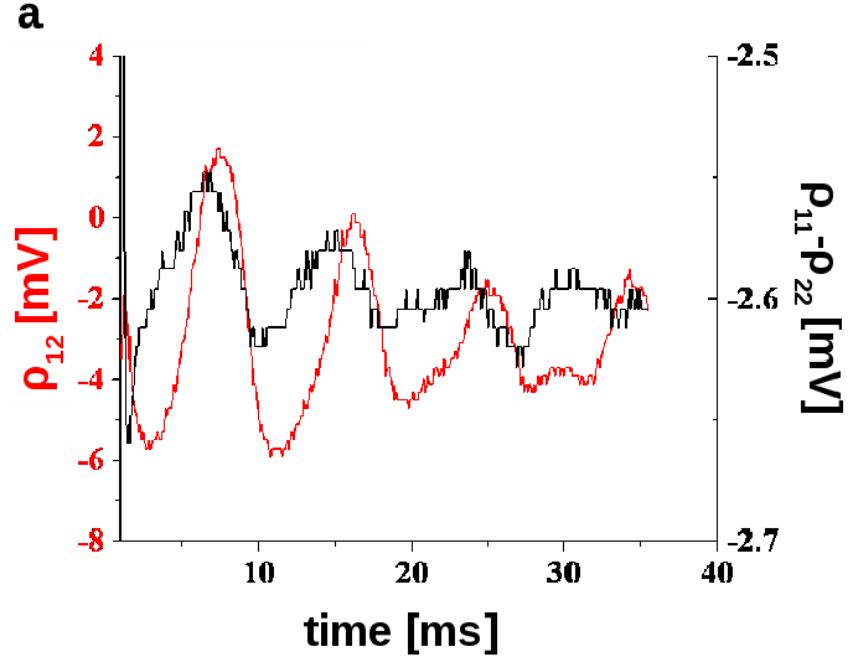
Figure 3.11: Measurement of the decay of the Rabi oscillations in W and ρ_{21}.

vibrations at 100 Hz of cavity components, causing differential cavity fluctuations of 0.3 pm/round-trip.

If the radiation of amplitude $\mathcal{E}$ (Rabi frequency $\kappa\mathcal{E}$) is off-resonance with a two-level system by an amount $\Delta\omega$, the Rabi frequency becomes $\sqrt{\kappa^2\mathcal{E}^2 + \Delta\omega^2}$. For the ring laser, the off-resonance amount $\Delta\omega$ can be controlled with a Pockel's cell (Fig. 2.1), the initial condition is set favorable to the counter-clockwise direction as shown in Fig. 3.7. The Rabi cycling is measured indeed to correspond to $\sqrt{|\tilde{r}|^2/\tau^2 + \Delta^2}$. In resonance case $\Delta\omega = 0$), measurement of ρ_{12} leads to $r/\tau_{RT} = 138$ Hz $\pm$ 15 Hz. With $\Delta\omega$ of 171 Hz $\pm$ 12 Hz, the off resonant measurement is $r/\tau_{RT} = 237$ Hz $\pm$ 21 Hz, which behaves as a two-level system off-resonance.
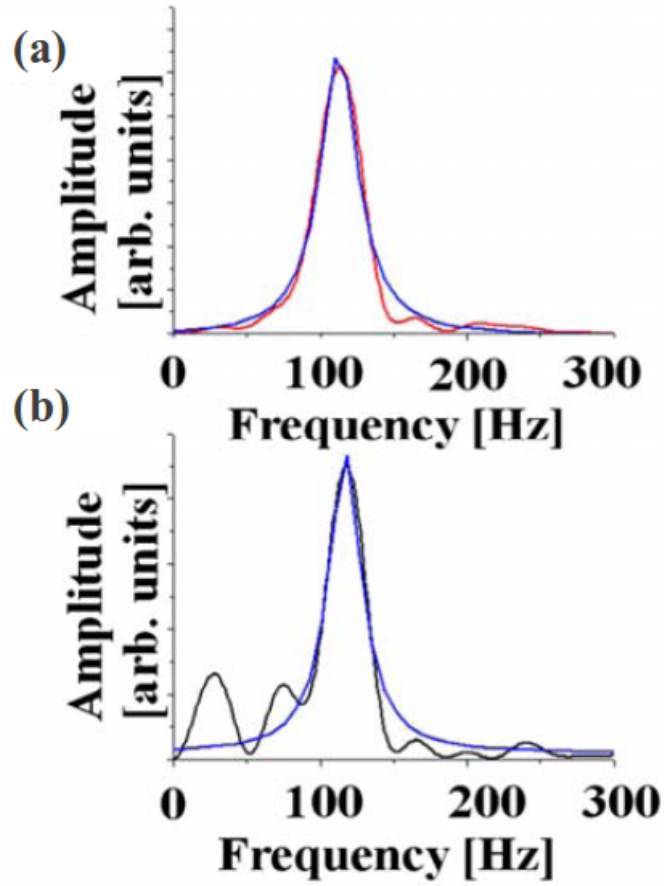
Figure 3.12: The Fourier transformations of the relative decay measurements are shown. a: off-diagonal elements, b: diagonal elements

The analogy presented here reveals previously unexplained observations on a Kerr-lens mode-locked ring laser [26]. Rather than being bidirectional, the operation was observed to switch direction at rates (tens of Hz) that did not seem to correspond to any cavity parameter. The slow switching rate might be due to similar "Rabi cycling", caused by the scattering coefficient of the gain crystal, which is where the pulses meet in the case of pure Kerr-lens mode-locking.

28

3.5   Summary

The analogy between a two–level system and a bidirectional mode-locked ring laser have been demonstrated analytically and experimentally. In the latter, the two "quantum states" $|1\rangle$ and $|2\rangle$ are the sense of circulation of the ring beams. The short pulses makes it possible to apply purely conservative coupling between the counter circulating pulses. Resonant interaction between a step-function resonant electromagnetic field and the two-level system leads to Rabi oscillation between the population of the upper and lower states. Similarly, Rabi oscillation have been observed between the population of the "upper" $(\tilde{\mathcal{E}}_2\tilde{\mathcal{E}}_2^*)$ and "lower" $(\tilde{\mathcal{E}}_1\tilde{\mathcal{E}}_1^*)$ states of the ring laser. The same density-matrix equation that describes the evolution of the two-level system apply to the ring laser, where the diagonal elements represent the intensity of the counter circulating pulses, and the off-diagonal element the interference of the two beams $\tilde{\mathcal{E}}_1\tilde{\mathcal{E}}_2^*$ that is recorded on a detector. The Rabi oscillations of the off-diagonal element are 90º out of phase with those of the population difference. The interaction can be made off-resonance. The Rabi oscillation frequency increases as expected, as the interaction is detuned from resonance. The Rabi oscillations decay with a time constant that appears to be associated with a mechanical vibrations of the laser support.

The development of new sensors is the analogy's impact. Most spectroscopic techniques involve some measurement of $|\rho_{12}|$, as a function of the driving field (measurement of the Rabi frequency $\kappa\mathcal{E}$ leading to the determination of the dipole moment) or detuning $\Delta\omega$. The dependence of the spectrum of $|\rho_{12}|$ on scattering in the ring laser is a very sensitive measurement of the backscattering coefficient $|\tilde{r}|^2 =$ (Rabi frequency)$\times\tau_{RT})^2$ (as small as $0.25 \cdot 10^{-12}$ in the lower data point of Fig. 3.10). The quantity $\Delta\omega$ in the ring laser is an intracavity conversion of a minute phase difference between the two circulating pulses, and results in a modulation observed on ρ_{12}. Any resolution enhancing technique that has been devised in spectroscopy, such as Ram-

sey fringes [10, 9], could be transposed to a laser phase sensor with two intracavity pulses. Pulsed coupling $\tilde{r}$ could be applied (for instance by using a rotating disk), to perform measurements within the beat note bandwidth.

Chapter 4

Theory of Intracavity Phase Interferometry (IPI)

4.1 Introduction

IPI is a very potent tool to measure minute phase shifts. In comparison to extra-cavity interferometry, IPI uses the unique attribute of mode-locked lasers that converts a phase shift into a frequency shift. Conventional interferometry, e.g. by Michelson Interferometer, measures a change in amplitude for phaseshift, however, the accompanyig amplitude noise is a limiting factor to taking sensitive measurements. Nevertheless, it is a very powerful tool in our modern society. For example, the Laser Interferometer Gravitational Wave Observatory (LIGO) project pushes the sensitivity to the classical limits by employing several enhancement techniques, as well as very good vibration control, and placing the interferometer in vacuum, using Fabry-Perot- cavities for enhancement and almost perfect optics. For further LIGO improvements, quantum mechanical approaches are also discussed, e.g squeezed states to finally reach the sensitivity to detect gravitational waves. How-

ever, these advanced sensitivity measurements cost multi-billions of dollars and are not very useful for a table top experiment. Using IPI, standard Michelson interferometer limits can be surpassed without using any active stabilization methods. Instead, a free running mode-locked laser cavity is used to get more precise sensitivity measurements. This chapter discusses how the Michelson Interferometer operates, gives an overview of how IPI converts a phaseshift into frequency, how the carrier to envelope offset is used in the IPI experiments, and how two pulse trains with the same repetition rate are created to convert the phaseshift into a frequency.

4.2   Michelson Interferometer

This section is a quick review of the Michelson Interferometer and its limits. The experimental setup consists of one, a light source (usually a laser), two, a beam splitter to separate the beam into two arms, and three the end mirrors to retro-reflect the beams, which are overlapped at the output port of the beam splitter and sent to a detector. By displacing one of the end mirrors in one arm, the difference in path length Δx results in a phase shift $\Delta\varphi$ of one of the beams in regard to the other by $\Delta\varphi$= k Δx, where k is the wave vector . Therefore the interference intensity is changed and detected.

For a setup with a perfect beam 50:50 beam splitter and 100% reflectivity mirrors in both arms, the phaseshift dependent intensity can be written by the following equation:

$$I = \frac{I_0}{4}(2 + 2\cos(\Delta\varphi)) \tag{4.1}$$

The Michelson interferometer has two operation regions, including working in the dark fringe region. This means, no light reaches the detector. A very sensitive
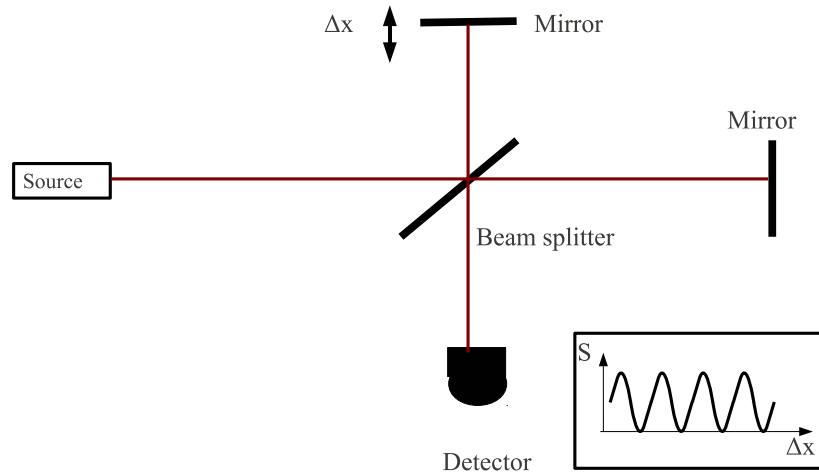
Figure 4.1: Sketch of a Michelson Interferometer setup

detector can be used to see a change from the single photon level to the saturation level. Also, in the dark fringe, by increasing the power, the sensitivity is increased significantly since almost no light is reaching the detector. The disadvantage is the non-linear response of the system in the dark fringe region.

If a linear response is required, the preferred method to extract data, the maximum slope regime is needed, where the cosine is approximatly a linear function. However, the trade-off to working in a linear response is the finite intensity reaching the detector and the possibility of saturation which limits the sensitivity of the system.

In comparision, the advantage of IPI over Michelson interferometer, is its linear response (where no dead band is present) but the saturation of the detector is not limiting since a frequency is measured instead of a change in intensity. Therefore, IPI will display a good sensitivity while still allowing for a large measurement range.

Another operation mode of the Michelson interferometer, is to slightly tilt one of the end mirrors as shown in figure 4.3. The tilting result in a vertical fringe
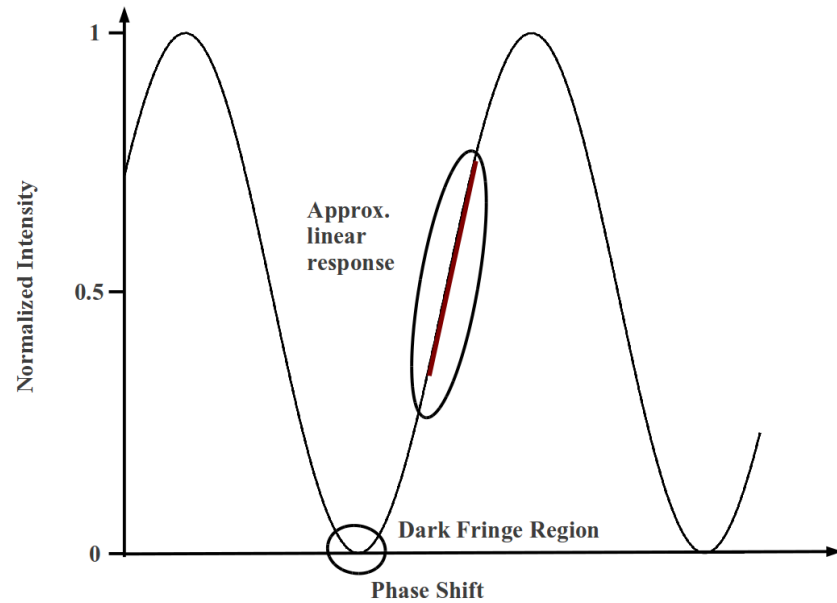
Figure 4.2: The two differet regions where a Michelson Interferometer can operated at. The red line indicates the linear response.

pattern that can be recorded with a vertical detector array. A phase shift can be introduced in either arm, resulting in a change of the vertical fringe spacing. The grating structure of the detector array combined with the optical fringes will display a Moire pattern as illustrated in figure 4.4. The moire structure displays a spatial variation with the wavelength $\lambda_m \propto 2 \; \mathrm{d}^2/\Delta\varphi$, where d is the distance between two detector arrays and $\Delta\varphi$ the introduced phase shift.
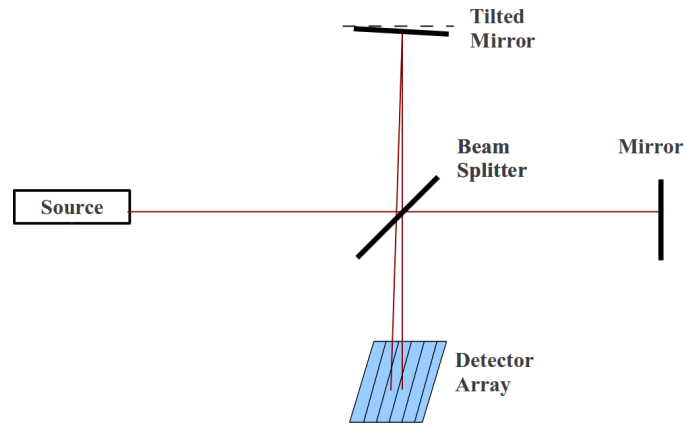
Figure 4.3: Experimental setup to record the moire pattern produced by the fringes of the light in combination with a detector array.
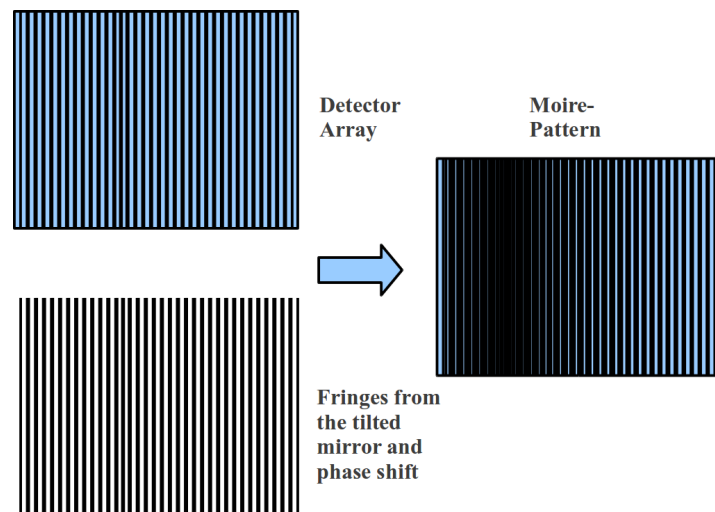
Figure 4.4: Combining the fringe pattern due to a slight misalignment of one mirror in combination with the phaseshift to be measured and the detector array pattern result in a Moire pattern.

4.3 Mode-locked lasers and Carrier-to-Envelope Offset

The IPI mode-locked laser uses the phaseshift of the carrier wave underneath the pulse envelope to convert the phaseshift into a frequency. Measuring the frequency

with IPI instead of the amplitude measurement of the standard interferometer elimiates amplitude noise and increases dynamic range without sacrificing sensitivity. This section discusses how mode-locked lasers convert a phasashift into a frequency through the carrier envelope offset.

Mode-locked lasers produce a continuous train of equivalent pulses separated by the roundtrip time of the cavity τ_{RT}. These pulses are defined by their envelope $\mathcal{E}(t)$, of width τ_p, center frequency ω_0 and carrier to envelope phase φ_m. Two consecutive pulses have the same envelope, but may have a different phase. This can be expressed with $\varphi_m = \varphi_0 + m\Delta\varphi_m$ where φ_0 is the constant carrier to envelope phase (CEP) for reference pulse with m=0. To better illustrate it, the situation is sketched in fig 4.5.
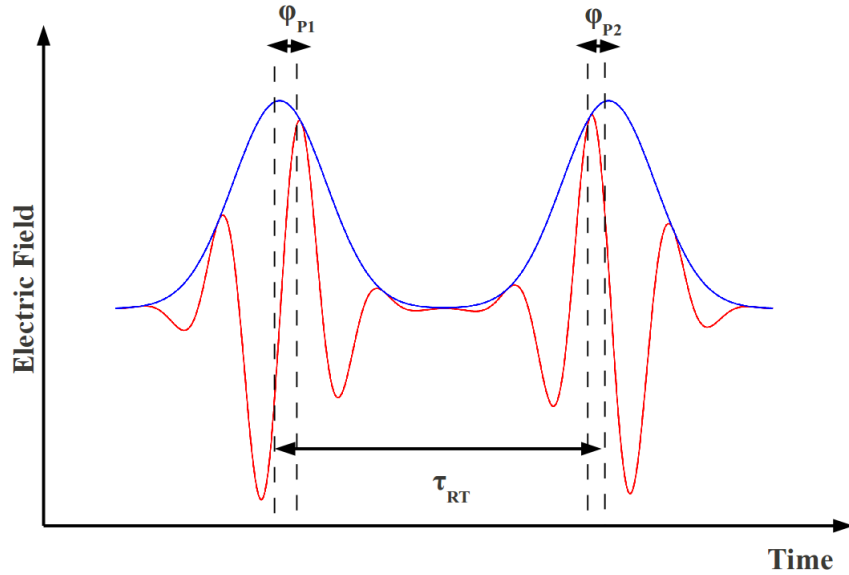
Figure 4.5: Two conscutive pulses with the envelope and the carrier field.

In the time domain a pulse train can be described in following manner [27]:

$$E_{train} = \mathcal{E}(t - \tau_{RT})e^{-i(\omega_0(t - \tau_{RT}) + \varphi_1)} + \mathcal{E}(t - 2\tau_{RT})e^{-i(\omega_0(t - 2\tau_{RT}) + \varphi_2)}$$

$$+\mathcal{E}(t - 3\tau_{RT})e^{-i(\omega_0(t - 3\tau_{RT}) + \varphi_3)}.... + c.c \qquad (4.2)$$

$$= e^{-i\omega_0 t - i\varphi_0} \sum_m \mathcal{E}(t - m\tau_{RT})e^{-i\omega_0 m\tau_{RT} - i\varphi_m)} + c.c.$$

This is an infinite sum of individual pulses, starting from -∞ to ∞. The phase shift from pulse to pulse is due to the difference in group and phase velocity. This difference adds a phase shift $\Delta\varphi$ to every consecutive pulse. There are also a large number of optical cycles between two consecutive pulses, $\omega_0\tau_{RT}$ can be written as $\omega_0\tau_{RT} = 2N\pi + \Delta\varphi$ and set $e^{2N\pi i} = 1$. The phase of the mth pulse is thus $m\Delta\varphi$. Combining it with the mathematical fact that any periodic function can be expressed as a convolution between a sum of delta functions and a non periodic function, Eq. 4.2 can be rewritten as a convolution between a pulse envelope and comb of delta function:

$$E_{train} = (\mathcal{E}(t)e^{-i\omega_0 t - i\varphi_0}) \star \sum_m e^{-im\Delta\varphi}\delta(t - m\tau_{RT}) \qquad (4.3)$$

Even though the equation is mathematically correct, it is hard to make a physical connection between the train of δ-functions and the phase factor $e^{im\varphi}$. The Fourier transformation of Eq. 4.3, according to the convolution theorem, is the product of each individual Fourier transformation:

$$E(\Omega) = F(\mathcal{E}(t)e^{-i\omega_o t})F(\sum_m e^{-im\Delta\varphi}\delta(t - m\tau_{RT})) =$$

$$= \mathcal{E}(\Omega - \omega_0)\frac{1}{\tau_{RT}}\sum_n \delta(\Omega - \frac{2\pi n}{\tau_{RT}} - \frac{\Delta\varphi}{\tau_{RT}}) \qquad (4.4)$$

In the frequency picture, an infinite train of pulses will lead to series of δ function that are equally spaced by $\frac{1}{\tau_{RT}}$. The pulse shape described by $\mathcal{E}(t)$ will define the

shape of the comb and is centered around the frequency ω_0. The constant phase shift from pulse to pulse leads to a shift of the comb itself. This can be seen by writing the frequency of the mth comb:

$$\Omega_n = \frac{2\pi n}{\tau_{RT}} + \frac{\Delta\varphi}{\tau_{RT}} \tag{4.5}$$

If no phase shift is present, $\Delta\varphi=0$, the 0th comb tooth coincides with the origin. However, if the phase shift is present the first tooth of the comb has a finite value different then 0. This is called the Carrier-to-Envelope offset (CEO) frequency, f_{CEO}. The CEP of one pulse does not have to be zero but rather can have any value. The CEO only describes the phase shift from one pulse to the next one.

$$\nu_q = f_q + f_{CEO} \tag{4.6}$$

where $\nu = \omega/2\pi$ is the optical frequency.
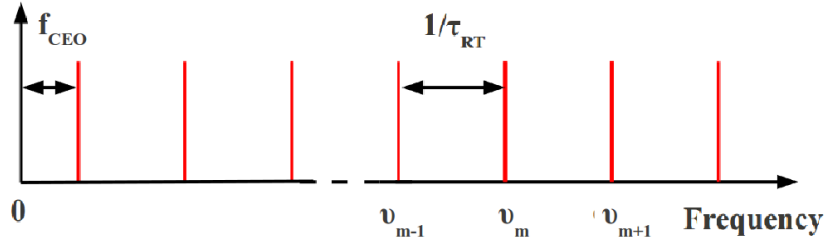
Figure 4.6: Frequency picture of an infinite pulse train with a pulse to pulse phase shift resulting in the carrier-to-envelope offset CEO.

Defining a CEP phase has some ambiguity since phase is always defined with a reference. For ultra-short pulses, a zero CEP pulse is required for some applications. The zero CEP is where the carrier wave oscillation is maximum and is aligned with the envelope peak. The perfect frequency comb, meaning $f_{CEO}=0$, does not

necessarily have a zero CEP. Only the change in CEP from pulse to pulse is the important factor to consider for stabilization schemes. However, for certain nonlinear phenomena especially higher odd orders, the CEP needs to be taken into account and addressed.

For this calculation, a infinite pulse train starting from $-\infty$ to ∞ was assumed. More physical and realistic pulse trains have a finite starting point, mostly at t=0, and a normal experiment, a certain sampling time of t=T. The Fourier transform of a finite Dirac-comb $\sum_{m=-T/2}^{T/2} \delta(\omega t - m\pi)$ is a finite sum over cosine- functions in the form of $1 + \sum_{m=-T/2}^{T/2} cos(2\pi\Omega m)$ The result differs such that the δ-functions of the frequency comb will have a finite width with $\Delta\nu \propto \frac{1}{T}$. This is sketched in fig. 4.7. In the limit where T is approaching ∞, the width becomes a δ-function.
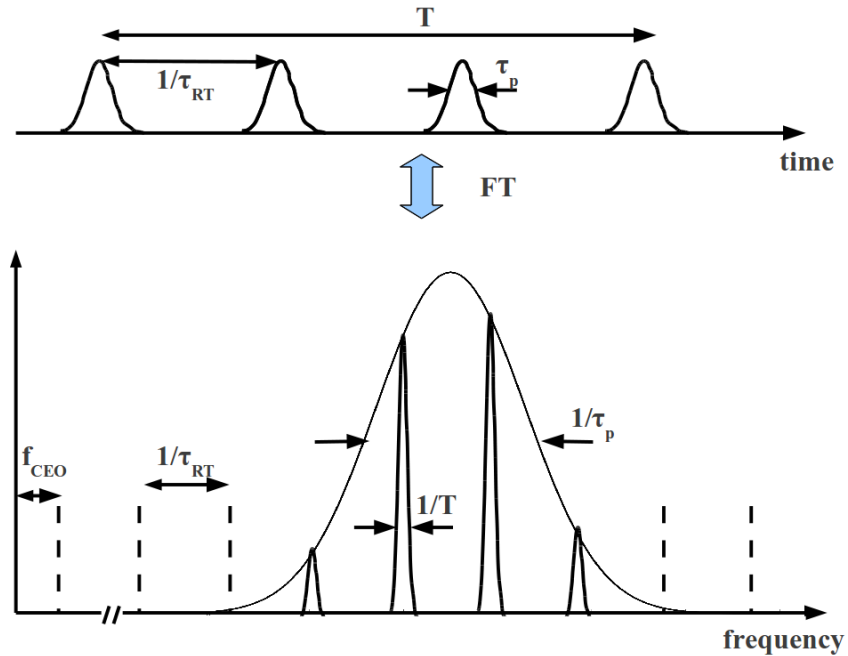
Figure 4.7: The frequency picture of a physical pulse train.

4.4   IPI and CEO

For IPI, we are using the CEO to convert a phase shift into a frequency measurement. This is the major difference between IPI and a standard extra-cavity interferometer where a phase shift is converted into an intensity change. Two pulse trains with the same round trip time τ_{rt} have the same frequency spacing. However, a difference in the CEO can be detected by overlapping the two pulse trains on a detector. This results in a beatnote between the two pulse trains

$$\Delta\nu = \frac{f_{CEO,1} - \Delta f_{CEO,2}}{2\pi\tau_{RT}} = \frac{\Delta\varphi}{2\pi\tau_{RT}} \tag{4.7}$$

Frequency combs have mandatory equal spacing and each comb line contributes to the overall signal and gives a very good signal strength with large signal visibility. Also, since the conversion is from phase into frequency, the whole measurement is mostly independent of amplitude fluctuations and does not require a cumbersome stabilization scheme. Exceptions to the rule are the non-linear refractive index measurements where the experiment relies on the difference in intensities between the two pulse trains. The experimental data suggests that even with an unstable cavity the intensity fluctuations have only second order impact on the measurement.

Looking at the signal in the time domain, the two pulses with the different phases overlap on the detector. Due to the different phase shift every round trip between the two pulses, the interference between the two pulses is periodically modulated.

Superficially, the IPI seems independent of intensity fluctuations with the above time domain picture. As mentioned above, from the experimental data e.g. the beatnote bandwidth shows good performance even with an unstable cavity. Good performance is observed even with the OPO where large amplitude fluctuations were observed. However a detailed analysis is difficult because the pulse to pulse fluctuations are fairly small and most of the behavior is observed over larger timescales.
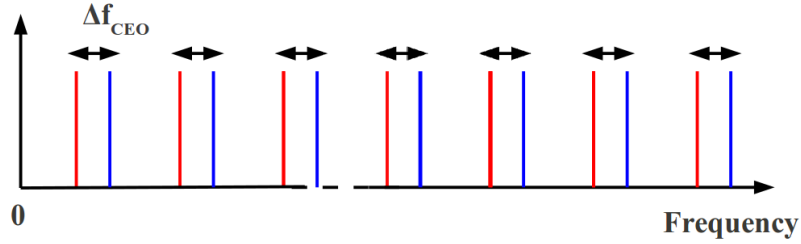
Figure 4.8: Two frequency combs with the same repetition rate but different CEO will result in a beatnote where every comb line is contributing to the signal

4.5 Creating Two Pulse Trains With The Same Repetition Rate

To overlap the two pulses with the different phases on the detector, the experiment created two-pulse trains with the same repetition rate inside the same cavity. The main obstacle for this method is creating two pulse trains with an identical repetition rate. Creating the same pulse trains from two different lasers is complex because building control electronics are difficult for the two separate cavities. Instead, one laser cavity is more feasible, which is standardly used for the IPI setup. The first demonstration of the IPI was done by Lai et al[7] with a dye laser mode-locked with a dye jet saturable absorber. The next implementation was a ring Ti:Sapphire laser system, mode-locked with a saturable absorber dye jet [26]
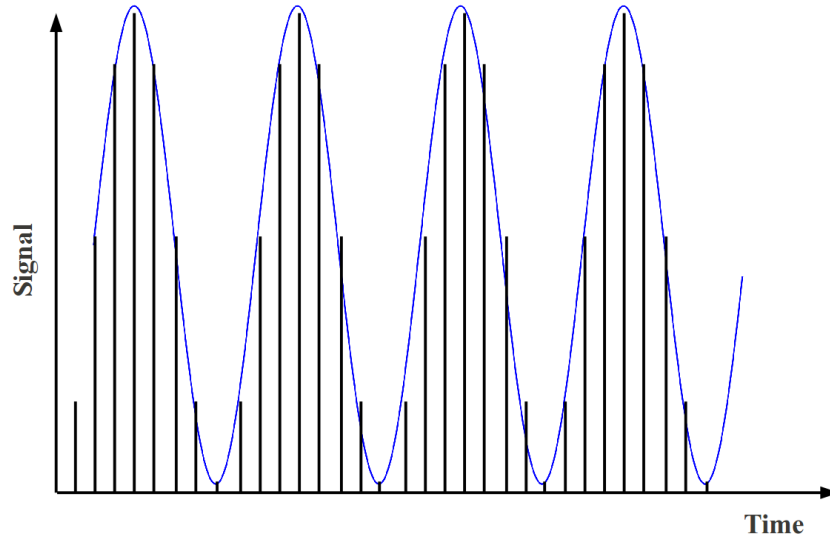
Figure 4.9: In time domain, the phase difference between the two pulse trains causes interference which is detected with the detector.

Two pulse trains in the same cavity, although more efficient than using multiple cavities, however, have a limitation: mutual injection locking. Mutual injection locking is also commonly observed in CW lasers. This is a well-known effect and limits the performance of HeNe-laser gyroscopes which use ring cavities. Any backscattering or reflections lock the frequency and the phase of these two pulse trains. This creates a dead band where no signal or frequency shift is detected, when a differential phase shift $\delta\varphi$ is imposed, as shown in Fig. 4.10.

IPI mode-locked system offers advantages over CW lasers. For CW lasers, this backscattering happens at every interface or optical medium ubiquitously in the cavity. As a result, the laser system must be driven far away from the locking region limiting the dynamic range of the whole measurement. An advantage of the IPI mode-locked system, with two pulses propagating in the cavity is avoiding the in-
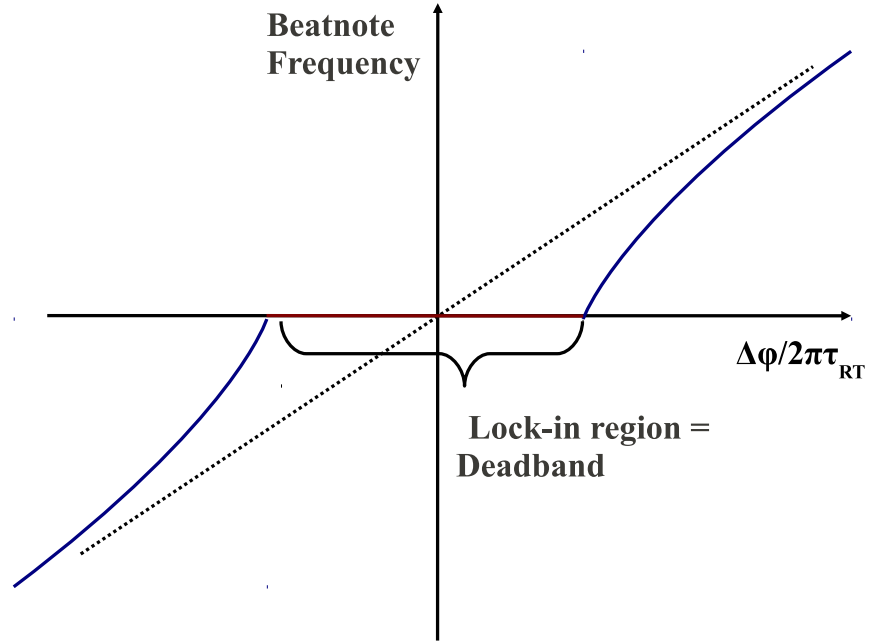
Figure 4.10: Locking between the two pulses occur for a certain phase shift region, called the deadband.

jection locking because the crossing points are controlled. For a mode-locked ring cavity, there are always two crossing points inside the cavity. IPI, by contrast, has both ring and linear cavities. In a linear cavity these two crossing points can be merged, if they occur in the middle of the resonator. The mutual injection locking occurs only if optics are placed at the crossing points.

The two pulse trains are independent even though they originate from the same laser cavity and the time-space separation enables one to distinguish them to perform the phase measurements. Creating these two independent pulse trains is quite challenging. In the following paragraph, the use of a ring cavity is discussed to create the two pulses. However the concepts apply equally to a linear mode-locked cavity. The Kerr-lens mode-locking (KLM) would be the preferred mechanism to create the

two pulses since KLM produces the shortest pulse width. However in a ring cavity KLM tends to be uni-directional and does not produce two counter propagating independent pulse trains [26, 28]. KLM method produces a uni-directional pulse train because of the laser dynamics. Material with a nonlinear refractive index n_2 and the spatial intensity distribution across the pulse creates a lensing effect. The effect will change the beam size significantly in some places compared to the linear, non mode-locked condition. Using an aperture where a smaller beam size is expected for the KLM case will force the laser to lase in the lower loss situation. Due to the difference in intensity of the two counter propagating pulse trains and the nonlinear nature of the effect, there can be a significant difference in beam size and therefore favoring one direction compared to the other one and only uni-directional operation is observable.

To force the laser to be bidirectional, an amplitude coupling mechanism is needed. Therefore, a saturable absorber is the favorable mode-lock mechanism. The method has been discussed by several publications already in detail [29, 30]. In short, if the two pulses cross inside a saturable absorber, where mutual saturation exceeds self-saturation, the loss of the cavity is decreased and therefore more favorable for lasing. The problem, however, is that a saturable absorber is a optical medium that scatters and can cause the locking effect. A moving dye jet used as a saturable absorber can be used to mitigate the problem. The phase of the backscattered light every round trip is randomized due to the moving particles. Taking the average over several round trips, the backscattering contribution averages out to zero and no locking is observed. This has been demonstrated experimentally by Lai et al[7]. The cavity was carefully designed with no optical elements at the second crossing point of the two pulses. Two measurements were performed; the Sagnac effect or gyroscopic response of the cavity and the Fresnel drag. A beatnote bandwidth of 100Hz was measured. A different approach besides mode-locked laser systems is optical parametric oscillation, synchronously pumped by a pulse train. This has been shown

first by Meng et al [23] with a bidirectionally, externally pumped OPO and followed with an bidirectionally intracavity pumped OPO. Discussion about the OPO is in Chapter 5.
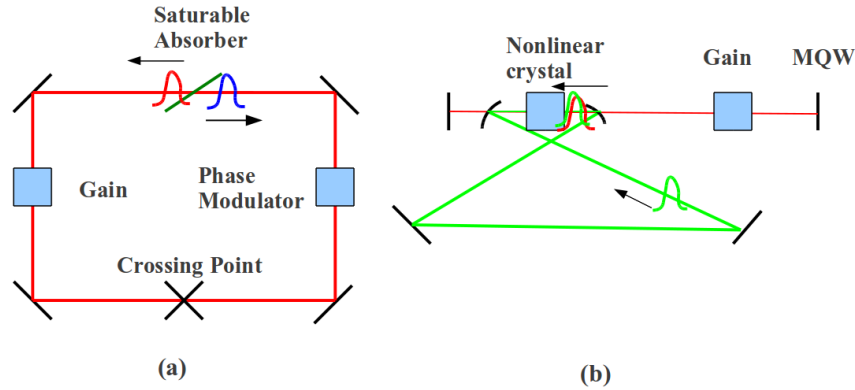
Figure 4.11: (a) The schematic of the ordinary ring laser mode-locked with a dye jet. As gain medium either dye or solid state materials can be used. The phase shift is applied with the help of an electric optical modulator. (b) Intracavity pumped OPO pumped with a mutliple quantum well (MQW) mode-locked pump laser.

   The previously described free running, unstabilized lasers have a good performance record because most noise contributions result in a common-mode noise, meaning both pulses are affected the same way. To improve the noise characteristics of a signal, common-mode noise can be suppressed by a differential measurement, like IPI. IPI measures the difference between the two frequency combs resulting in a beatnote measurement. Any noise with a time constant larger than the round-trip time that will affect both pulses equally, does not broaden the beatnote bandwidth. A very narrow beatnote bandwidth of 1Hz has been observed experimentally with a Ti:Sapphire lasers described above [26]. The measured linewidth of 1Hz is due to noise coming from a differential phase shift acquired by the two pulses rather then the common-mode noise. Several mechanisms result in a differential phase shift. One mechanism is mechanical vibrations of the optical elements in the cavity. The pulses hit the elements at different times resulting in a different phase shift due to

the differential Doppler shift. In a ring cavity, Fresnel drag is another example of a mechanism resulting in a differential phase shift where the refractive index is different for the beam traveling with or against an air current. A more detailed discussion about noise contributions affecting the line width of the beatnote and the limit of IPI can be found in Chapter 7.

4.6   Group and phase velocity

The CEO frequency of the pulse train is due to the difference of group v_g and phase velocity $v_{ph} = c/n$ inside the cavity. These two velocities are not independent of each other and are related through the following equation:

$$v_g = v_{ph} - \lambda \frac{\partial v_{ph}}{\partial \lambda} = c(n - \lambda \frac{\partial n}{d\partial \lambda})^{-1} \tag{4.8}$$

A change in refractive index is not only affecting the phase velocity but also the group velocity. IPI measurements are all based on a differential change in refractive index for the two pulses inside the cavity. Therefore, there will also be a change in group velocity, resulting in a different round trip time for the two pulses. However the repetition rate of both pulses stays the same as discussed in Chapter 4.5. For the OPO, the repetition rate is determined by the pump pulse. In the case of a saturable absorber mode-locked Ti:Sapphire laser, the mutual saturation forces both pulses to have the same repetition rate. In the OPO some mechanism should should correct change in group velocity. The mechanism is a slightl shift in frequency *envelope* resulting in a change in center frequency ω_0 of the two pulses. However the position of the comb lines and separation stays unchanged (see Fig. 4.12). The beatnote frequency measured in an IPI measurement is not affected. Only the signal strength is altered since the overlap of the two combs is reduced. The reduction in signal strength is similar to a change in fringe visibility in standard interferometric
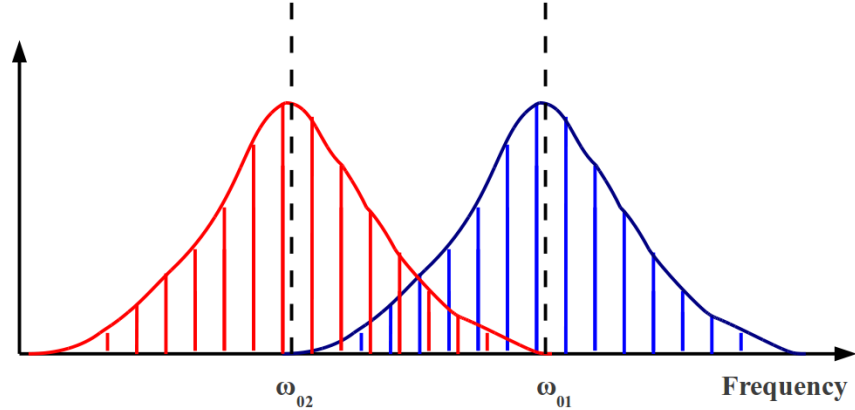
Figure 4.12: The effect of different group velocities on the two frequency combs is shown. The result is a shift of the two envelopes to a center frequency of ω_{01} and ω_{02} for pulse train 1 and pulse train 2 , while the comb lines and spacing between is unchanged. For the IPI measurement, the beatnote is not altered. Only the overlap of the two comb structures is changed reducing the signal strength similar to reducing the fringe visibility in normal interferometric measurements.

measurements. A similar spectral split of two circulating pulses has been obeserved in a Ti:sapphire laser, KL mode-locked by a ZnS crystal [31]

4.7   Summary

This chapter sets the framework for IPI: the CEO of a mode-locked pulse train is used to convert a minute phase shift into a frequency signal. Two-pulse-per-cavity lasers are needed to implement IPI. Previous work shows already a pristine sensitivity for unstabilized laser systems. Applications range from measurements of rotation, non-linear refractive index, backscattering, magnetic field, Fresnel drag, acceleration, electro-optical coefficients and many more. In principle, any differential or directional phase shift can be measured.

Chapter 5

OPO as a Tool for IPI

5.1 Introduction

A synchronously pumped OPO is a great tool for IPI. One of its advantages is that no gain coupling is present between the two pulses inside the cavity since gain is only available during the time the pump pulse is present inside the nonlinear crystal. OPOs can operate at a large variety of wavelengths and have a precise tuning capability. Also, stabilization schemes are much easier to implement. The repetition rate of the pump laser and the wavelengths can be stabilized by implementing a feedback loop for the pump and OPO cavity lengths.

Externally pumped OPO An initial approach was to pump an OPO external to the pump cavity, splitting the output of the pump laser in two beams which are sent in opposite directions to a periodically poled $LiNbO_3$ (PPLN) inside a "signal cavity" [32]. This approach has not given the expected resolution, because nm fluctuations of the pump spot resulted in beat note instabilities and beat note bandwidth

of the order of tens of kHz.

Intracavity Pumped OPO A solution proposed and implemented [23] is an intracavity pumped OPO, where a periodically poled $LiNbO_3$ (PPLN) is common to the pump laser and signal cavities. Two pulses are generated in the signal cavity because the pump pulse makes two passages through the PPLN. There is no fluctuation of pump spot position, since both pulses share the same spatial mode of the laser cavity. The crossing point (where scattering might occur) of the two pulses is determined by the position of the PPLN in the pump cavity. This type of laser is extremely difficult to align, and to operate in a stable bi-directional mode. It has been shown that the nonlinear gain of the OPO couples the pump and signal cavity. The coupling enhances the q-switching tendency of the pump cavity. Another effect is that mainly only one pulse is present in the OPO cavity even though the two counter propagating pulses should generate the two independent pulses in the OPO. A suggested solution would place a nonlinear loss that depends on the intensity of the signal pulse inside the OPO cavity. This stabilizes both the signal and pump cavity and stable operation can be observed. This might be the reason why Meng et al[23] were able to do a measurement. Due to tight focusing inside the $LiNbO_3$, enough second harmonic (nonlinear loss) was generated by the signal pulse to enable the measurement. Recent efforts for this dissertation to reproduce an intra cavity pumped OPO has not been successful yet. Trying to put a second nonlinear crystal inside the OPO cavity is a difficult alignment task as well as trying to achieve the 1% conversion that is needed for stabilization.

Pump Sources for OPO The main source of instability for the intracavity pumped OPO is the memory effect in the pump laser gain due to the long lifetime of the gain medium, especially for the Ti:Sapphire. Semiconductor lasers have a much shorter upper state relaxation time in the order of nanoseconds which prevents Q-switching

instabilities. The short lifetime, combined with the good availability and low cost are the main motivation for investigating semiconductor lasers as a OPO pump source. Two lasers are presented in the dissertation: the tapered amplifier (TA) and the optically pumped-external-cavity surface-emitting semiconductor laser (VECSEL).

5.2   Two pulse, external cavity OPO cavity

5.2.1   General

A considerably simpler and more effective method, than the methods discussed in the introduction, is pumping the OPO directly at the output of a Ti:sapphire mode-locked laser; the Ti:sapphire laser has *half* the length of the OPO cavity. The crossing point of the two pulses is in the middle of the OPO cavity, where there is no optical element that could couple both beams. There is no gain competition, and no coupling through pump depletion in this extracavity scheme.

The pump laser in the experiment is a Ti:Sapphire laser, mode-locked with a multiple quantum well as saturable absorber. In the Ti:sapphire laser, a birefringent filter is inserted for wavelength tuning. The output coupler (OC) is 8%. The laser's output power is 400mW at 790nm with 1.6ps pulsewidth and a repetition rate of 180MHz. The OPO crystal is a 3cm long, AR coated periodically poled LiNbO$_3$ (PPLN) with a periodicity of 20.36um. An optical isolator was not used to avoid the back reflection from the front surface of the OPO. This is more an issue for short crystals where the surface is close to the focus and therefore acting like a cat eye configuration which retro-reflects back into itself. For the long 3cm PPLN, the surface is far enough from the focus point and the reflection then diverges enough not to couple to the pump cavity which would destroy the mode-locking. The phase difference $\Delta\varphi$ is applied by a thin ($\approx$ 1mm) LiNbO$_3$ electro-optical phase modulator

51

(EOM). A pellicle beam-splitter is used as an output coupler of about 1% output coupling.
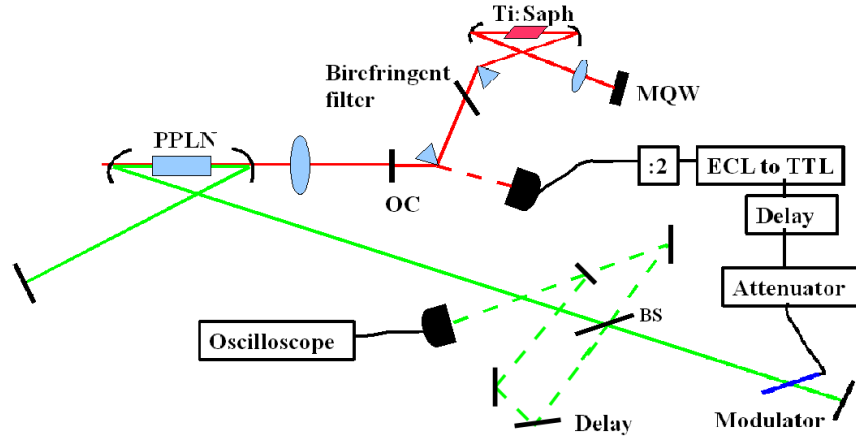
Figure 5.1: Pump and signal cavities. The modulator is driven with the appropriate phase by the repetition rate signal from the pump cavity divided by 2. The beat note signal is detected by overlapping the two outputs of the pellicle beam-splitter (BS) with the right delay.

The output is then sent to a delay line and a detector. The delay is adjusted so the two counter propagating pulses are overlapping at the detector. The driving circuit of the EOM takes the repetition rate signal from the pump cavity, divides it by two, converts from an ECL to a TTL signal, and sent to a electronic delay line. The delay is adjusted so that the independent pulses will always see either the maximum or minimum of the square signal and avoiding the edges of the square pulse (setting that provides the largest beat note signal). The maximum peak to peak voltage is 2.3V. Fig. 5.2 shows one example beat note.

Taking the Fourier transformation of the signal reveals a bandwidth of 1Hz (see Fig. 5.3). Because of such a narrow beat note bandwidth, it is possible to resolve changes in phase $\Delta\varphi < (1\ \text{Hz}) \times 2\pi\tau_{RT} \approx 5 \cdot 10^{-8}$rad.
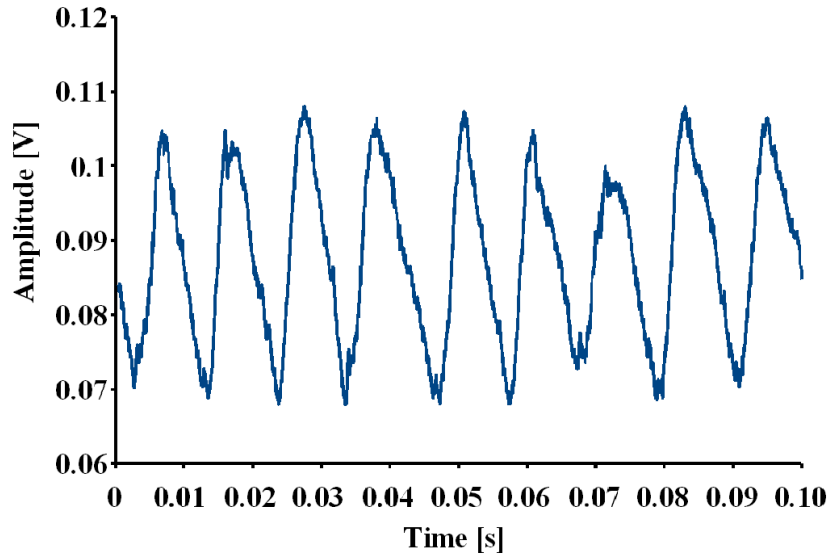
Figure 5.2: Typical beat note signal recorded with a oscilloscope.

The linearity of the beat note response with respect to the phase (proportional to the voltage applied to the modulator) is verified in Fig. 5.4. As expected, no dead band is observed. With the simple relation of $\frac{\Delta\nu}{\nu} = \frac{\Delta L}{L}$ where ν is the frequency of light and L the cavity length, the phase resolution is seen to correspond to an optical path resolution of 0.01pm. Optical elements such as mirrors don't have a flatness in picometer. Therefore the optical path resolution of 0.01pm has to be seen as an average across the wavefront of the laser beam.

5.2.2 Experimental Notes

The OPO is operating close to threshold. By inserting a half wave plate into the pump beam path before the OPO, an estimate of a pump threshold was about 320mW. This is close to the maximum power available for pumping the OPO. This explains
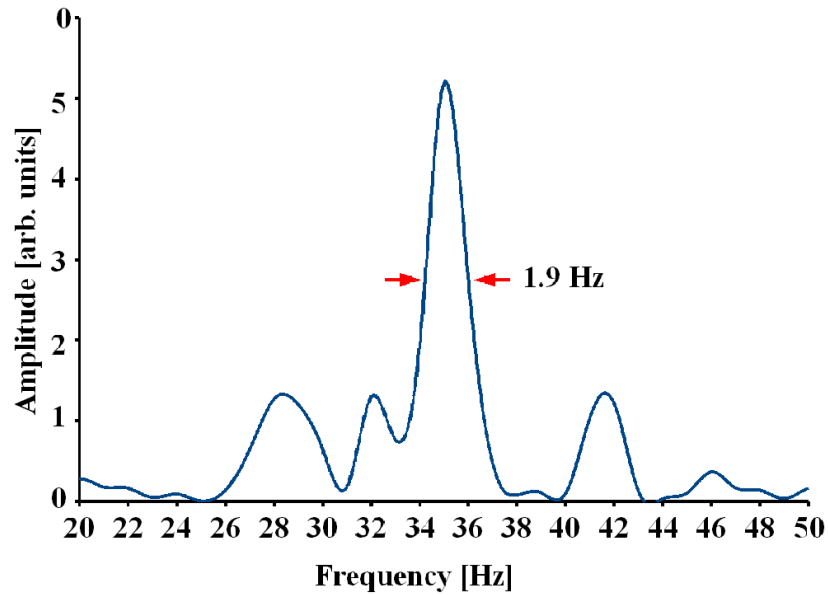
Figure 5.3: Fourier transformation of a beat note signal. The signal is recorded over the time of 1 s.

several alignment problems encountered in the beginning. The research used several different crystals. Initially, a Brewster cut, 3mm long crystal was used. Alignment of this cavity is very hard since an alignment laser is required. Due to dispersion, the different colors exit the crystal at different angles. So the unphasematched second harmonic cannot be used to align the cavity. Next, the 3cm long parallel cut crystal was tried.

Due to the low energy available in the experiment, a telescope was used to expand the beam before focusing it inside the OPO crystal in order to obtain a shorter and tighter focal spot. The curvatures of the two mirrors were r=10cm and r=40cm. The second mirror is used to image the focal point of the smaller curvature mirror in the OPO crystal. This allows for a tighter focusing and a better nonlinear conversion. Note that only a fraction of the crystal length is effectively used; the length is determined
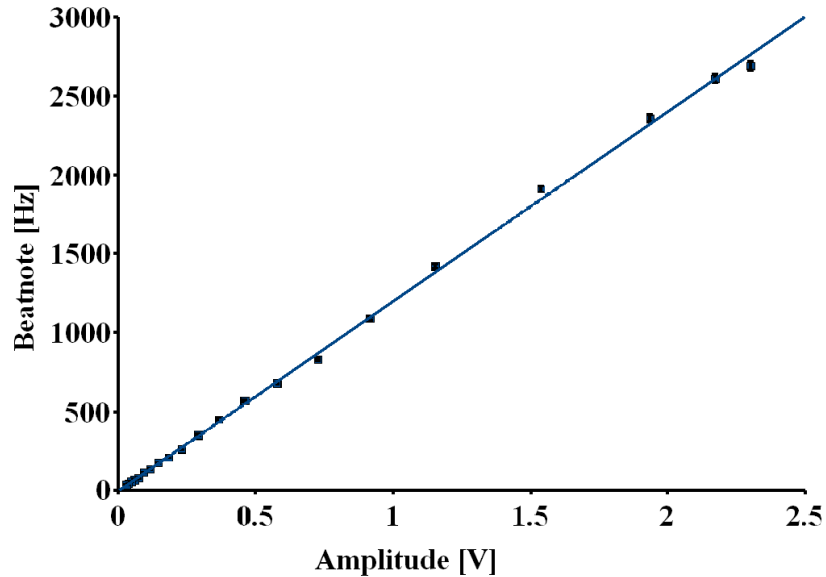
Figure 5.4: The dependence of the beat note frequency on the applied voltage. A linear dependence is seen as expected. The error bars are included in the graph. Due to the small bandwidth, these error bars are comparatively small ($\approx 1\%$) and not visible. With a electro-optic coefficent of 32.2pm/V, the expected slope is 1.1kHz/V which is close to the measured 1kHz/V.

by either the beam waist or the GVD between the pump and signal, resulting in a spatial walk-off. The second harmonic of the pump is sufficient to align the cavity in the case of a parallel face crystal. The OPO cavity must be in a stable configuration e.g. the distance of the two collimating mirrors is within the stability range. This can be done by either using an external alignment laser or by carefully monitoring the spot size of the second harmonic of the pump (blue). The next step is overlapping the blue beam on itself after one round trip. After this step, the end mirror of the OPO is moved to match the pump repetition rate (or common multiple of it) and it should start lasing.

5.2.3 Nonlinear index measurement

Nonlinear indices n_2 are normally measured with the method called Z-scan [33, 34]
The sample to be measured is inserted in a high power focused beam and translated
along the z-axis (propagation axis) around the focal point. The nonlinear index
causes a change in the divergence of the beam which can be measured by a change
of intensity with a detector. It is a simple and successful method.

IPI can also be used to measure n_2. The advantage over the Z-scan is, again, not
measuring a change in intensity but directly measuring the phase shift introduced.
Another advantage of IPI is only a single measurement is required and a scan is not
needed. For this measurement, the setup is modified by the following: the phase
modulator inside the cavity is removed. Instead a Pockels cell is inserted in pump
beam path and driven with the same signal as in the previous experiment, amplified
to 20V. This will alter the polarization of every other pump pulse slightly and changes
the gain for the two OPO pulses, since the phase matching is polarization dependent.
The difference in intensities of the two OPO pulses, I_1 and I_2 then create a beatnote:

$$\Delta \nu = \frac{ln_2(I_1 - I_2)}{\lambda \tau_{RT}} \tag{5.1}$$

where l is the length of the sample used.

As a sample, PPLN itself was used for a proof-of principle experiment.
The beatnote bandwidth mostly observed in this experiment was 50Hz, 10 times
larger than in the other experiment. There are two sources for this increased band-
width: the electronic noise imported by the Pockel's cell, and the coupling between
amplitude and frequency noise introduced by the nonlinear effect. The beat note
bandwidth translates into an n_2 error of $\pm 2.2 \times 10^{-17}$ cm^2/W which corresponds to a
phase error of 8.6×10^{-7}. The uncertainty for an unknown sample placed in the OPO
cavity and to be measured should be twice so $\pm 4.4 \times 10^{-17}$ cm^2/W. When a sample
is placed in the cavity, the pulse width of the OPO pulse will be altered due to the
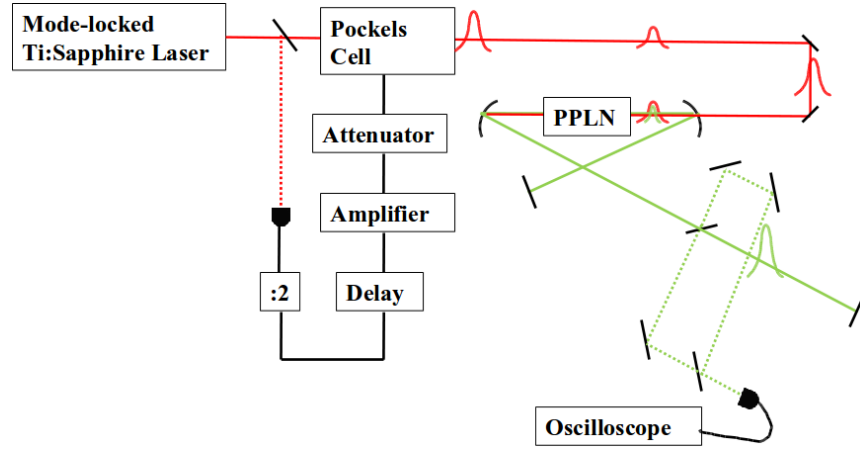
Figure 5.5: The setup for the n_2 measurement: A Pockels cell is inserted between the pump and OPO cavity. As sample, the PPLN itself is used.

added group velocity dispersion (GVD). The change in pulse width has to be taken into account for the determination of the intensities in the cavity but do not change the measurement in itself.

From the slope of figure 5.7, one can extract n_2=1.28$\times 10^{-16}$cm^2/W at the wavelength of 1404nm. Comparing to a previous measured value with the z-scan method at 1064nm of n_2=1.8$\times 10^{-16}$cm^2/W [33, 34], it is in the same order.

Improving the system should make this a powerful and sensitive tool to measure n_2. A better calibration of the intensity difference will reduce the error bars in the x-direction. Also a more stable operation of the pump and the OPO should improve the beatnote bandwidth and therefore increase the resolution by at least a factor of 10 or 100 if the previous shown bandwidth of 0.17Hz can be reached.
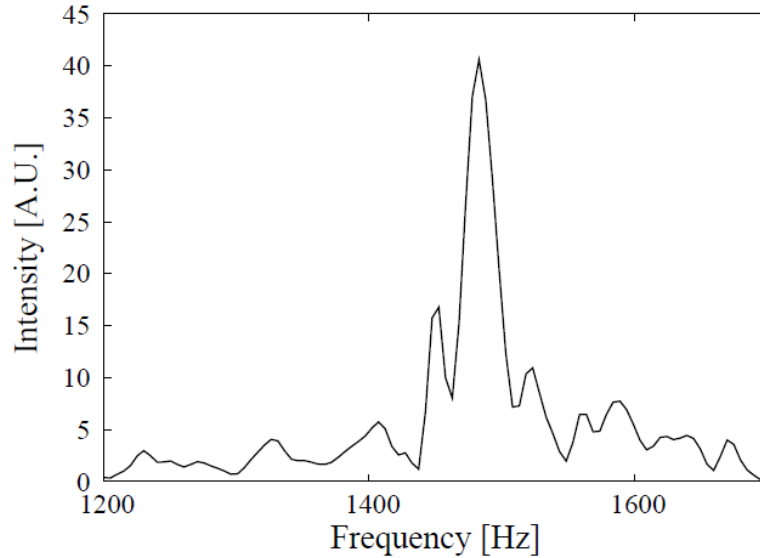
Figure 5.6: Fourier transformation of the one beatnote signal of 1.5kHz shows a relative wide bandwidth of 50Hz.

5.3 Intracavity Pumped OPO

5.3.1 General

Attempts have been made to build a ring intracavity OPO before. They were successful in measuring a beatnote, however they were lacking long term stability due to coupling the pump cavity and OPO cavity [35]. Nevertheless, the harmonic pumping scheme, or when the OPO cavity is a common multiple of the pump cavity, is also a possibility for a linear intracavity setup to avoid the instabilities. It also can be setup as a ring where the two pulses are propagating in the same direction.

The biggest advantage of using an intracavity pumped OPO is access to much more intracavity pump power. Typical 100MHz mode-locked Ti:Sapphire lasers pumped by a 5W Nd:YAG laser have output powers between 100mW and 400mW. Larger
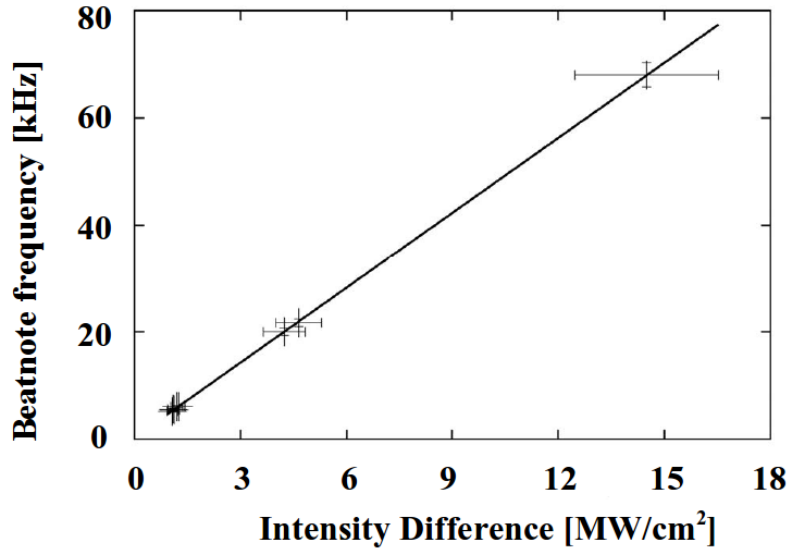
Figure 5.7: The beatnote is measured versus the intensity difference of the two pulses. This is achieved by varying the peak-to-peak voltage on the Pockels cell. The error bars for the intensity difference are fairly large and originate from difficulties converting the voltage difference into an intensity difference. This is done by measuring the output pulse train with a fast detector and a lock-in amplifier where the reference is the signal applied to the Pockels cell.

powers can be extracted by using a a 10W 532nm laser to pump the Ti:Sapphire. However this comes with a huge dollar price and a risk of damaging the laser crystal. In addition, more power extraction did not work. By using a low loss cavity e.g. no output coupler, several watts inside the cavity can be achieved. This 10-fold increase in intracavity power makes it possible to achieve a higher power OPO, much further above the threshold than in the externally pumped case; therefore more losses can be introduced into the OPO cavity and this ability will be needed when inserting IPI's optical elements.

Another consideration has to be taken into account: the back reflection. The back reflection from a short nonlinear crystal will couple to the cavity and will cause the

mode-locking to stop. An optical isolator cannot be used inside a linear pump cavity since the isolator would prevent lasing, a Brewster angle crystal is used in such an experiment. Like previously stated, the alignment is more difficult because of material dispersion and the different beam paths of the different wavelengths outside of the crystal. The use of an alignment laser seems to be the easiest method of getting the OPO to oscillate.

5.3.2 Experiments

Andreas Velten's thesis [36] also showed the ability to achieve a beatnote measurement with an intracavity OPO.

Velten conudcted two different experiments. The first one used the same crystal as in 5.2. Since an isolator was not used for the 3cm parallel phase crystal in the extra cavity OPO to avoid coupling from the back reflection into the main cavity, the assumption was to use the same crystal inside the pump cavity as well. The output coupler was removed and a focusing mirror was inserted behind the PPLN crystal so the PPLN was inside the Ti:sapphire cavity. The threshold of the OPO oscillation was surprisingly high at about 5W of the 532nm pump power. Overall this setup was not very stable. Small amplitude fluctuations of the Ti:Sapphire were amplified by the OPO. Also, operation close to the threshold of the OPO did not help the stability. (Only 5.2W of 532nm light was available.) However, the instabilities precluded measuring a beatnote.

The second experiment used a different crystal, a 1cm Brewster cut PPLN for a wavelength region between 1.07μm to 1.26μm. The decision was made to move to this wavelength regime since the system eventually should be used for biological applications and the water absorption can be minimized in that window. The mirrors were also exchanged for high reflecting mirrors ($>99.8\%$). The threshold of the OPO cavity was reduced to 4.7W in this configuration and a fairly stable operation of the

OPO could be achieved if the 532nm pump was set above 5W. Bi-directional operation e.g. the forward and backward traveling pump pulse creates two OPO pulses, was not observed as expected. However with the harmonically pump scheme (OPO cavity length was 2/3 of the pump) a beatnote measurement was possible.

5.3.3   Length Measurement

A nanoscope is proposed for an OPO cavity for minute length changes. By using a combination of a Pockels cell and a polarizing beam splitter, these two independent pulse trains can be sent to different cavity arms. One is used as the reference cavity, the second arm as a measurement cavity. By placing samples inside the measurement arm, one can measure the change in thickness by monitoring the phase shift introduced by the change in the refractive index. For such an application, shorter pulse lengths are more desirable to increase the spatial resolution. The intracavity OPO should be more suitable. All the optics needed for this experiment introduce a big loss to the OPO cavity and higher pump power is desirable. A more detailed discussion about this project can be found in 8.3

5.4   Pump sources for the OPO

The main motivation for using semiconductor lasers is the short upper state relaxation time, which prevents Q-switching instabilities. The instabilities are normally observed with Ti:Sapphire lasers and especially Ti:Sapphire lasers used for intracavity pumping OPOs. Dye lasers were routinely used for intracavity pumping of OPO without any problem, because of the property of fast relaxation time.

Another advantage is that seminconductor lasers may be a cheaper pump source for the OPO. They are compact, fairly efficient and cheap in comparison to most

solid state sources and suitable for a wide variety of applications, especially communication technology. Mode-locked semiconductor lasers were first used in the early 1980's [37, 38]. However the technical difficulties of achieving short pulse duration and high output power are still not resolved for edge emitting laser diodes. Also the small area of edge emitting laser diodes are limited in the power since small areas mean high intensities and therefore damaging the facet is very likely. This limits the outputpower in the order of milliwatts and energies up to 20pJ. [39].

Two approaches to solve the high power and short pulse problem are considered: tapered amplifier (TA) in a ring oscillator configuration and optically pumped-external-cavity surface-emitting semiconductor laser (VECSEL) [40]

5.4.1   Tapered Amplifier

The work described here was done together with equal contributions by Andreas Velten and Ye Liu.

A tapered amplifier consists of a normal, index guided region at the input side on which the beam is focused. After the initial amplification and the waveguide ends, the beam is allowed to diffract in a transverse direction. This is the tapered region where the beam is gain guided. [41, 42]. Two cylindrical lenses are then needed to re-collimate the beam too achieve good beam quality. Tapered amplifiers are more commonly used in a master-oscillator power amplifier (MOPA) setup, where the temporal and spatial characteristics of the output of a low-power oscillator are well maintained through amplification in a tapered structure [43, 44]. Instead of the standard master-oscillator power amplifier (MOPA) configuration,the tapered amplifier is used as gain medium inside its own cavity. For the setup a diode was used from Eagleyard , 780nm, 1W, EYP-TPA-0780-01000-3006-CMT03-0000 pre-packaged with
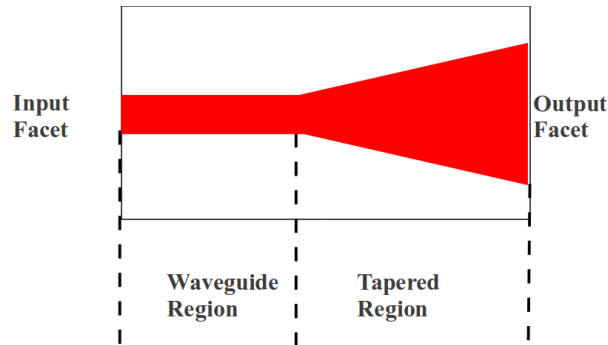
Figure 5.8: A typical structer of a tapered amplifier is shown. At first, the input beam is pre-amplified in the waveguide region of the TA. To reach higher powers without damaging the material, the beam is then allowed to diffract and gain guided in the tapered region.

the focusing and collimating optics as well as the optical isolator included. The later is required to protect the diode from any back reflection. The advantage of this configuration is the good beam quality that is defined by the cavity itself. Also to avoid any damage to the semiconductor itself, only a small amount of the available power can be coupled back. This leads to an unusual laser configuration were most of the power is coupled out. It also has a very high gain per roundtrip as compared to most solid state mode-locked oscillators.

Initially the optimal operation parameters were determined by a MOPA configuration. As input we used a Ti:Sapphire laser tuned to 780nm. (Fig 5.9). Gain saturation is starting at 7mW of input power with a maximum outputpower at maximum pump current of 610mW. This corresponds to a small signal gain of 87 or

19.4dB.
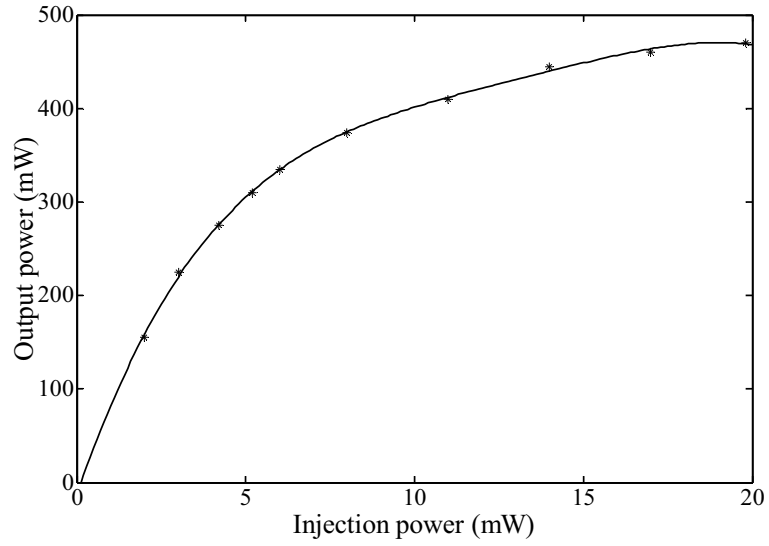
(a)
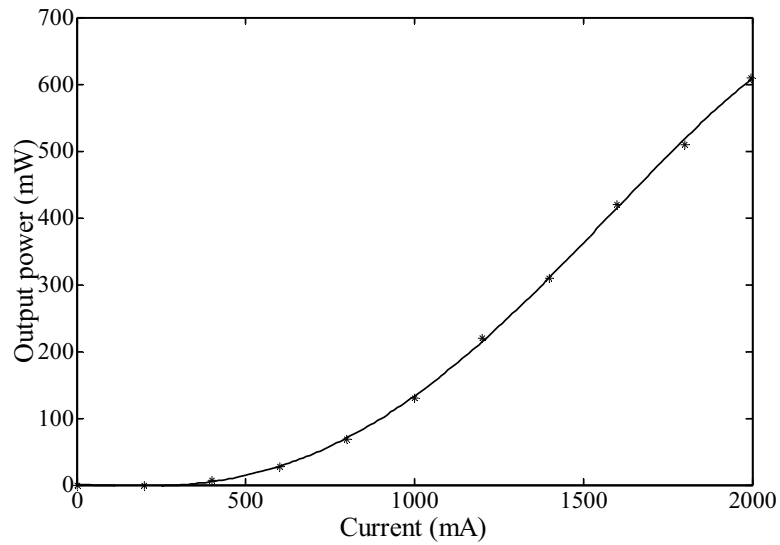
(b)

Figure 5.9: A standard master oscillator setup up is used to determine the optimum input power in our cavity

The experimental setup of the cavity is shown in 5.10. A polarizing beam splitter (PBS) and a half-waveplate is used (HWP1) as an output coupler and to control the power coupled back to the TA to avoid burning the input facet. The second half-wave plate is used to reorient the polarization matching it with to the input for maximum gain.
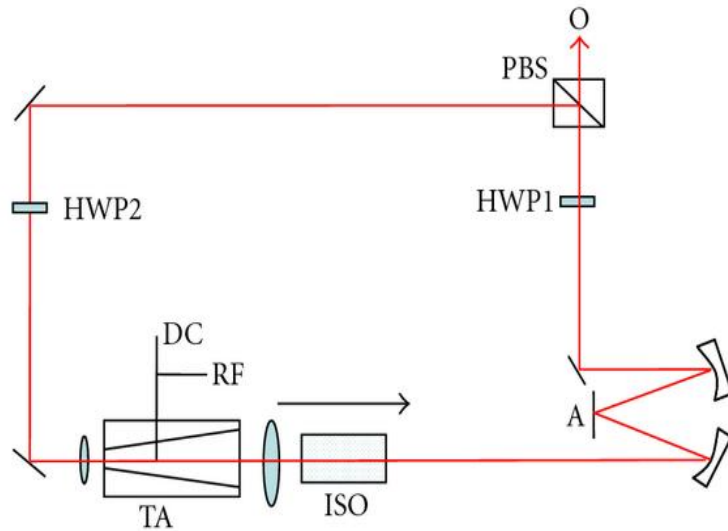
Figure 5.10: Schematic of hybrid mode-locked external ring cavity semiconductor laser. For mirror A, a normal mirror was used in cw configuration and a multiple quantum well mirror for mode-locking. The radius of curvature of both focusing mirrors is 10cm.

In position A in figure 5.10 we either placed a high reflection mirror to operate in CW or the MQW well mirror for mode-locking. In the CW case a threshold of the cavity was measured to be at 1.1A of pump current with a wavelength of 781nm. The output beam profile was fairly round and the Gaussian fit was very good. To better quantify the beam profile a M^2 measurement was performed where beam profiles were measured at several distances. An example of such a beam profile is shown in Figure 5.11 for the vertical and horizontal axis. The measurement shows a M^2 of

1.07 which supports the claim that the beam profile is determined by the cavity itself rather than the tapered amplifier.
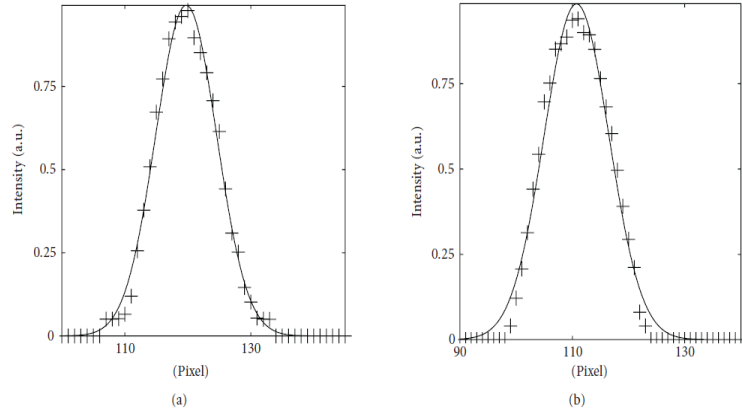
Figure 5.11: Laser-beam profiles with Gaussian fit in the horizontal (a) and vertical axis (b).

Initially, to mode-lock the TA, a MQW saturable absorber–centered at 795nm–was inserted. Since the TA has a high gain, a 10 layer MQW was used to introduce a large non-linear loss and a deeper modulation. However, the modulation alone is not strong enough to achieve a stable mode-locking. On the oscilloscope only a sinusoidal modulation on the amplitude was observed. An RF signal was applied to the Bias-T to jump start the mode-locking. In this configuration a stable mode-locking operation was observed, indicated by the pulse train in fig. 5.12. The stability observed here is typical of a Ti:Sapphire laser operating in the "soliton regime" and not often observed with a short lifetime medium such as semiconductors. The stability seems to indicate that the pumping the OPO by a semicunductor laser is worth persuing. The repetition rate was about 88MHz and the output power 40mW. The autocorrelation of the pulse showed an almost perfect sech^2 fit with a duration of 500fs (fig. 5.14). This is compared to the optical spectrum. The FWHM of the spectrum is about 2.15nm . The time-bandwidth product of 0.527 is larger than

400ns/division
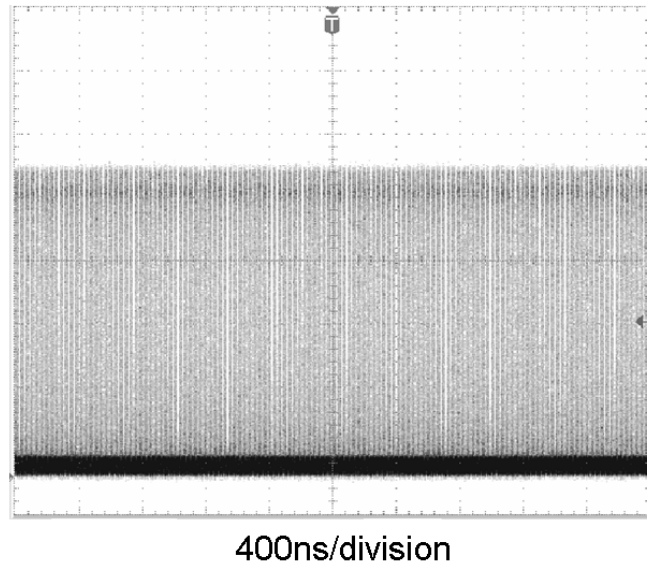
Figure 5.12: A oscilloscope trace of the stable pulse train

the theoretical value for a sech pulse of 0.315 [45]. This is not surprising since no dispersion compensation is used and a significant chirp on the pulse is expected.
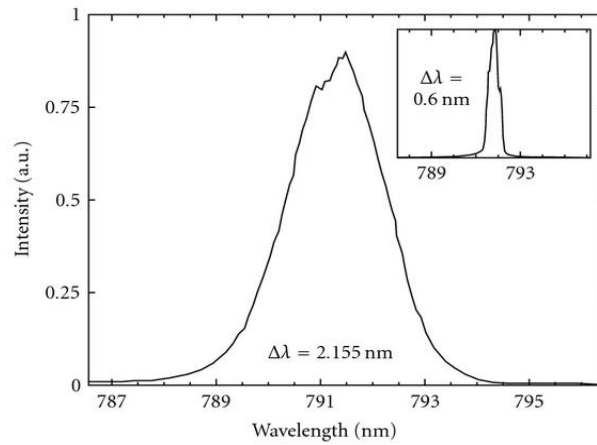
Figure 5.13: Optical spectrum with RF modulation on. Inset, RF modulation off.
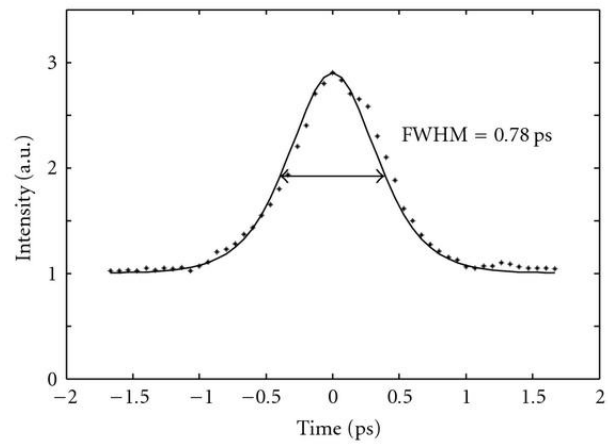
Figure 5.14: Intensity autocorrelation trace of generated pulse with pump current of 1.3A.
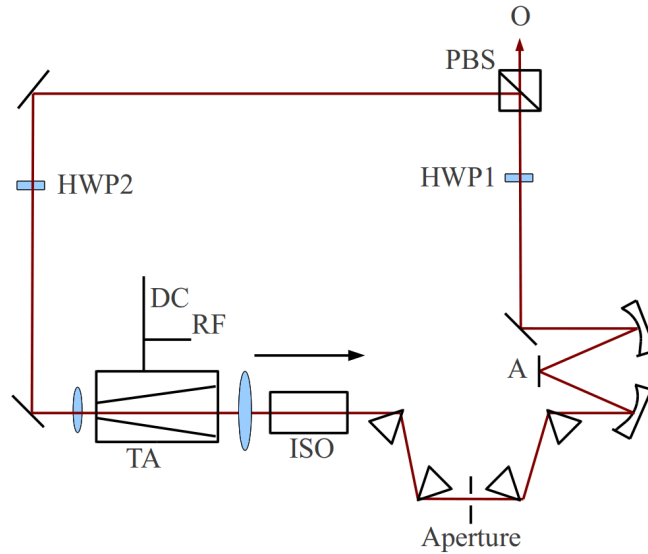
Figure 5.15: Schematic of hybrid mode-locked external ring cavity semiconductor laser with prism inserted. For mirror A, a normal mirror was used in cw configuration and a multiple quantum well mirror for mode-locking as before. The aperture was placed on a translation stage and had a width of 1mm.

The large tunability of the TA from about 40nm (according to manufacturer specification) can be used to tune the laser cavity by inserting two prism pairs. After the first pair, the spectrum is spread out and a slit on a translation stage is inserted for wavelength selection (fig. 5.15). The tuning characteristics are shown in fig. 5.16. It shows a range of operation of 20nm in CW case and 10nm for mode-locking. The discrepancy between the manufacturers specification and our cavity are fairly large. This can be partially due to limited bandwidth of the mirror coatings and the distributed Bragg reflector (DBR) of the MQW.

Even though the TA is a novel and great device (1.4kW peak power, 0.68nJ pulse energy and 60mW outputpower), it has limited use to pump the OPO. The TA's pulse energy is too low to pump the OPO. The pulse energy is limited by the comparably short lifetime of the excited electrons in the TA. The short lifetime
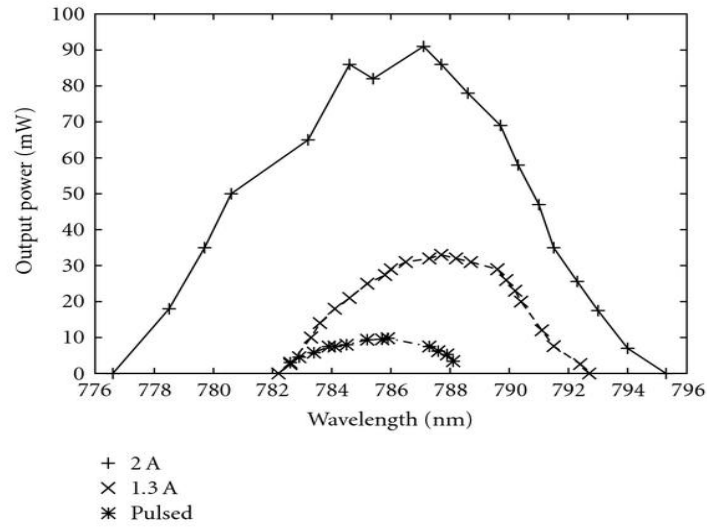
Figure 5.16: Output power versus wavelength for the cw laser at 2A (+), 1.3A (x), and for the mode-locked operation at 1.3A. The TA temperature is set at T=28.5°C
.

limits the amount of energy that can be stored in the TA at a given pump current. Since it is on the order of 1 nanosecond, decreasing the repetition rate below 1GHz will not result in an increase in pulse energy. A continuous wave output power of 1W (maximum output power at 795nm for comercially available TA diodes) would thus leads to a maximum pulse energy of about 1nJ. However, 2 nJ are normally needed for pumping an OPO. The pulse energy is the most important factor if ideal experimental conditions are achieved: length of the crystal is matched to the focusing optics and the walk-off (see Appendix A).

5.4.2 VECSEL

The limitation of the TA prompted looking at other approaches with semiconductor laser devices. One alternate approach, building a 795nm vertical external cavity semiconductor laser (VECSEL), was attempted due to Pulaski's big success using a ring MQW laser pumped with a dye laser [22] and the Keller and Tropper groups' success with optically pumped VECSEL devices used in CW and mode-locked configuration at the 980nm and 808nm region. Even though ultimately building a laser at that wavelength was unsuccessful, the related data is useful as a reference.

Darwin Serkland from the Sandia National Labs designed and grew a first sample batch for us with MOCVD. In Appendix B, the design is outlined. On a GaAs substrate, first 40 alternating layers of 100% AlGaAs of 659.1A thickness and 25% AlGaAs of 569.0A where grown for the DBR mirror centered at 795nm. For the gain medium, a stack for 10 quantum well sections where used. The barriers where optically pumped at a wavelength below 680nm. On top, an anti-reflection coating was applied to avoid a Fabry-Perot self lasing of the device.

A simulation of the index and electric field is shown in fig. 5.17. The anti-nodes co-align with the quantum well gain structure for maximum gain. Also the center of the gain is designed such that the gain peak is at a slightly lower wavelength than the mirror peak taking into account the expected wavelength shift of 0.3nm/K due to the heating of the sample. A photoluminescence (PL) measurement verified the offset of the two peaks, (fig. 5.19). A simple two mirror cavity (DBR and curved mirror as end mirrors) was used (fig. 5.18).

For pumping, a fiber coupled diode laser (650nm, 2W maximum outputpower) was focused onto the sample. The spot size was estimated to be 500μm. After excessive alignment adjustments, the device did not lase for several reasons.
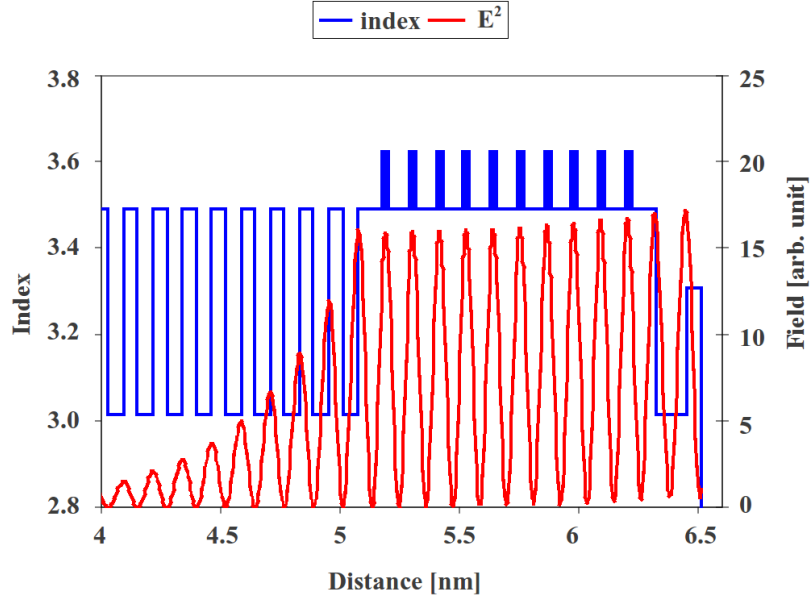
Figure 5.17: The index simulation and electric field is plotted.

One of the possible reasons is heating. Several experimental and theoretical studies of the problem show that gluing or optically contacting the sample to a window made out of Sapphire, Diamond or Silicon Carbide will significantly increase the heat dissipation and help with the threshold of the cavity. One of the samples was bonded to a Sapphire window with optical resin. The bonding was not optimal since rings where visible between the sample and the window. However, in the center, a region of good bonding was available. Even with this approach, still no lasing was observed. This might imply that the PL peak (maximum gain) is too far off of the DBR spectrum, which is creating too much loss for laser operation.

The next approach was using the gain medium in transmission, rather than in
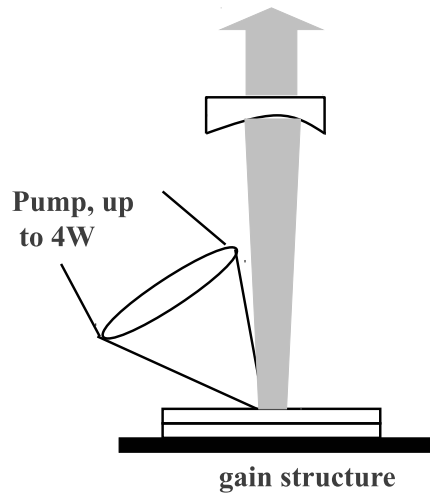
Figure 5.18: VECSEL pumping geometry: as pump two 2W, fiber coupled, 670nm diode lasers were used.

reflection, e.g no DBR needed. A sapphire window was coated and wedged on on side. The semiconductor sample, grown by Andreas Stintz, was removed from the substrate and bonded to the coated side of the Ti:Sapphire. The coating was designed such that the whole sample could be used at Brewster angle to minimize the losses during transmission (for more details, see the thesis of Andreas Velten [36]). Up to date we have not been able to achieve any lasing for our 795nm VECSELs.
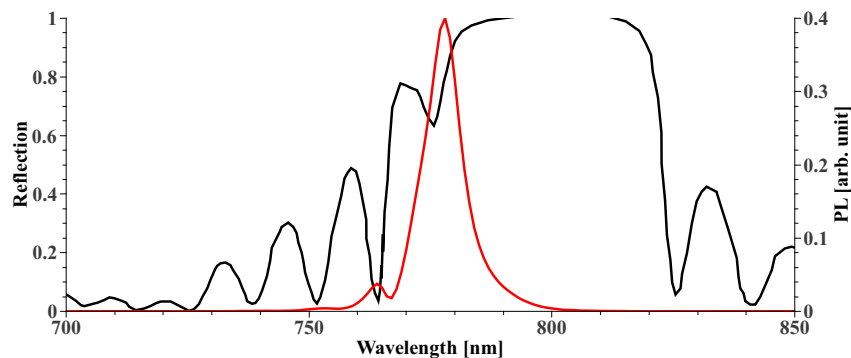
Figure 5.19: Spectrum of mirror and photoluminescence peak are shown

5.5   Summary

In this chapter the data shows it is possible to create two independent pulse trains inside the OPO cavity with only a unidirectional pumping scheme. This is achieved by changing the length of the OPO cavity to a common multiple of the pump cavity length, harmonic pumping scheme. Harmonic pumping can be applied to any number of pulses inside the cavity, limited by the occupied space e.g. pulsewidth. Kokabee et al [46] have built an OPO with a repetition rate upto 16GHz. The experiment presented in the dissertation achieved a very stable operation shown by the narrow bandwidth of the beatnote frequency taken over 2s. This bandwidth was pushed even further down to 0.17Hz by Andreas Velten [36, 47]. Translated in length measurement, it corresponded to 3fm or resolution. Besides measurement of the electro-optical coefficient shown in figure 5.4, this can be used to measure non-linear index of samples placed inside the cavity.

Two semiconductor lasers are discussed as possible alternatives for a OPO pump source, the tapered amplifier and the VECSEL. The TA is able to produce a stable pulse train with fairly high output power and short pulse width (1.4kW peak power, 0.68nJ pulse energy, 60mW outputpower and 500fs pulse length) but has limited use for pumping the OPO because the required energy for pumping the OPO can not be achieved due to the short life time of the gain. The required energy for pumping the OPO can not be achieved due to the short life time of the gain. The energy limitation problem prompted looking at the VECSEL. Efforts are described in this chapter to build a optical pumped VECSEL at 795nm wavelength. To date we have not been able to achieve any lasing for our 795nm VECSELs. Possible reasons are flaws in the specific design and unsolved heating problems. Nevertheless a VECSEL at that wavelength should be possbile.

Chapter 6

Application of IPI to Magnetometry

6.1 Introduction

The work presented in this chapter discusses applying the precise sensitivity of mode locked lasers to phase perturbations as described in Chapter 4. As detailed below the magnetic field acting on an intracavity sample is converted into a frequency, proportional to the field to be measured. It is one of the various applications of IPI [27], in which a phase difference between two pulse trains is directly converted to a frequency, rather than the convential amplitude change, as discussed in the previous chapters. This demonstration experiment is performed with a bidirectional mode locked ring laser, designed so the two counter circulating pulses have the same repetition rate $1/\tau_{RT}$, forcing them to meet at the same crossing point at each round-trip. The two pulse trains generated by this laser have the same pulse period τ_{rt}, but not necessarily the same carrier frequency $\nu = 1/T$ where T is the light period. Therefore, they can be made to interfere on a detector, creating a beatnote at the

frequency $\Delta\nu = \nu_c - \nu_{cc}$. Note that for the same carrier frequency, this beatnote frequency can also be expressed as the difference in carrier to envelope offset frequencies (CEO) f_0 of either pulse train: $\Delta\nu = f_{0,c} - f_{0,cc}$. The CEO of a pulse train is the difference in carrier to envelope phase of two consequtive pulses ϕ_{CEP}, divided by the pulse period: $f_{0,i} = \Delta\phi_{CEP,i}/(2\pi\tau_{RT})$, and corresponds to the lowest frequency mode of the extended comb [27, 48]. The large signal to noise ratio of the beatnote observed in IPI stems from the fact that the teeth of the frequency comb of a mode-locked laser are rigorously equally spaced. Thus every mode of the clockwise pulse train produces the same beat frequency $\Delta\nu$ with a corresponding mode of the counter-clockwise pulse. The principle of intracavity phase to frequency conversion in mode-locked lasers has been exploited to measure rotation, electro-optic coefficients, and a nonlinear refractive index [36]. The experiment presented here shows that a magnetic field causes a phase shift $\Delta\phi_{CEP}$ between two intracavity pulses, resulting in a measurable frequency difference $\Delta\nu$ between the two corresponding pulse trains emitted by the laser.

This chapter discusses new applications of IPI measuring phaseshift instead of amplitude–optical magnetometry that could possibly provide better magnetic field measurements.

6.2   Faraday Rotation

The conversion of a magnetic field into a differential phase shift employs the Faraday effect, by which left or right handed circular polarization experiences a different optical path

$$(n_+ - n_-)\ell = \Delta n\ell, \tag{6.1}$$

when propagating in a material along the direction of a magnetic field. n_+ and n_- are respectively the indices of refraction corresponding to either circular polarization. The difference in optical path implies a phase difference

$$\Delta\varphi = 2\pi\Delta n\ell/\lambda \tag{6.2}$$

at each round trip for the circulating pulses. This differential phase shift results also in a rotation of a linear polarized beam, usually quoted in degrees: $\theta = 180°\Delta n\ell/\lambda$. The tradition of measuring the Faraday effect through polarization rotation is so deeply entrenched that the physical constant associated to this effect is the Verdet constant $V = \theta/(\ell B)$, expressed in degrees/(unit length $\times$ unit of magnetic flux density).

The phase difference $\Delta\varphi$ per round-trip τ_{rt} results in a relative shift in mode frequency (or CEO shift) between the two counter propagating frequency combs of:

$$\Delta\nu \quad = \quad \frac{\Delta\varphi}{2\pi\tau_{RT}} = \frac{VB\ell}{180° \ \tau_{RT}} \tag{6.3}$$

Unlike the traditional measurement of Faraday rotation, the measurement of a beat frequency is independent of the amplitude of the laser, hence is not affected by amplitude noise. The improvement of signal to noise brought by IPI is similar to the one brought by FM over AM modulation in radio communication.

6.3 Proof of Principle Experiment

A proof of principle experiment is presented, using a Ti:sapphire ring laser mode-locked by a dye jet as saturable absorber (Hexa-Indo Tri- Carbocyanine Iodide or HITCI dissolved in Ethylene Glycol). This is not the ideal laser system for such an application, but the easiest to implement. Other possible laser systems will be discussed in Section 6.5. The requirement that the two pulse envelopes overlap at a
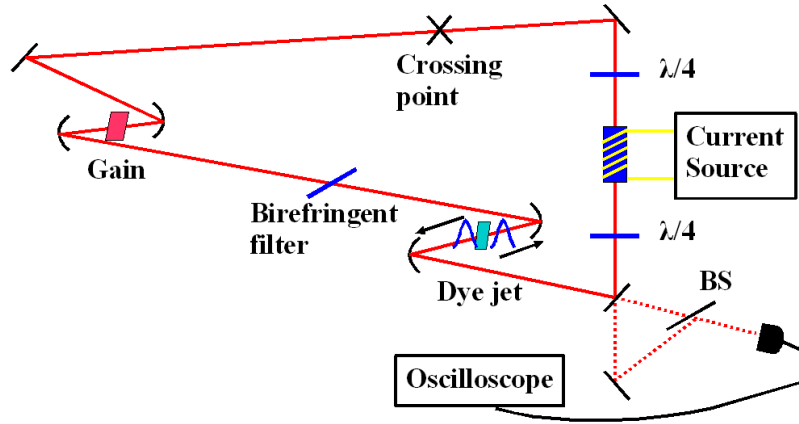
Figure 6.1: Experimental Setup: Ti:Sapphire cavity with dye jet as saturable absorber and a birefringent filter for wavelength tuning. The cross indicates a pulse crossing point half way around from the dye jet. The sample with solenoid is placed between two quarter wave plates. A delay line (dotted lines) overlaps the two counter propagating pulses at a detector

fixed crossing point, at each round-trip, is satisfied with a flowing saturable absorber jet, which tends to modify the group delay to center the envelopes in the absorber [27], without introducing any phase or frequency coupling between the two pulses. The magnetic probe is placed between two quarter wave plates. The magnetic probes used are rods of $\ell = 9$ mm BK7, and $\ell = 10$ mm Terbium Gallium Garnet (TGG), both anti-reflection coated for 790nm. The magnetic field is generated by a solenoid with 17 windings wrapped around the different samples. The probes are shielded with Mu metal from other contributions, such as the earth's magnetic field. The magnetic field is assumed to be uniform along the propagation axis and across the beam size, which is much smaller than the sample diameter. The laser generates two

trains of 30 ps (FWHM) pulses at a repetition rate of 125MHz and a wavelength of 790 nm.

The method is sufficiently sensitive to easily measure the Faraday effect in BK7, as illustrated by the linear relationship between the beat note and magnetic field in Fig. 6.2. A similar measurement made with a 1 cm long TGG crystal, typical material used in Faraday isolators, is shown in Fig. 6.3. A slope of 30nT/Hz is observed which corresponds indeed to the published Verdet constant at 790nm of 4.5×10^3 ^{o}T^{-1}m^{-1} [49]. The larger error is in determining the magnetic field strength due to imperfect shielding of the sample. Contributions to the error are from the earth magnetic fields and magnetized parts of the optical table. The TGG sample (5mm) is smaller in diameter then BK7 (25.4mm), therefor a better shielding is achieved and the error is estimated to be smaller.
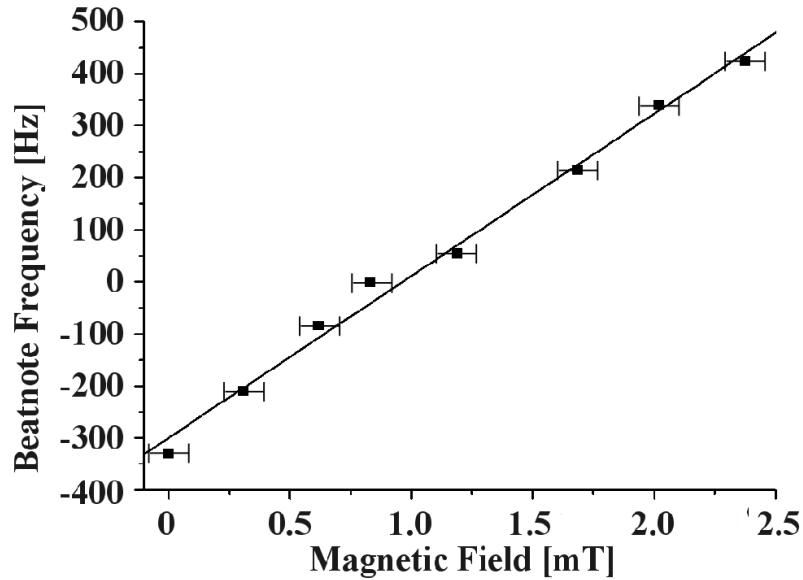
Figure 6.2: Beat frequency versus magnetic flux along a 9mm long rod of BK7. Verdet constant for Bk7: V=166 ^{o} T^{-1}m^{-1} at 800nm [1].
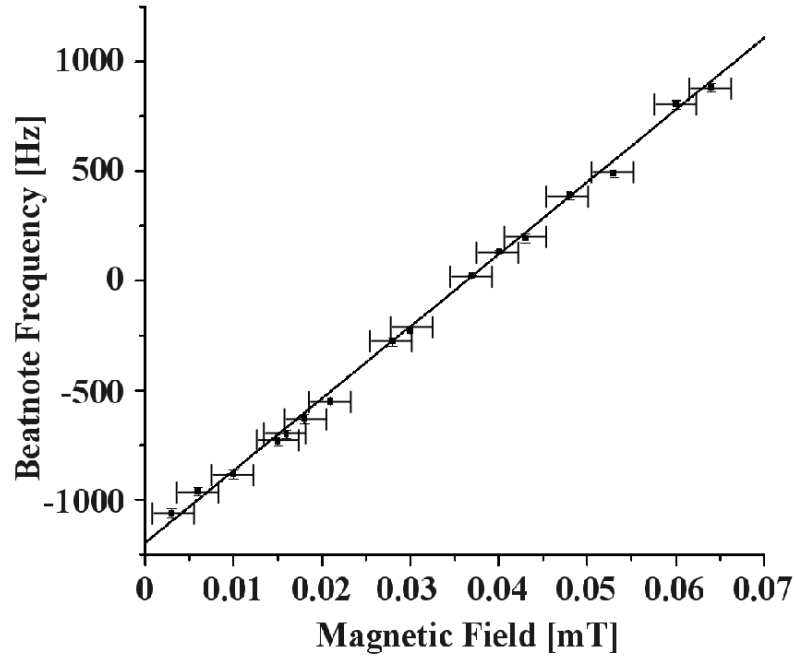
Figure 6.3: Beat frequency versus magnetic flux along a 1cm long crystal of TGG

6.4 Resolution, Sensitivity and Accuracy

6.4.1 Resolution and Sensitivity

A measure of the resolution is given by the bandwidth of the beatnote. The Fourier transformation of a beatnote recorded over a time of more than 2s, is plotted in Fig. 6.4, showing a bandwidth of 1 Hz. The change in magnetic field scale is indicated on the top of the figure. With such a narrow bandwidth, a field variation of 10 nT (which is 1/3 of the bandwidth) can be resolved. A variation of 10 nT corresponds to only 8×10^{-9} rad, which is one order of magnitude less than the smallest measurable polarization rotation measurable with other techniques [50].
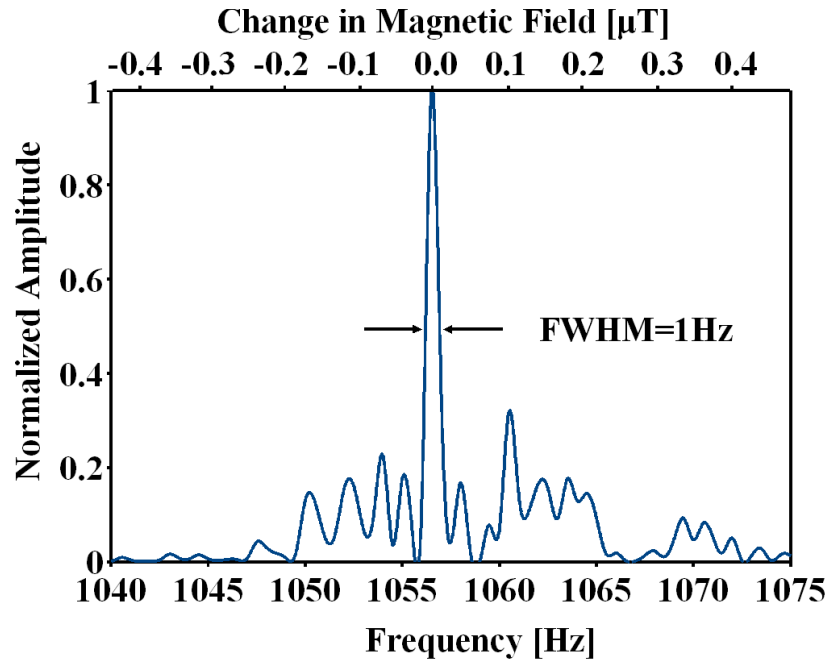
Figure 6.4: Fourier transformation of beat note signal. The FWHM is indicated to be 1Hz

The bandwidth of the beat note, for this particular ring laser, has the following contributions:

1. Fresnel drag caused by air currents

2. Gyroscopic response (Sagnac effect)

3. Mirror vibration

4. Schawlow-Townes linewidth

The contribution of the Fresnel drag is important but can be reduced by enclosing the beams, and even eliminated by putting the cavity in helium or vacuum. The gyroscopic response can be eliminated by using a figure 8 cavity, which is a "zero area"

cavity. The importance of the contribution from mirror vibration can be assessed by considering that random displacements of 1 pm displacement of a mirror in 10 ns would broaden the beat note bandwidth to 120 Hz (such a displacement corresponds to a resonant mechanical vibration at 100 Hz of 1 micron amplitude). In the case of a linear optical parametric oscillator cavity of the same length, with two circulating pulses, the first two contributions are eliminated (because each of the intracavity pulses goes through the same cavity element in the same sequence). A beat note bandwidth of 0.17 Hz is measured [36]. Even without considering active stabilization, this bandwidth can be further decreased by reducing the size of the laser, for instance from 3 meter perimeter down to 30 cm, making it possible to gain in mechanical stiffness, leading to a resolution of the order of 0.01 Hz in beat note bandwidth, which is eventually limited by the Schawlow-Townes linewidth of the laser. For the current system we estimated a linewidth of a few mHz (high Q cavity with overall loss of 2% and an intracavity power of 4W) [51].

A reduction in size increases the *sensitivity* of the magnetic field measurement, since the frequency to be measured is, according to Eq. (6.3), inversely proportional to the cavity round-trip time. It can therefore be estimated that a 30 cm perimeter cavity, with the same TGG sample, would resolve a change in magnetic flux of 100 pT.

6.4.2   Accuracy

As can be seen from Figs. 6.2 and 6.3, there is a "bias beatnote" at zero applied magnetic field. One contribution is from the earth magnetic field that is not completely shielded off. There is, however, a contribution to the beatnote at zero magnetic field when the two counter-circulating pulses do not have the same intensities due to difference in power. As the two counter-circulating pulses traverse the gain medium,

or any cavity element of length d, a differential phase shift $\Delta\varphi = 2\pi n_2(I_+ - I_-)d/\lambda$ (where I_+ and I_- are the intensities of the two counter-circulating beams in that element) is introduced, which will contribute to the beat note. The arrangement of Fig. 6.1 has in fact been used [36] as the most sensitive device for measuring a nonlinear index of refraction. For an absolute magnetic field measurement, the laser would have to be stabilized and a zero intensity difference between the counter-circulating pulses would have to be maintained. Another option is to calibrate independently the laser in zero magnetic field to determine the bias.

In addition to making an absolute magnetic flux measurement difficult, the nonlinearities affect indirectly the beat note bandwidth, by introducing a contribution to the beat note bandwidth from differential intensity fluctuations.

6.5   Improved systems

The Ti:sapphire laser used in these preliminary demonstration experiments is not a practical system, in view of the dye jet used as saturable absorber. Other laser systems can also provide a bidirectional operation without phase coupling between the two counter-circulating pulses, as needed for IPI experiments. Most promising is the synchronously pumped OPO (either external cavity or intracavity as discussed in Chapter 5) for which a beat note bandwidth of 0.17 Hz has been measured. Miniaturization of these lasers is not the only way to improve their sensitivity and resolution. Another improvement is to substitute for the TGG crystal an atomic vapor, which could bring another factor 1000 improvement [52, 53] or better (see Chapter 8.2). Magnetometers based on coherent population trapping are particularly well adapted to IPI detection scheme. The coherent population trapping can be tuned in by making the repetition rate of the mode-locked laser match a submultiple of the hyperfine splitting of, for example, Rb87 [27]. Another approach to atomic vapor

magnetometry relies on nuclear spin resonance [54]. The final detection in the later approach is still based on Faraday rotation, which can be replaced by the method of IPI presented in this paper.

6.6   Conclusion and Discussion

A sensitive magnetic field measurement has been presented which exploits the CEO change for two counter propagating pulses inside a ring cavity. A change of 10nT in magnetic field can be resolved which corresponds to a polarization rotation of the order of 10^{-9}rad.

More work can be done on this project. As discussed above, using atomic vapor as magnetic sensor material is the next step to improve the system. But more can be done with this experiment.

Also using fiber laser technology, one can make an all-fiber magnetometer. In our group, it was shown that one can can build a bidirectional mode-locked ring cavity, useful for IPI measurements [55]. Incorporating hollow-core-fibers (HCF), filled with atomic vapor would make this a small, portable and useful magnetometer. Ghosh et al [56] showed that specially coated HCF can be filled with atomic vapor and coherent interaction experiment can be performed. The length of the interaction allows for low vapor concentration as well as low light concentration. Even using opposing polarization of the two pulse trains in the fiber laser would allow for a linear cavity without having to worry about the coupling between two pulse trains avoiding the deadband. Work is in progress to build such a device.

Chapter 7

Limit to the Beatnote Linewidth

7.1 Introduction

The following chapter discusses the noise contribution to the beat note measurement
and the ultimate bandwidth that could be achieved. The discussion includes review-
ing previous work on linewidth broadening origins in the frequency comb mode as
well as the coupling between repetition rate and phase fluctuations, gain coupling
and center wavelength drifts in a mode-locked laser.

Meng [8] already mentioned that squeezed states may be used to exceed the classical
limit of the beatnote bandwidth. Since squeezing requires using non-linear processes,
like OPO, the OPO used for IPI may be a way to conduct squeezing because squeez-
ing could minimize the phase noise in the beat note measurement. However, a better
understanding of the limit is required, prior to using OPO for squeezing. Although
this Chapter will discuss the limit on the beat note bandwidth, implementing squeez-
ing experimentally or how it improves the limit will not be covered.

7.2 Influence of the Cavity Length on the beatnote

Shorter cavity lengths theoretically improve the sensitivity of IPI by more sensitive beatnotes measurements. As previously stated, vibrations of cavity mirrors can be linked to the 1Hz bandwidth of the beatnote. A very simple derivation links the change in cavity length ΔL to the beatnote:

$$\frac{\Delta \nu}{\nu} = \frac{\Delta L}{L} \tag{7.1}$$

A 1 Hz bandwidth with a cavity length of 3m means that the change of cavity length that can occur in the time-interval between the two pulses is 0.01pm. Vibrations of 10Hz with an amplitude in the order of 0.1μm will result in this change. This is not the only mechanical instability in the system.

For ring lasers, especially the previous described magnetometer experiment, changes in the air currents, even with an enclosed laser system, will affect the beatnote bandwidth [57]. Here the change in cavity length can be expressed as the air current:

$$\Delta L = 2(n^2 - 1)\frac{lv}{c} \tag{7.2}$$

where n is the refractive index of the gas and v is the speed of this medium. A 0.01pm change in cavity length would mean an average air speed over the length of the cavity of 0.94×10^{-5}m/s. The index of refraction of air at 800nm is n=1.000267 [58]. In linear cavities, this does not play a big role since both pulses will always share the same path over the roundtrip time. It is an important factor in the ring

laser: simply blowing air through the beam path results in a large beat note change.

Overall, mathematically the change in beatnote versus the change in rountrip time also plays an important role. Taking the first derivative of the beatnote signal with respect to the roundtrip time allows for a better analysis of the problem,

$$d\Delta\nu = -\frac{\Delta\varphi}{2\pi\tau_{RT}^2}d\tau_{RT} = \Delta\nu\frac{\Delta\tau_{RT}}{\tau_{RT}}. \tag{7.3}$$

For the free running Ti:Sapphire, the fluctuation of the repetition rate are normally several kHz in one second which can be observed with a standard frequency counter. A 1kHz change in repetition rate means a timing jitter of 20ps for a 100MHz laser over 1s. This translates into a change in beatnote of 0.32mHz bandwidth. This calculation assumes a phase sensitivity that is currently seen by the experiments of 1×10^{-8}rad. Hence a repetition rate stabilization of the cavity itself is not needed until all the other mechanical noise contributions are completely eliminated.

For a synchronously pumped OPO, the cavity length can change without the change in repetition rate. For the small changes caused by various perturbations, the group velocity v_g of the pulse can self adjust such that the overall repetition rate is the same by adjusting the center frequency of the pulse and therefore the speed it travels through the cavity. This is especially true for the synchronously pumped OPO, where the repetition rate is predetermined by the pump cavity.

7.3 Schawlow-Townes Linewidth

The Schawlow-Townes linewidth determines the resolution of IPI. There are several publications about the linewidth of a frequency comb concluding that the theoretical limit is the Shawlow-Townes linewidth [51, 59]. In the first order, the linewidth can be described by a modified Schawlow-Townes formula for CW lasers [60]. The

Schawlow-Townes linewidth is thus primarily the cavity round trip frequency, the ratio of the photon energy to the intra-cavity energy,

$$\Delta\nu_{ST} = \frac{h\nu\theta l_{tot}T_{OC}}{4\pi\tau_{RT}^2 P_{out,av}} = \theta l_{tot}\left[\frac{1}{\tau_{RT}}\frac{h\nu}{W_{cav}}\right] \tag{7.4}$$

where l_{tot} is the total loss of the cavity, T_{OC} is the transmission of the output coupler and $P_{out,av}$ the average output power of the laser itself. $\theta \approx \frac{N_2}{N_2-N_1}$, where N_i is the population of the lower (1) or upper state [61], is the spontaneous emission factor and in generally ≥ 1 for a four-level system due to the low population in the lower lasing state.

For three-level systems and quasi-three level systems (the two lower levels of the four levels are close enough such that the thermal energy is enough to occupy the lower laser level) spontaneous emission is much stronger and harder pumping is needed to achieve the same gain due to the higher ground state population and therefore θ is larger than 1. For semiconductors, another modification has to be considered. The linewidth enhancement factor α is a measure of coupling the phase noise to the intensity. Therefore Equation 7.4 has to be multiplied by a factor of $(1+\alpha)$. In the CW case, the linewidth is interpreted as the contribution of spontaneous emission of the gain medium into the CW beam as well as coupling of quantum noise through the mirrors of the cavity. This phase noise will then broaden the linewidth of the laser. It is the same for a mode-locked laser. However Paschotta et al [51] showed that this is only true for the modes close to the center frequency for a passively mode-locked laser and generally true for an active mode-locked system. At the wings of the comb the linewidth increases due to quantum noise induced timing jitter. Menyuk et al [62] and Wahlstrand et al [63, 64] also showed that the linewidth increased in the wings of the comb.

Equ. 7.4, was used to estimate the linewidth (at the center frequency) for the experiment. Our typical Ti:Sapphire is a four level system gain medium, therefore $\theta = 1$. Normally the experiment used a high Q-cavity laser with low losses. All the elements are at Brewster angle and use high reflective mirrors typically with a R>99%. Overall one can estimate the losses total 5%. An average output power is about only a few hundreds of μW to a few mW, depending on the pump power used. Typically the cavity operates far above threshold. For the output a 1% reflection of one of the Brewster angle oriented elements was used e.g. prism, electro-optical modulator or beam splitter. For this chapter 1mW was used. Rountrip time of a typical laser is 10ns and the center wavelength 800nm. This leads to a $\Delta\nu_{ST}$ of 100μHz for such a Ti:Sapphire system.

In Equation 7.4, a limitation hampers the sensitivity of IPI. Decreasing the cavity length increases the repetition rate and inherently increases the sensitivity of the measurement because the beatnote signal is inversely proportional to the round trip time. However the Schawlow-Townes linewidth is also inversely proportional to the roundtrip time for constant energy and to the square of the rountrip time for constant output power. If the energy is kept constant, than the Schawlow-Townes linewidth is inversely proportional to the roundtrip time. This implies harder pumping is needed. In the case of the Ti:Sapphire, this problem can be neglected since the Schawlow-Townes linewidth is significantly smaller than the smallest bandwidth ever measured and the crossing point of both curves is in the order of ps round trip time, by far exceeding the technical capabilities.

7.4   Contribution by Other Parameters

Uncorrelated fluctuations in the laser wavelength will eventually play a role in the noise of the IPI signal since dispersion will contribute to the phase shifts we are measuring. So far, no changes have been observed in the center wavelength significant enough to cause any problems. These fluctuations are normally smaller than ± 0.1nm. This observation is limited by the resolution of the spectrometer. But in regards of the linewidth of the IPI signal, the wavelength fluctuations do not play a role. Wahlstrand et al [64] did a detailed analysis of the linear response of a mode-locked Ti:Sapphire laser to perturbation via the formalism of stochastic differential equations.

$$\frac{d\vec{v}}{dt} = -A\vec{v} + \vec{S} \tag{7.5}$$

where v is the transposed vector of all the fluctuations: gain fluctuations Δg, energy fluctuations ΔW, center frequency fluctuations $\Delta \omega_0$, central pulse time $\Delta \tau$ and the phase fluctuations $\Delta \phi$. The vector $\vec{S}$ represents all the noise sources for all the parameters and A is a matrix that couples the change in one parameter to another parameter. Overall 15 differential equations for $\langle \Delta v_i \Delta v_j \rangle$ have to be solved for a complete analysis of the linewidth of the combs as well as the contribution from each individual parameter. Overall, they concluded that for a free running laser, the noise is dominated by the timing jitter. Also the linewidth can vary by a factor of 100 for comb lines as far as 200THz away from the center frequency. However they are concerned with ultrashort pulses, duration of the order of 10fs. In this dissertation experiments, the shortest pulses achieved in IPI are pulse widths of hundreds of fs to ps. This results only in a comb width of 10THz or less and therefore the approximation using the Schawlow-Townes linewidth seems to be adequate. However there is still a need for an exact analysis simulation to determine the exact values for the experiment.

IPI's great advantage over single pulse train measurements is that noise always affects both pulses the same way. Any noise with a time constant longer than the round trip time of the laser does effect both pulses the same way and therefore does not affect the beatnote measurement. This unique attribute is the main reason why the unstabilized, free running lasers have a great performance record. As long as the timing jitter does not change significantly with respect to the beatnote bandwidth, both combs will jitter synchronously and the overall differential phaseshift measurement is not affected over the measurement period. However, long term drifts still will have an impact on the overall performance of the device. Intensity shifts, especially with the Ti:Sapphire, where both pulses do not have the same intensities contribute in a drift of the beatnote frequency offset and therefore make an accurate and absolute measurement difficult. The wavelength of such a system can also drift over several nanometers which will effect the dispersion of the material. This is especially true for the atomic magnetometer. The repetition rate can slip as much as the whole comb separation in the long term. Overall, these long term drifts can be controlled via standard stabilization schemes and by controlling the environment of the laser cavity (e.g. temperature, air flow) and should not be an ultimate limit of IPI.

7.5   Linewidth of an OPO comb

At first glance, OPOs seemed to be significantly different than an ordinary gain medium since no spontaneous emission is present. However different regimes in an OPO have to be considered: "below threshold," "close to threshold," and "above threshold." Graham et al [65] calculated the linewidth, using quantum mechanics for the different regimes for the CW OPO. For the "below threshold" regime, the linewidth of the signal is only dependent on the quantum noise fluctuations of the idler and vice versa, but not dependent on mode noise itself. Approaching "closer

to threshold,"the linewidth behaves like an high gain amplifier or laser that is below threshold. In this "close to threshold" regime, spontaneous conversion of the vacuum noise and the vacuum noise of the signal frequency in the surroundings takes over. In the "above threshold" regime the linewidth becomes an adiabatic diffusion between the pump and the sum of signal and idler phase which results in two terms in the linewidth of the signal: the pump laser linewidth plus the contribution of the spontaneous conversion and quantum noise. This also means that whichever is larger is the dominating factor (see Boyd, Nonlinear Optics [66]).

It is uncertain, how the dominating factors equate to a synchronously pumped OPO, since the above description is for the CW OPO specifically. Assuming the OPO linewidth can be calculated trough the Schawlow-Townes linewidth with Equation 7.4, the linewidth value is 0.31mHz. The experimental conditions in Chapter 5 were used to calculate the linewidth value (output power of 100 μW). Overall, the total losses where about 3%. The center wavelength of the OPO was at 1.5 μm. Compared to the measured linewidth of 0.17Hz, this is only one order of magnitude away from reaching the measurement limit. At a roundtrip time of 2ns, the Schawlow-Townes linewidth becomes larger than the beatnote itself, resulting in a decreased resolution due to the bandwidth. The question remains if ultimately we will be limited by the quantum limit or by the increased sensitivity to the mechanical noise.

In a synchronously pumped OPO, there are more constraints to the system. The repetition rate is only determined by the pump pulse. This can be explained by looking at the amplification process inside the OPO crystal. When the pump pulse is either behind or ahead the OPO pulse, the front or tail of the OPO pulse will not see gain and therefore also slows down or speeds up. Another way to describe this process is by using the dispersion of the OPO cavity. The center frequency of the OPO pulse will shift to always overlap with the pump pulse inside the gain crystal.
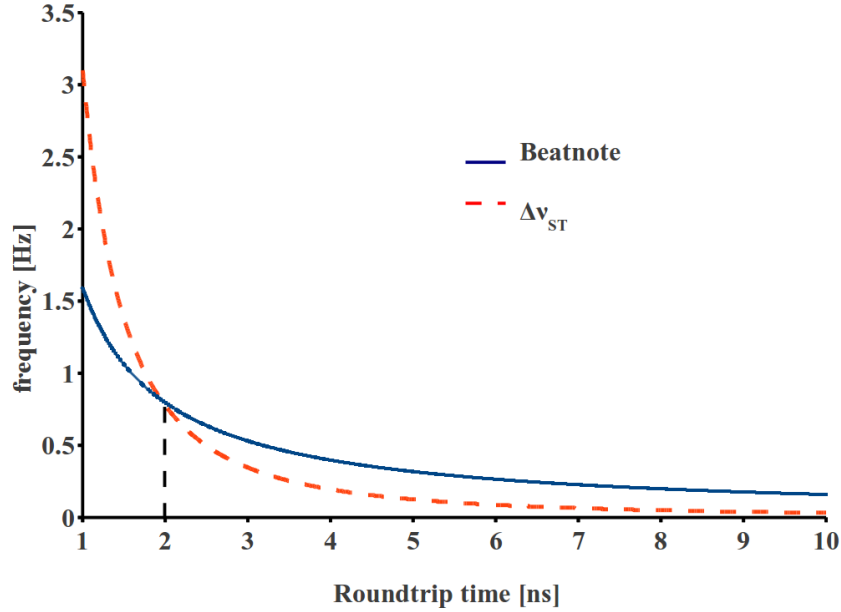
Figure 7.1: OPO cavity: Plotted here is the beatnote signal vs roundtrip time for a constant phase shit of 1×10^{-8} (solid blue) and the Schawlow-Townes linewidth vs the roundtrip time (dashed red) assuming a constant average outputpower.

This only occurs over a short length scale limited by the phase matching condition, mirror reflectivity, dispersion properties of the OPO cavity, and the pulse width. Experimentally one can see this effect of wavelength adjustment by changing the length of the OPO cavity. Normally, we were able to move the end mirror for 200μm in the case of a picosecond pulse, but only a few 10s of μm in the case of a pulse with a few hundreds of femtosecond width. The wavelength adjustment is happening while the repetition rate of the OPO stays the same. This has been characterized before by Dudley et al [67]. Therefore the timing jitter of the OPO is only dependent on the timing jitter of the pump pulse. A more careful investigation by Dudley et al revealed that the timing jitter of the OPO is not only dependent on the timing jitter of the pump pulse. Their OPO was pumped by a mode-locked Ti:sapphire. In the case were the GVD of the OPO cavity was compensated by a pair of prisms the

timing jitter was actually less than that of the pump. They claimed it is partly due to the difference in group velocity (walk-off) and that no spontaneous emission is present. However they also observed, when the GVD was not compensated, an increased timing jitter. This was mainly due to the increase in amplitude fluctuations that couples to the phase of the pulse.

Since the experiment is already measuring a very small bandwidth of the beatnote, the pump timing jitter does not affect the measurement significantly. As already discussed, the change in repetition rate with the Ti:Sapphire laser has only a small effect on the change in beatnote. This insignificant effect is also true for the OPO since the physics have not changed. The difference is that the OPO repetition rate can only fluctuate if the pump repetition rate fluctuates too.

Phase conservation during the parametric conversion process must be considered because phase noise will also be converted and limits IPI measurement [68].

$$\varphi_p = \varphi_i + \varphi_s - \frac{\pi}{2} \tag{7.6}$$

The phase conservation also means that the CEO of the pump has to be conserved.

$$f_{CEO,p} = f_{CEO,i} + f_{CEO,s} \tag{7.7}$$

The idler is created new every round trip in a singly resonant OPO. The CEO of the pump is fixed by its cavity. That means the phase shift introduced by the IPI to the signal has to be imposed onto the idler with a negative sign to still fulfill Equ. 7.7.

$$f_{CEO,p} = (f_{CEO,i} + \frac{\Delta\varphi}{2\pi\tau_{RT}}) + (f_{CEO,s} - \frac{\Delta\varphi}{2\pi\tau_{RT}}) \tag{7.8}$$

Equation 7.8 allows us to measure the beatnote by overlapping two consecutive idler pulses. However, how the phase noise of the pump is compensated must be considered. The restrictions only apply to the sum of the two phases, but not the difference. Also, the signal pulse is restricted even further by its own cavity. Any

pulse to pulse fluctuations in the pump phase can be only absorbed into the idler and therefore should have a broader bandwidth of the beatnote of the idler. Measuring the beatnote of both signal and idler at the same time and analyzing its bandwidth and fluctuations is a simple experiment to set up and will help understand the noise contributions in IPI measuremnets with an OPO.

Again one has to mention that IPI only measures the difference between two pulse trains of the signal. Long term drifts in phase, repetition rate and frequency will affect both pulses the same way and are negligible as long as dispersion of the material used to impose the phase shift can be neglected. The pulse to pulse fluctuations are generally much smaller than the long term effects and should not have a large contribution to the beatnote bandwidth.

7.6   Summary

Before considering using squeezed states with the OPO setup, there is still the need for a better analysis of the actual noise limit of IPI. Futher analysis is needed to calculate and measure all the A_{ij} coefficients in equation 7.5 for the Ti:Sapphire experiment. In theory, the limitation for the linewidth of IPI is the Schawlow-Townes linewidth of a mode-locked laser which is very small for the Ti:Sapphire cavities used in the IPI experiments. The discussion presented in this chapter revealed the reason why our unstabilized laser systems perform very well: noise larger than the round trip time affects both pulses the same way and repetion rate fluctuations have can be neglected.

The Schawlow-Townes formula can be applied to the OPO, assuming that the spontaneous emission is similar to the spontaneous parametric conversion of the vacuum fluctuations. If the Shawlow-Townes linewidth is the limit of the OPO

beatnote bandwith, the measured 0.17Hz linewidth is only one order of magnitude away from the calculated Schawlow-Townes linewidth and the sensitivity cannot be further refined. However, other effectsrepetition rate is only determined by the pump and the sum of the phases between signal and idler is related to the pump phasemust be researched further for potential limits to the beatnote bandwidth and IPI resolution.

Chapter 8

Future Work

8.1   Introduction

In this dissertation, two applications of two-pulse per cavity lasers were presented. First, IPI and the newly developed OPO cavity with great stability was discussed, as well as new IPI applications to optical magnetometry. Second, the two-level analogy reveals previously unexplained dynamics of a Kerr-lens mode-locked ring laser and possible uses as a scattering sensor. In the following chapter, future research work is proposed to improve the optical magnetometry sensitivity with IPI using atomic vapor. A totally different application of IPI is also discussed–using the great displacement resolution to build a phase imaging system, named Scanning Phase Intracavity Nanoscope (SPIN). Finally, a high repetition rate OPO is proposed where multiple pulses are propagating inside the cavity in a harmonical pump scheme. Chapter 5 proved that these pulses are independent from each other. However, by seeding the idler, the phase of the all the signal pulses can be locked which should lead to a high repetition rate OPO comb.

97

8.2 Atomic Magnetometer Using IPI

The proof-of-principle experiment presented in Chapter 6 shows that IPI can be used as an optical magnetometer, measuring phase changes in the order of 10^{-8} rad. As briefly described at the end of that chapter, using atomic media should improve the sensitivity significantly. Several options can be implemented as an atomic magnetometer: the Zeeman effect, spin precession, and coherent population trapping. Each option has been studied extensively before, however they have never been used inside a laser cavity as a magnetometer. In the following sections, each method will be examined in more detail with respect to IPI.

8.2.1 Zeeman Effect

The Zeeman effect describes, when a magnetic field is present, the energy shift and splitting of energy levels with different magnetic moments. The effect is only valid for weak magnetic fields, where spin-orbit coupling is still occurring. For larger magnetic fields, the effect is called the Paschen-Back effect where the spin-orbit coupling is overcome. For even larger fields, the splitting becomes quadratic (non-linear). Sublevel m=1 of a j=0-j=1 transition (see figure 8.1) upon application of a magnetic field with a component B_z along a z-axis, can be written as

$$\Delta E = \mu_B g_f m_f B_z \tag{8.1}$$

where g_f is the hyperfine g-factor accounting for corrections to the dipole-moment, m_f the magnetic quantum number and μ_B their Bohr magneton. The shift in Energy results in a change in the resonance frequency $\omega_0 + \Delta\omega = (E + \Delta E)/\hbar$ If the magnetic field is measured through Faraday rotation, one can use a classical model to estimate the changes in index of refraction associated with the level shift
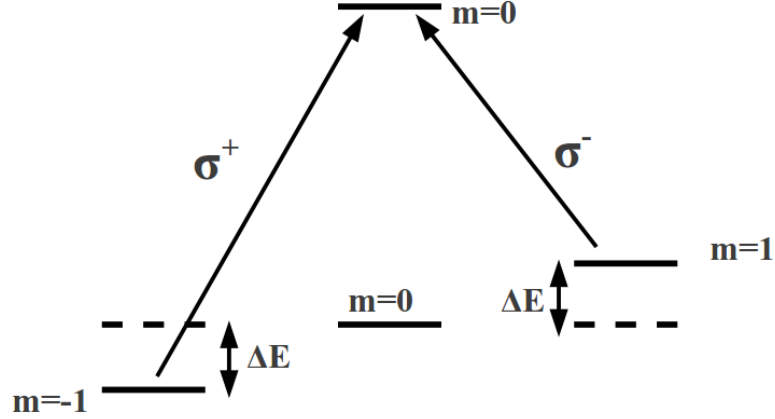
Figure 8.1: Zeeman Energy shift for small magnetic field. σ^- and σ^+ is for left and right circular polarized light. m is the magnetic quantum number

$$n(\omega) = 1 + \frac{Ne^2(\omega_0 - \omega)}{\epsilon_0 m_e \omega_0} \frac{1}{(\omega_0 - \omega)^2 + \Gamma^2} \tag{8.2}$$

where N is the atom density. ϵ_0 the permittivity of free space, e and m_e the charge and the mass of the electron and Γ the damping rate or natural bandwidth of the transition. Assuming an oscillator strength in the order of 1 as well for g_f and m_f, ω being close to resonance, μ_B=9.2×10^{-28}J/T, ϵ_0=8.8×10^{-12}F/m, e=1.6×10^{-19}C, N of 10^{14}cm^{-3}, $m_e = 9.1\times10^{-31}$ kg, Γ in the order of MHz, λ of 10^{-6}m,ω_0 of 10^{15}rad/sec and a sample length L of 1cm allows for an estimation of the change in phase when a magnetic field is applied,

$$\Delta\phi = \frac{2\pi(n(\omega_0 + \Delta\omega) - n(\omega_0 - \Delta\omega))L}{\lambda} \approx 10\frac{rad}{T} \times B_z. \tag{8.3}$$

As seen before, with our unstabilized IPI measurements, a phase shift in the order of 10^{-8} can be measured. This implies a magnetic field of 10^{-9}T when using the Zeeman effect. A problem with a real system is that there is a thermal distribution across all the hyperfine levels due to the Boltzmann distribution e.g. the atoms are

not all polarized. Therefore sensitivity is reduced because not all of the atoms are contributing to the change in refractive index.

8.2.2 Spin Alignment or Optically Pumping

Optical pumping has already been studied extensively with Alkali-atoms in extra cavity settings [54] and it has been shown to be an optical magnetometer with a sensitivity in the order of femto-Tesla and even atto-Tesla called the SERF magnetometer and can be applied to the IPI method.

Besides the effect of total polarization (spin alignment), the increase in the coherence time T_2 up to 1s and longer reduces the bandwidth of the spin precession significantly and therefore gives the high sensitivity of a few femto Tesla. The T_2 time can be modified by reducing the spin relaxation due to the collisions with the cell wall. One collision with a glass wall would lose the spin alignment immediately and the transit time of an atom through the laser beam will determine the linewidth of the measurement. Coating the cell walls with parafine would extend the amount of collisions up to 10,000. Recently, a cell has been constructed where this number was further increased up to 10^6 [69].

The pump (here circular polarized light) aligns all the spins along the k-vector. The magnetic field in the perpendicular direction makes the spin vector precess creating a S_x contribution which is probed with a linear polarized probe beam. Circular dichroinism will result in a rotation of the linear polarization.

8.2.3 Coherent Population Trapping

Coherent population trapping (CPT) and its associated effects like electromagnetic induced transparency and dark states can be used as another technique for optical
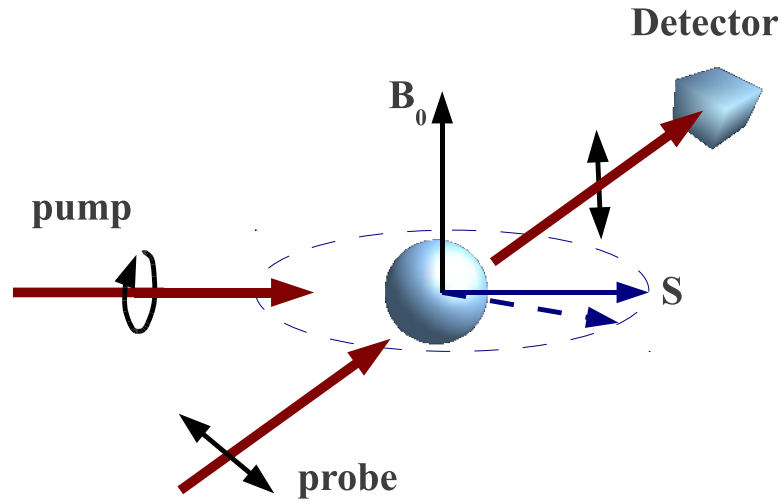
Figure 8.2: The optical pumping scheme used for magnetic field measurement.

magnetometry. Its narrow feature in comparison to the normal Zeeman splitting is making for a much steeper refractive index curve.

An atom that has a *Lambda*-transition (see figure 8.3) is interacting with two CW laser fields which are close to resonance with either of the dipole transition $< 1|$ to $< 3|$ and $< 2|$ to $< 3|$. The two ground states $< 1|$ and $< 2|$ are separated by $\Delta\omega_{12}$ and the transition is dipole disallowed. If the difference between the two laser frequencies matches the energy splitting between the two lower state $\Delta\omega_{12} = \omega_{13} - \omega_{23}$ destructive interference between the two dipole transitions occurs and a reduction in absorption and fluorescence can be observed. Due to the long lifetime of the transition between $< 1|$ and $< 2|$ the linewidth of EIT is much smaller than the Doppler width of the states itself. It is in the order of kHz. formula 8.3 and easily reach femto-Tesla resolution. This has been shown by Kitching's group [52]

.

CPT can also be observed with a pulse train if the repetition rate of the pulse train is a submultiple of the lower state energy separation.[70]. The frequency comb
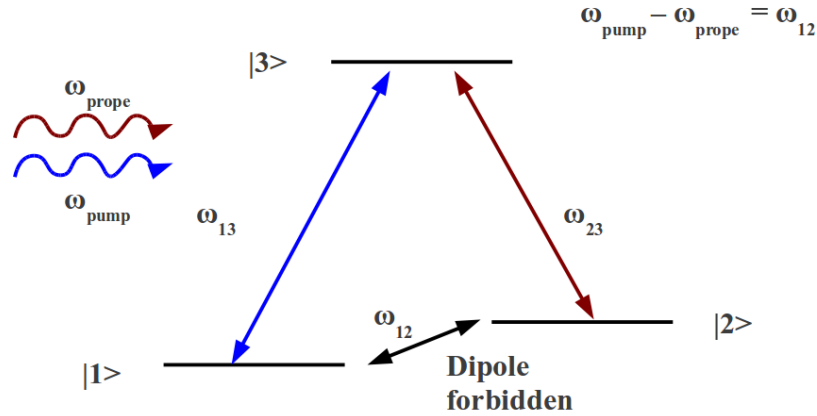
Figure 8.3: A typical Λ transition in an atom is shown

structure provides both frequencies necessary to excite the two transitions and establish the coherence. Experiments have been carried out with Rubidium 87 and its D1 transition at 795nm. When the repetition rate was exactly tuned to a submultiple of the hyperfine splitting of the ground state a dip in the fluorescence was observed. The linewidth of this dark resonance is only 15kHz. This sharp line in absorption implies a very steep change in refractive index which can be used for our magnetometer.

Placing the atomic sample inside the cavity will face several challenges. One, the absorption dynamics of the Rubidium will potentially have an effect on the basic laser operation. The second challenge is the dynamics of the interaction between two opposing polarized pulse trains and the atoms has not been studied yet. Both challenges have to be studied extensively in experiments and with simulations simultaneously to fully understand these dynamics before repetition rate CPT can be applied to IPI and magnetometry.

8.2.4 Sensitivity

Whichever method is used, the sensitivity of magnetic field measurements using atomic vapor is inversely dependent on the density and coherence time [71]. The formula describing the atomic projection noise can be written,

$$\delta B = \frac{1}{g\mu_B} \frac{\hbar}{\sqrt{N\tau T}}, \qquad (8.4)$$

where N is the number of atoms, μ_B the Bohr magneton, g the Lande factor of the ground state, τ the coherence time and T the measuring time assumed to be much larger then τ [71]. Improving the sensitivity for standard optical magnetometer will require either an increase in the density, increase in the coherence time, or increase in measurement time. In addition to the atomic projection noise, the shot noise has to be considered with standard optical magnetometry where an amplitude measurement is performed. For an optimized experiment, both contributions play a crucial role. For the IPI magnetometer, the experiments were not limited by the detector's amplitude shot noise; however,the experiments with IPI using rubidium 87 should be limited by the comb line linewidth as discussed in Chapter 7. Whichever is larger, either the linewidth or the projection noise, will limit the experiment. The experiments done by Ladan Arissian used a rubidium cell, density in the order of 10^{14}cm^{-3}, a coherence time of 10^{-3}s and g=2 for the D1-line, would result in a sensitivity of 10^{-17}T in a measurement over the time of 1s.

Estimating the Verdet constant of the previous published optical magnetometers converts the ultimate limit of Eq. 8.4 into a beatnote. Publications suggest that the Verdet constant for an atomic vapor system is of the order of 100nrad/(ft cm). This converts into a beatnote of 0.15Hz when a 10 cm vapor cell is assumed as well as 10ns roundtrip time and is a factor of 10 below the smalles beatnote bandwidth measured with a Ti:Sapphire laser of 1Hz. As of now in the case of the Ti:Sapphire
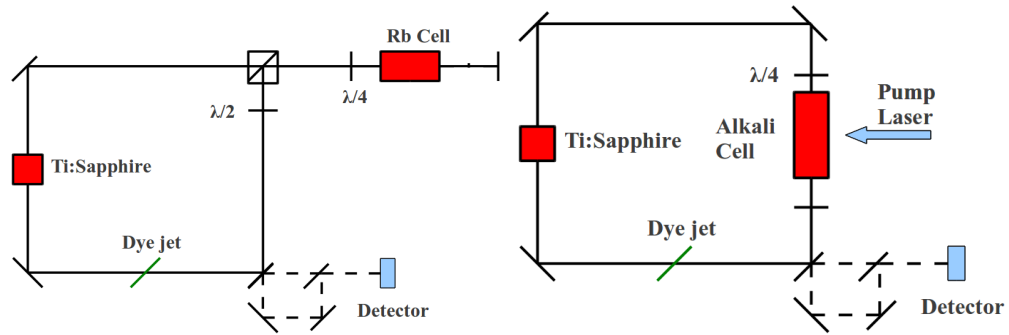
Figure 8.4: Two possible experiments: on the left, the proposed CPT magnetometer using IPI is shown. On the right, the implementation of optical pumping is sketched.

laser we would be still limited by the mechanical noise but a field of 0.1ft should be resolvable. IPI is also limited by the integration time. With the example described here, a 40 second long measurement has to be performed until the projection noise limit is exceeding the Fourier limit.

8.2.5 Experimental Setup

Implementing the three concepts described above is fairly simple. For the Zeeman magnetometer and the optical pumping experiment, the cavity does not have to be changed significantly. The TGG sample has to be replaced with an atomic vapor cell. Either rubidium or potassium can be used for vapor. This is sketched on the right side of figure 8.4.

Another setup is a laser ring cavity with a tail. This is the preferred method for the CPT magnetometer since a co-propagation is needed to avoid problems with the Doppler broadening. For the tail, a polarizing beamsplitter is inserted in the cavity. In the tail section a quarter wave plate and the atomic vapor cell is placed. In one direction, the p-polarization is transmitted through the beamsplitter. On the return path passing the quarter-wave plate a second time, the polarization is rotated by 90°
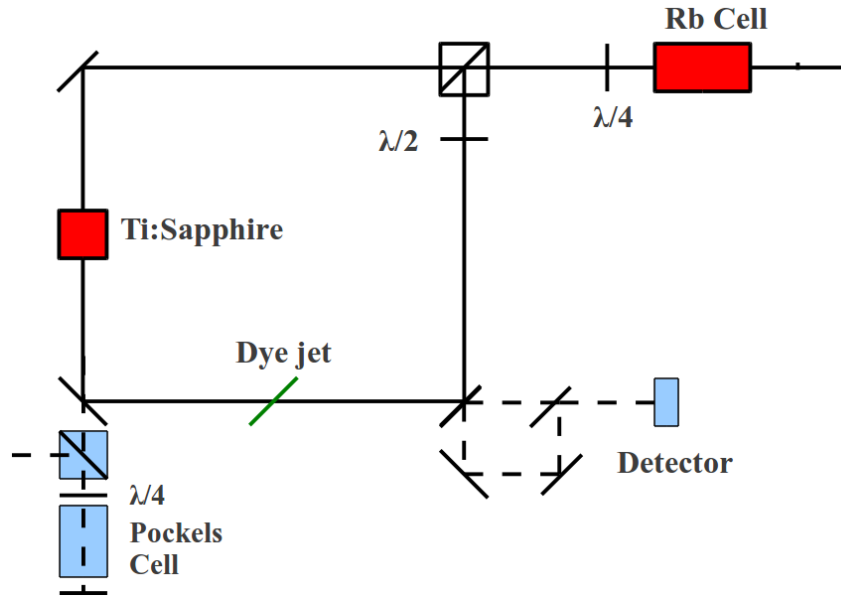
Figure 8.5: Combining the optical pumping and the sensor into one experiment. For pumping, the laser is operating uni-directional. This is done the same way as for the two-level analogy by a feedback. Switching off the feedback, the bi-directional operation can be used to measure the beatnote introduced by magnetic field.

to s-polarization and reflected by the beamsplitter. A half-wave plate is needed to rotate its polarization back to preferred orientation. The counter-propagating pulse is transversing the elements in reverse order.

A third setup might also be possible. Uni-directional control of the two-level system can be used to eliminate the CW-pumping laser needed for the spin-alignment or optical pumping experiment. In this case, the spins are aligned along the propagating light axis. A magnetic field along the propagation axis will also lead to a projection of the spin in the x-direction (S_x) that can be probed by the two opposed circular polarized pulse trains.

8.3 SPIN: Scanning Phase Intracavity Nanoscope

Another proposed IPI application is a phase imaging system for weakly reflecting biological samples. SPIN is an alternative to classical imaging systems, imited by the diffraction limit, $\lambda/2n_A$ where n_A is the numerical aperture of the microscope objective. Standard imaging systems can be further improved by using non-linear light techniques such as non-linear fluorescence and fluorescence labeling of individual molecules. However, the techniques limit the observation region to only certain parts of cells and molecules of interest, potentially loosing the big picture. For high-resolution imaging, electron microscopes can be used. High resolution, few nanometers, can easily be reached. The disadvantage is that thin samples have to be prepared, which kills the living sample and no in-vivo imaging can be done. Using IPI with its sub-wavelength displacement resolution as an imaging system would address both issues simultaneously: high depth resolution and in-vivo.

The idea is to use a linear cavity as shown in figure 8.6. A modulator is placed inside the cavity to change the polarization of one circulating pulse with respect to the other one. A beamsplitter diverts the two pulses into two different arms of the cavity, the sample arm and the reference arm. A beatnote is detected due to the difference in path length between the two arms. Placing the sample on a x-y translation stage allows for a phase map of the sample that can be converted into a 2-D image.

The resolution in the transverse direction is limited by the beam size to a few micrometers. One method to achieve transverse resolution is tomographic reconstruction. Another method is to combine SPIN with a second imaging technique.One ccan ues as second imaging technique, an off-axis, coherent illumination for the extension of imaging interferometric microscopy, as proposed by Neumann et al [72]. This technique collects higher diffraction orders from an illuminating beam, overlap them with the 0th-order of a reference beam, and image both together. The coverage of the spatial frequencies of the image is increased with the higher orders and more infor-
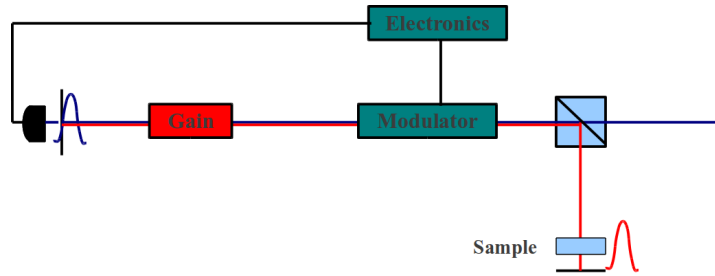
Figure 8.6: SPIN configuration: the pulses are split into two different arms, the reference and the sample arm. The beatnote is created by the change in path length due to the sample. The modulator is driven by the pulse repetition rate. Several schemes for this are possible.

mation can be extracted with an appropriate recovery algorithm. The transverse resolution of such a setup is estimated to be $\lambda/4$. Combining SPIN setup and the off-axis imaging system can be achieved by using the illumination method (interference of grazing and small illumination incidences of figure 3.b in reference [72] with the 0th order illumination as intracavity laser beam. For the illuminating beam, part of the pulse is coupled out and send to the sample with the proper delay (see fig. 8.7). Both beams have to be collected behing the sample and the image can be reconstructed. In this configuration, SPIN is providing the depth resolution and the off-axis coherent imaging system, the transverse resolution. Additional flexibility is proovided with a half-sphere on top of the sample wich would allow illumination from different angles of both beams.

The two arm configuration has already been shown to work with a a vanadate laser mode-locked with a MQW [73]. A displacement of 3nm of the end mirror in one arm resulted in a 1kHz change of beatnote. The scattering of the stationary MQW introduced a large deadband limiting the usefulness of this laser. A better solution for studying the performance of such a cavity design in regards of a phase imaging system is a linear Ti:Sapphire cavity mode-locked with a saturable absorber dye jet
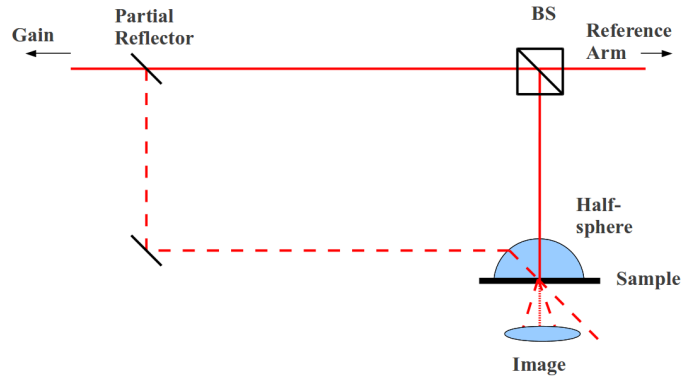
Figure 8.7: Combining SPIN with a second imaging technique to increase tranverse resolution. The sample pulse is coupled out by a partial reflector and overlapped with the proper delay with the cavity pulse at the sample via a half-sphere. The cavity pulse provides the 0th order as referene, the second pulse the higher orders and both are imaged.

which does not have a [26] deadband as previously shown. A setup sketch is shown in figure 8.8. The dye jet is placed in the center of the cavity. This ensures two pulse operation because saturation of the dye can be reached quicker resulting in a lower loss for the laser.

The best laser for SPIN is the linear OPO with two pulses inside this cavity. OPO is a purely solid state laser that can be tuned over a large wavelength region. Two different OPO cavity approaches can be used for SPIN. An external cavity, harmonically pumped OPO as demonstrated in chapter 4 or and intra-cavity pumped OPO. Both designs have benefits and disadvantages. The external cavity approach has been shown to be an excellent and stable source, but a high power pump laser is needed. The power problem can be avoided by using an intracavity pumped OPO. Stable two pulse operation is not a simple task in an intracavity OPO. The coupling between the two cavities result in an instability. Theoretical simulation suggest that this can be solved by introducing a non-linear loss inside the OPO cavity [36] but experimental implementation has not been achieved up to now.
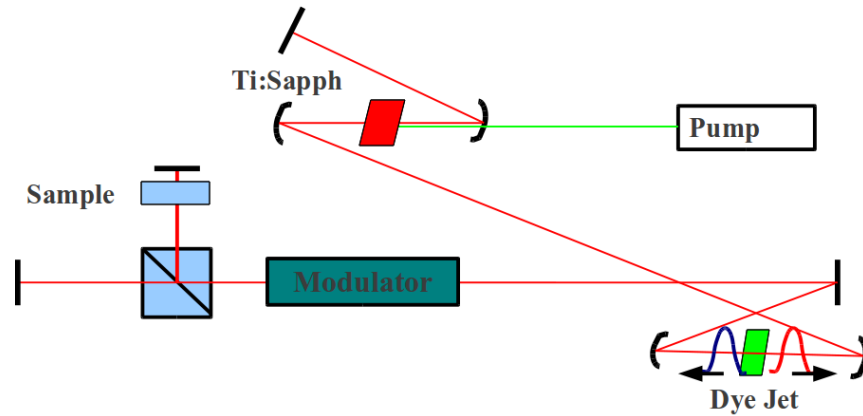
Figure 8.8: Cavity configuration for SPIN with a Ti:Sapphire gain crystal and dye jet.

The signal applied to the Pockels cell, diverting the two pulses into the two arms, has to be considered more carefully. Ideally a square pulse is used. The $\lambda/2$ voltage level are normally a few hundreds of Volts for low voltage modulators and a square pulse is almost impossible to create in this high voltage range. Therefore a sinusoidal wave has to be used. The problem with a sinusoidal wave is the time needed for the pulse traveling through one of the arms and back to the Pockels cell and will result in a change in the voltage level. This results in a partial rotation of the pulse and
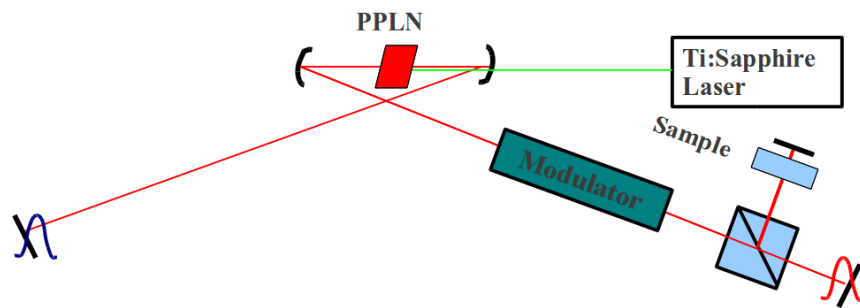
Figure 8.9: The external cavity OPO setup. A mode-locked pump laser, in this case Ti:Sapphire will pump the PPLN crystal. The OPO cavity has to be a multiple e.g. 2 times of the pump cavity to create the two independent pulses.
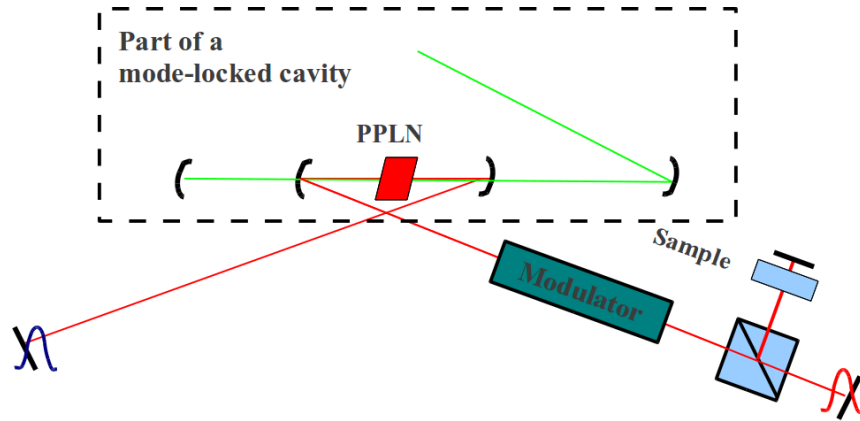
Figure 8.10: The internal cavity setup is sketched. The pump pulse is passing the PPLN twice in one round trip, possible creating the two independent pulses inside the cavity. Harmonically pump scheme can be implemented in this design as well.

therefore introduces a loss to the cavity. A 10cm path length takes 0.3ns traveling time. The change in voltage at the peak value using V(t)=V_0(1+cos(ωt)), where V_0 is the peak voltage, ω the frequency of the signal, for a 1.5m linear cavity (10ns roundtrip time) is 2% resulting in a cavity loss in the same magnitude. This can be avoided by voltage larger than the $\lambda/2$ voltage as sketched in Fig. 8.11. The pulse is passing through the modulator slightly before and on the return path slightly after the peak voltage is reached. The same concept applies to the second pulse in the cavity at zero wave voltage.

A problem arises when the Pockels cell is driven by the repetition rate of one pulse. The cell will also act as a phase modulator similar to the EOM in Chapter 5 and introduces a bias beatnote between the two pulses. Driving the Pockels cell by double the repetition rate of one pulse while simulatenously oscillating between -V$_{\lambda/2}$ to +V$_{\lambda/2}$ can eliminate the beatnote (see figure 8.12). The first pulse will see an alternating positive or negative V$_{\lambda/2}$ every round-trip resulting in the cancellation of the acquired phase that creates the beatnote. For the second pulse, the cancellation can take place already on the return path.
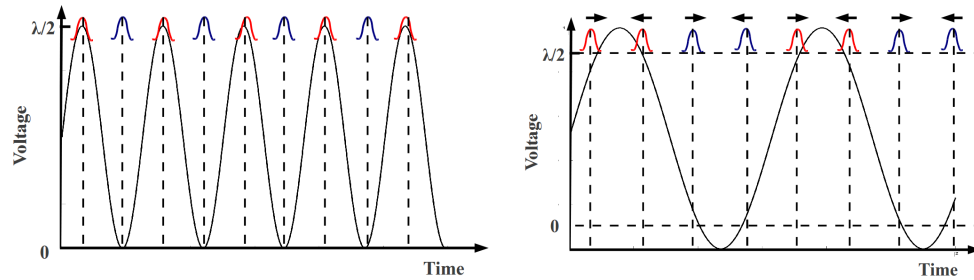
Figure 8.11: One the left side, the ideal situation is shown. The modulator is driven by the repetition rate of one pulse and a short tail is assumed. The pulse 1 (red) and pulse 2 (blue) will always hit either the zero voltage or the $\lambda/2$ voltage so they are diverted into the two different arms. On the right the figure takes into account that the tail has a finite length. Driving the modulator with a biased signal such that zero and $\lambda/2$ voltage is not at the peak allows for minimum loss. The arrows indicate the first path and the return path of one pulse.

The best signal possible would be the series of step functions as shown in figure 8.13. The pulse width can be chosen to accommodate the cavity tail length, thereby providing the ability to adjust the separation between the blue and red pulse, reducing the requirement of the modulator placement inside the cavity. A similar circuit
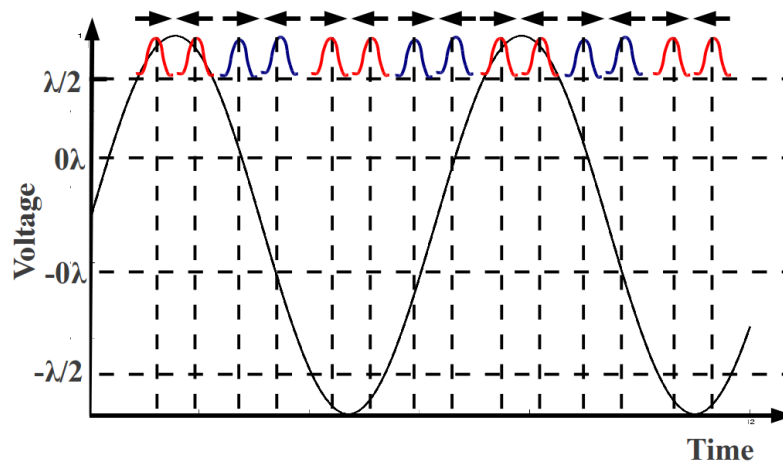
Figure 8.12: The modulator driven by twice the repetition rate of one pulse.
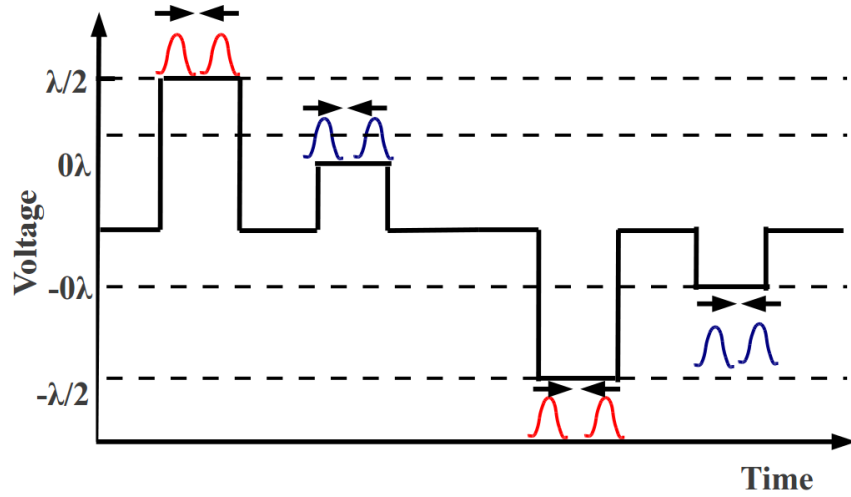
Figure 8.13: Ideal signal with square pulses.

that produces such a pulse train has been published by Braga et al [55]. for moderate voltage levels of a few volts. The technical difficulty is the high voltage needed.

The applications is not only limited to phase imaging. IPI can also be applied to measure the amplitude of phonon waves in mirror coatings. The mirror of the sample cavity can be coated with any high reflective coating that is excited at a periodicity of the laser cavity itself. The two-pulse externally pumped OPO cavity is a great candidate for this sensor. The unused portion of the pump pulse has still enough power to excite the optical phonon in the coating and the same repetition rate as the OPO. As coating, Bismuth is a prime candidate as coating for studying the performance of this nanoscope sensor. Several studies have been carried out investigating the properties of optical phonon and can be compared to our device [74] .

8.4 High Repetition Rate OPO

Another OPO application, unrelated to the two previous examples, is high-repetition rate OPO used for astronomy. In astronomy, stable frequency combs with a large, in the GHz, frequency separation are required as reference signals. The signals are normally provided by optical techniques like high repetition rate, mode-locked Ti:Sapphire Laser systems. The research proposes a different method:using a harmonically, synchronously pumped optical parametric oscillator (OPO), where the pump laser is stabilized in repetition rate as well as phase. Small cavities require the use of a short gain crystal to minimize dispersion. Also negative GVD mirrors (NGVD) have to be used to compensate the cavity's group velocity dispersion. The mode-locking mechanism is challenging due to the smaller crystal used and therefore less nonlinearity is present to achieve Kerr lens mode-locking. Short pulse operation is achieved up to 10GHz with an outputpower of 1W [75]. Higher repetition rates are difficult to achieve due to the required space for placing the NGVD mirrors as well as the size of the gain crystal.

Optically pumped VECSELs mode-locked with an on-chip saturable absorber can push the limit even further. Short pulse widths is a challenge for such devices and only 100fs pulsewidths have been achieved to date. Harmonically pumped OPOs can be used to achieve high repetition rate lasers without miniaturizing the cavities. Kokabee et al [46] have successfully achieved a 16GHz picosecond OPO this way. In this research, it was shown that these multiple pulses inside the OPO cavity are independent of each other, especially in phase as shown in chapter 5.

The unique feature of synchronously pumped OPO is that the repetition rate τ_{RT} of the OPO pulse train is determined by the pump repetition rate. The feature implies that the frequency spacing of the OPO comb is fixed assuming a perfectly stable pump pulse train. However, the CEP is not fixed. The CEP is the electric field phase in respect to the center of the envelope of the pulse. This pulse to pulse

varying phase converts directly into a frequency, the CEO. In the frequency picture, the comb picture, the CEO can be seen as an offset frequency from zero. In an OPO, the pump frequency becomes converted into a signal and idler frequency. The conversion process in an OPO has to fulfill three main conservation laws:

1. energy

2. momentum

3. phase

The first two laws are normally considered as the phase matching condition where the wavelength has to be conserved e.g $\omega_{pump} = \omega_{idler} + \omega_{signal}$ and the wave vectors $k_{pump} = k_{signal} + k_{idler}$ have to be conserved respectively. The proposed method will use the third conservation–the phases also have to be conserved: $\varphi_{pump} = \varphi_{signal} + \varphi_{idler} - \pi/2$. A perfect stabilized pump source (repetition rate, wavelength and phase) and the phase matching condition puts constraints on the system. By injecting a continuous wave seed laser at the idler wavelength, the idler's phase and the frequency are fixed. This leaves a perfectly stabilized frequency comb with all parameters controlled: repetition rate, wavelength, and phase.

To create the high repetition rate OPO, the OPO cavity length must be changed to a common multiple of the pump cavity, the harmonical pumping scheme.The first pump pulse will create a signal pulse circulating in its cavity until it interacts with another pump pulse for amplification. The pump pulses in between the first pump pulse will create a signal pulse, also circulating within the cavity. This leaves us with a higher harmonic of the original pump repetition rate. For example, creating a 300MHz OPO from a 100MHz pump laser, 3 separate pulses are circulated in the OPO cavity. The 300MHz OPO can be achieved by either a 3 times larger cavity or a 3/4th smaller cavity than the pump cavity length. This scheme can be applied to any multiple of the original pump repetion rate.

Combining both methods, the phase locking with a seed laser and the high repetition rate OPO will give the desired perfect frequency ruler needed in several other fields e.g Astronomy. The wide tunabillity of the OPO's center wavelength will make this device a very versatile spectroscopic tool.

Chapter 9

Conclusion

This dissertation is centered around the two-pulse-per-cavity mode-locked laser systems and their applications.

The first experiment discusses how two-pulse-per-cavity lasers can also be used for an analogy between the laser cavity and two-level atoms. This analogy, provides new insight into the dynamics of two-pulse coupling in mode-locked ring lasers. The analogy might explain observations like a Kerr-lens mode-locked ring laser, which switches directions of operation at rates of tens of Hz, rather than being bidirectional.

In the second experiment, an external pumped OPO is introduced with a cavity tvice the length of the pump. The cavity length enables creating two independent pulse trains. The phase independence between the two pulses was obtained from the beatnote measurement with an electro-optical modulator. Further, no coupling or deadband was observed and a very narrow beatnote bandwidth was measured, implying long-term stability.A slightly modified setup measured the non-linear index of PPLN with very good error bars and a value consistent with previously reported

numbers. For a complete survey, a brief discussion of the intra-cavity pumped OPO is described, including the problems encountered.

Novel approaches for OPO pump sources are also presented and studied. For the first time, the research demonstrated a hybrid mode-locked tapered amplifier laser in a ring cavity. The high average output power and broad tunability will the make the laser adaptable for many applications. Due to the limitations in pulse energy, however,the tapered amplifier laser is inadequate to pump an OPO. Therefore, the research next considered VECSELs. Currently, a mode-locked 795nm VECSEL has not been achieved.

Continuing with IPI research, the experiments innovated a new application for IPI, optical magnetometry. A proof of principle experiment was presented with promising performance where a solid state (TGG) probe is used. Atomic vapor was discussed as a a probe to improve IPI magnetometer performance.

Finally, fundamental IPI limits were discussed. For Ti:Sapphire the limit is the Schawlow-Townes linewidth. Before approaching this limit the mechanical noise has to be suppressed significantly. For the OPO, a more difficult limit arises.The OPO can be treated like a laser, but due to the phase-matching mechanism as well as the synchronously pumping, a more complex system evolves.

The last chapter proposed a number of experiments to improve the performance of optical magnetometer and an application of IPI for phase imaging.

Appendices

Appendix A

Pump Energy and OPO Gain

A simple calculation can be made to show that the threshold of an OPO is only related to the Energy of the pump pulse. Starting from the threshold condition for a single resonant OPO (found in Chapter 2 of [66])

$$g^2 L^2 = 2 \times l \tag{A.1}$$

where g is the nonlinear gain, L the length of the gain crystal and l the loss of the cavity for the signal frequency. For this calculation it is assumed that perfect conditions are present. This means perfect phase matching $\Delta k = 0$ is achieved and the crystal length is adapted to the pulse widths as well as the focusing arrangement is chosen such that a minimum beam size is achieved over the length of the crystal. The gain can be derived as the following:

$$g = \sqrt{\frac{4\omega_s^2 \omega_i^2 d_{eff}^2 A_p^2}{k_s k_i c^2}} \tag{A.2}$$

were i and s stand for signal and idler, d_{eff} is the effective nonlinear coupling coefficient and A_p the dimensionless electric field amplitude of the pump pulse. The

Appendix A. Pump Energy and OPO Gain

intensity I is related to A_p: $I_p = 2n\epsilon_0 c |A_p|^2$. Normally for nonlinear process the peak intensity is used for $I_p = I_{ave}\tau_{rt}/\tau_p$. For the length of the crystal we choose it to be proportional to the Rayleigh length of the pump beam $L = \rho = \pi w_0^2/\lambda$ and that L is proportional to the pulse width τ_p of the laser we get the following expression:

$$g^2 L^2 \propto I_{ave} w_0^2 \tau_{rt} = W_p \tag{A.3}$$

where W_p is the pulse energy.

Appendix B

Optically Pumped VECSEL Structure

The structure of the VECESL:

		Al content	Thickness [A]
Substrate	SI GaAs		
Start	GaAs		1073
	AlGaAs	0.3	575
Mirror 40x	AlGaAs	0.3	575
	AlGaAs	0.67	41
	AlGaAs	0.81	42
	AlGaAs	0.9	43
	AlGaAs	0.92	390
	AlGaAs	0.9	43
	AlGaAs	0.81	42
	AlGaAs	0.64	41
Intermediate	AlGaAs	0.47	191
	AlGaAs	0.35	186
	AlGaAs	0.28	183
	AlGaAs	0.23	22
Gain QW 5x	AlGaAs	0.2	439
	AlGaAs	0.08	74
	AlGaAs	0.2	92
	AlGaAs	0.08	74
	AlGaAs	0.2	439
Intermediate	AlGaAs	0.28	183
	AlGaAs	0.35	186
	AlGaAs	0.47	191
Top layer	AlGaAs	0.67	41
	AlGaAs	0.86	42
	AlGaAs	0.96	43
	AlGaAs	0.98	394
	AlGaAs	0.96	43
	AlGaAs	0.86	42
	AlGaAs	0.67	41
	AlGaAs	0.47	39
	AlGaAs	0.37	39
	AlGaAs	0.32	38
	AlGaAs	0.3	345
	AlGaAs	0.3	115

References

[1] A. Jain, J. Kumar, F. Zhou, L. Li, and S. Tripathy. A simple experiment for determining verdet constants using alternating current magnetic fields. *American Journal of Physics*, 67:714–717, 1999.

[2] T. H. Maiman. Stimulated optical radiation in ruby. *Nature*, 187:493–494, 1960.

[3] F. J. McClung and R. W. Hellwarth. Giant optical pulsations from ruby. *Journal of Applied Physics*, 33:828–829, 1962.

[4] L. E. Hargrove, R. L. Fork, and M. A. Pollack. Locking of hene laser modes induced by synchronous intracavity modulation. *Appl. Phys. Lett*, 5:4–5, 1964.

[5] P. F. Moulton. Spectroscopic and laser characteristics of Ti:Al$_2$O$_3$. *J. Opt. Soc. Am.B*, 3:125–133, 1986.

[6] C. L. G. Alzer, M. A. G. Martinez, and P. Nussenzveig. Analog of electromagnetically induced transparency. *Am. J. Phys.*, 70:37–41, 2002.

[7] Ming Lai and Jean-Claude Diels. Wave-particle duality of a photon in emission. *Journal of the Opt. Soc. Am. B*, 9:2290–2294, 1992.

[8] Xianmei Meng. *Ultra-short Pulse Optical Parametric Oscillator Sensor*. PhD thesis, University of New Mexico, Albuquerque, New Mexico, 2003.

[9] M. M. Salour and C. Cohen-Tannoudji. Observation of Ramsey-s interference fringes in the profile of Doppler-free two-photon resonances. *Physical Review Letters*, 38:757–760, 1977.

[10] N. F. Ramsey. A molecular beam resonance method with separated oscillating fields. *Physical Review*, 78:695–699, 1950.

References

[11] R. P. Feynman, F. L. Vernon, and R. W. Hellwarth. Geometrical representation of the Schroedinger equation for solving maser problems. *J. Appl. Phys.*, 28:49–52, 1957.

[12] C. Cohen-Tannoudji, J. Dupont-Roc, and G. Grynberg. *Atom-Photon Interactions*. John Wiley & Sons, New York, 1992.

[13] F. Aronowitz. The laser gyro. In Ross, editor, *Laser Applications*, pages 133–200. Academic Press, New York, 1971.

[14] F. Aronowitz and R. J. Collins. Lock-in and intensity-phase interaction in the ring laser. *J. Appl. Phys.*, 41:130–141, 1970.

[15] J. Killpatrick. The laser gyro. *IEEE Spectrum*, 4:44, October 1967.

[16] F. Aronowitz and R. J. Collins. Mode coupling due to backscattering in a He-Ne traveling-wave ring laser. *Appl. Phys. Lett.*, 9:55–58, 1966.

[17] Izumi Kataoka and Yukio Kawahara. Dependence of lock-in threshold and winking pattern on the phase-interaction of scatering waves in the ring laser. *Japanese Journal of Applied Physics*, 25:1365–1372, 1986.

[18] J.-C. Diels and I. C. McMichael. Influence of wavefront conjugated coupling in the operation of a laser gyro. *Opt. Lett.*, 6:219–221, 1981.

[19] R. J. C. Spreeuw, R. Centeno Neelen, N. J. van Druten, E. R. Eliel, and J. P. Woerdman. Mode-coupling in a He-Ne laser with backscattering. *Physical Review A*, 42(7):4315–4324, October 1990.

[20] Xianmei Meng, Jean-Claude Diels, Dietrich Kuehlke, Robert Batchko, and Robert Byer. Ultra-short pulse opo ring laser. In *CLEO 2000, technical digest*, volume CMW7, page 122, San Francisco, Ca, 2000. Optical Society of America.

[21] Paul Pulaski. *Semiconductor laser gyroscopes*. PhD thesis, The University of New Mexico, Albuquerque, New Mexico, 1997.

[22] Paul Pulaski and Jean-Claude Diels. Unidirectional multiple-quantum-well laser. In *CLEO, 1995*, page 153 (CTuQ4), Baltimore, MA, 1995. Optical Society of America.

[23] Xianmei Meng, Raphael Quintero, and Jean-Claude Diels. Intracavity pumped optical parametric bidirectional ring laser as a differential interferometer. *Opt. Comm*, 233:167–172, 2004.

References

[24] Rafael Quintero-Torres, Mark Ackerman, Martha Navarro, and Jean-Claude Diels. Scatterometer using a bidirectional ring laser. *Opt. Comm.*, 241:179–183, 2004.

[25] M. Navarro, O. Chalus, and Jean-Claude Diels. Mode-locked ring lasers for backscattering measurement of mirror. *Optics Letters*, 31:2864–2866, 2006.

[26] Matthew J. Bohn and Jean-Claude Diels. Bidirectional Kerr-lens mode-locked femtosecond ring laser. *Opt. Comm.*, 141:53–58, 1997.

[27] Ladan Arissian and Jean-Claude Diels. Investigation of carrier to envelope phase and repetition rate — fingerprints of mode-locked laser cavities. *Journal of Physics B: At. Mol. Opt. Phys*, 42:183001, 2009.

[28] Matthew Bohn. *The Ti:sapphire ring laser gyroscope*. PhD thesis, The University of New Mexico, Albuquerque, New Mexico 87131, May 1998.

[29] J.-C. Diels and I. C. McMichael. Degenerate four-wave mixing of femtosecond pulses in an absorbing dye jet. *J. Opt. Soc. Am. B*, 3:535–543, 1986.

[30] M. L. Dennis, J.-C. Diels, and M. Lai. The femtosecond ring dye laser: a potential new laser gyro. *Optics Letters*, 16:529–531, 1991.

[31] R. Jason Jones, Matthew J. Bohn, and Jean-Claude Diels. Solid state laser gyro using ZnS for kerr-lens mode-locking. In *CLEO, 1998*, page 434, San Francisco, Ca, 1998. Optical Society of America.

[32] Xianmei Meng, Jean-Claude Diels, Dietrich Kuehlke, Robert Batchko, and Robert Byer. Bidirectional, synchronously pumped, ring optical parametric oscillator. *Opt. Letters*, 26:265–267, 2001.

[33] M. Sheik-Bahae, A. A. Said, and E. W. Van Stryland. High sensitivity single beam n_2 measurement. *Opt. Lett.*, 14:955–957, 1989.

[34] Richard DeSalvo, Ali A. Said, David J. Hagan, Eric W. Van Stryland, and Mansoor Sheik-Bahae. Infrared to ultraviolet measurements of two-photon absorption and n_2 in wide bandgap solids. *IEEE J. Quantum Electron.*, QE-32:1324–1333, 1996.

[35] Andreas Velten, Alena Zavadilova, Vaclav Kubecek, and Jean-Claude Diels. Instabilities in intracavity pumped optical parametric oscillators and methods of stabilization. *Applied Physics B*, 98:13–25, 2009.

References

[36] Andreas Velten and Jean-Claude Diels. *Optical parametric oscillators for Intra-cavity Phase Interferometry: Performing ultra-sensitive measurements inside a mode-locked cavity.* PhD thesis, The University of New Mexico, Albuquerque, New Mexico, 2010.

[37] Y.Silberberg and P.W.Smith. Subpicosecond pulses from a modelocked semi-conductor lasers. *IEEE J. Quantum Electron.*, 22:759–761, 1986.

[38] E. P. Ippen, D. J. Eilenbergen, and R. W. Dixon. Picosecond pulse generation by passive modelocking of diode lasers. *Appl. Phys. Lett.*, 37:267–269, 1980.

[39] P. J. Delfyett, L. Flores, N. Stoffel, T. Gmitter, N. Andreadakis, G. Alphonse, and W. Ceislik. 200 femtosecond optical pulse generation and intracavity pulse evolution in a hybrid modelocked semiconductor diode laser- amplifier system. *Optics Lett.*, 17:670–672, 1992.

[40] A. Aschwanden, D. Lorenser, H. J. Unold, R. Paschotta, E. Gini, and U. Keller. 2.1-w picosecond passively mode-locked external-cavity semiconductor laser. *Opt.Lett.*, 30:272–274, 2005.

[41] G. Bendelli, K. Komori, S. Arai, and Y. Suematsu. A new structure for high-power tw-sla. *IEEE Photonics Technology Letters*, 3:42–44, 1991.

[42] J. N. Walpole, E. S. Kintzer, S. R. Chinn, C. A. Wang, and L. J. Missaggia. High-power strained-layer InGaAs/AIGaAs tapered traveling wave amplifier. *Appl. Phys. Lett.*, 61:741–742, 1992.

[43] J. Bowers A. Mar, R. Helkey, D. Mehuys, and D. Welch. Mode-locked operation of a master oscillator power amplifier. *IEEE Photonics Technology Letters*, 6:1067, 1994.

[44] Yihan Xiong, Sytil Murphy, J. L. Carlsten, and Kevin Repasky. Design and characteristics of a tapered amplifier diode system by seeding with continuous-wave and mode-locked external cavity diode laser. *Opt.Eng.*, 45:124205–1–124205–5, 2006.

[45] J.-C. Diels and Wolfgang Rudolph. *Ultrashort laser pulse phenomena.* Elsevier, ISBN 0-12-215492-4; second edition, Boston, 2006.

[46] O. Kokabee, A. Esteban-Martin, and M. Ebrahim-Zadeh. Efficient, high-power, 16 ghz, picosecond optical parametric oscillator pumped by an 81-mhz fiber laser. In OSA, editor, *Conference on Lasers and Electro-Optics/International Quantum Electronics Conference*, page paper CThP2, 2010.

References

[47] Andreas Velten, Andreas Schmitt-Sody, and Jean-Claude Diels. Precise intra-cavity phase measurement in an optical parametric oscillator with two pulses per cavity round-trip. *Optics Letters*, 35:1181–1183, 2010.

[48] Jun Ye and Stephen Cundiff. *Femtosecond Optical Frequency Comb: Principle, Operation and Applications*. Springer, New York, NY, 2005.

[49] A. Balbin Villaverde, D. A. Donatti, and D. G. Bozinis. Terbium gallium garnet verdet constant measurements with pulsed magnetic field. *J. Phys. C: Solid State Phys.*, 11:61, 1978.

[50] V. A. Ruilova-Zavgorodniy, D. Yu. Parashchuk, and I. A. Gvozdkova. Highly sensitive pump probe polarimetry: Measurements of polarization rotation, ellipticity, and depolarization. *Instruments and Experimental Techniques*, 46:818–823, 2003.

[51] S.C. Zeller R. Paschotta, A. Schlatter, H.R. Telle, and U. Keller. Optical phase noise and carrier-envelope offset noise of mode-locked lasers. *Applied Physics B*, 82:265–273, 2006.

[52] P. D. D. Schwindt, S. Knappe, V. Shah, L. Hollberg, and J. Kitching. Chip-scale atomic magnetometer. *Applied Physics Letters*, 85:6409–6411, 2004.

[53] Peter. D, D. Schwindt, B. Linseth, S. Knappe, V. Shah, and J. Kitching. Chip-scale atomic magnetometer with improved sensitivity by use of the mx technique. *Appl. Phys. Lett.*, 90:0811021–3, 2007.

[54] S.J. Seltzer and M.V. Romalis. Unshielded three-axis vector operation of a spin-exchange-relaxation-free atomic magnetometer. *Appl. Phys. Lett.*, 85:4804, 2004.

[55] A. P. Braga, J.-C. Diels, R. K Jain, R. Kay, and L. Wang. Bidirectional mode-locked fiber ring laser using self-regenerative, passively controlled, threshold gating. *Optics Letters*, 35:2648–2650, 2010.

[56] C. K. Renshaw S. Ghosh, A. Bhagwat, S. Goh, and A. L. Gaeta. Low-light-level optical interactions with rubidium vapor in a photonic band-gap fiber. *PRL*, 97:023603, 2006.

[57] Michael Dennis and Jean-Claude Diels. Behavior of a bidirectional co2 ring laser. In N. B. Abraham, Elsa Garmire, and Paul Mandel, editors, *OSA Proceedings of Nonlinear Dynamics in Optical Systems*, volume 7, pages 420–423, Afton, Oklahoma, 1991. Optical Society of America.

References

[58] J. Zhang, Z. H. Lu, and L. J. Wang. Precision measurement of the refractive index of air with frequency combs. *Opt. Lett.*, 30:3314–3316, 2005.

[59] P. T Ho. Phase and amplitude fluctuations in a mode-locked laser. *IEEE J. Quantum Electron.*, QE-21:1806 – 1813, 1985.

[60] A. L. Schawlow and C. H. Townes. Infrared optical masers. *Phys. Rev.*, 112:1940–1049, 1958.

[61] Anthony E. Siegman. *Lasers*. University Science Books, Mill Valley, CA, 1986.

[62] C. R. Menyuk, J. K. Wahlstrand, J. Willits, R. P. Smith, T. R. Schibli, and S. T. Cundiff. Pulse dynamics in mode-locked lasers: relaxation oscillations and frequency pulling. *Opt. Expr.*, 15:6677–6689, 2007.

[63] J.K Wahlstrand, J.T. Willis, T. R. Schibli, C.R. Menyuk, and S. T. Cundiff. Quantitative measurement of timing and phase dynamics in a mode-locked laser. *Optics Lett.*, 32:3426–3428, 2007.

[64] J.K Wahlstrand, J.T. Willis, C.R. Menyuk, and S. T. Cundiff. The quantum-limited comb lineshape of a mode-locked laser: Fundamental limits on frequency uncertainty. *Optics Expr.*, 16:18624–18628, 2008.

[65] R. Graham and H. Haken. The quantum-fluctuations of the optical parametric oscillator. i. *Zeitschrift fuer Physik.*, 210:276–302, 1968.

[66] R. W. Boyd. *Nonlinear Optics*. Academic Press, Boston, 2008.

[67] J. M. Dudley, D. T. Reid, M. Ebrahimzadeh, and W. Sibbett. Characterisics of a noncritically phasematched Ti:sapphire pumped femtosecond optical parametric oscillator. *Optics Communications*, 104(4,5,6):419–430, January 1994.

[68] D. T. Reid, B .J. S. Gale, and J. Sun. Frequency comb generation and carrier-envelope phase control in femtosecond optical parametric oscillators. *Laser Physics*, 18:87–103, 2008.

[69] M. V. Balabas, T. Karaulanov, M. P. Ledbetter, and D. Budker. Polarized alkali-metal vapor with minute-long transverse spin-relaxation time. *Phys. Rev. Lett.*, 105:070801, 2010.

[70] Ladan Arissian, Jean-Claude Diels, Andreas Stintz, and Vaclav Kubecek. Multiple quantum wells for ring and linear lasers with long lifetime gain. In Shori Hoffman, editor, *Solid State lasers IX*, volume 5707-52, pages 295–301, San Jose, CA, 2005. SPIE.

References

[71] D. Budker and M. Romalis. Optical magnetometry. *Nature Physics*, 3:227, 2007.

[72] A. Neumann, Y. Kuznetsova, and S. R. J. Brueck. Structured illumination for the extension of imaging interferometric microscopy. *Optics Express.*, 16:6785–6793, 2008.

[73] Xuan. Luo, A. P. Braga, L. Arissian, and J.-C. Diels. Intracavity phase measurement towards sub-manometer resolution. ASSP Conference, OSA topical meeting, paper MB7, 2009.

[74] T. Garl, E. G. Gamaly, D. Boschetto, A. V. Rode, B. Luther-Davies, and A. Rousse. Birth and decay of coherent optical phonons in femtosecond-laser-excited bismuth. *Phys. Rev B*, 78:134302, 2008.

[75] A. Bartels, D. Heinecke, and S. A. Diddams. Passively mode-locked 10 ghz femtosecond ti:sapphire laser. *Optics Letters*, 33:1905–1907, 2008.